Turbulent flow in and over an urban canopy in Vancouver, Canada

A Large Eddy Simulation using a real building and vegetation configuration based on LiDAR data

Master's thesis at ETH Zurich

Student: Pascal Egli

Date of submission: July 28, 2014

Supervisors

- Prof. Wolfgang Kinzelbach - Swiss federal Institute of Technology in Zurich ETHZ
- Prof. Marc Parlange - Swiss Federal Institute of Technology in Lausanne EPFL
- Prof. Andreas Christen - University of British Columbia in Vancouver UBC
- Marco Giometto - Swiss Federal Institute of Technology in Lausanne EPFL

In collaboration with the University of British Columbia in Vancouver

Faculty of Applied Sciences, Faculty of Forestry and
Department of Geography/Atmospheric Science Program

ETH
Eidgenössische Technische Hochschule Zürich
Swiss Federal Institute of Technology Zurich

EPFL
ÉCOLE POLYTECHNIQUE
FÉDÉRALE DE LAUSANNE

UBC
a place of mind
THE UNIVERSITY OF BRITISH COLUMBIA

Abstract

In this Master's thesis, turbulent flow of the atmosphere over the urban canopy of the 'Sunset' neighbourhood in Vancouver was studied using a Large Eddy Simulation (LES) model. A high precision Light Detection and Ranging (LiDAR) dataset was employed to represent the urban building geometry that served as a boundary condition and to implement the form drag force of trees as a function of the height-dependent Leaf Area Density (LAD) in this LES model. Eddy flux measurements of the Urban Climate Research Tower of UBC located in the study domain were sampled for wind direction and neutral atmospheric conditions in order to validate the modelling results. The simulations were carried out on a subset of 512 $\times$ 512 m with flat topography, regular building patterns and an areal fraction of trees of $\lambda_v = 0.12$. Modelling resolution was 2 m and model runs were carried out once without trees (only buildings) and once with trees. Velocity spectra from conditionally sampled tower measurements and from modelling results both show typical slopes of the inertial subrange (-5/3) and the production range (-1) as well as a slope change at the same frequency, which validates the modelling results. Time correlations of the longitudinal velocity u for varying lag and height show that characteristic length and time scales are larger when trees are present than if there are only buildings. Wind speeds for the simulation with trees are slightly lower than for the simulation without trees, while more small scale Turbulent Kinetic Energy (TKE) is generated in the Roughness Sublayer for the simulation with trees. The aerodynamic roughness length z_0 of the modelling subset was determined to be in the range of 0.36 - 0.40 m for a hypothetical simulation without trees, and in the range of 0.42 - 0.46 m for a simulation taking into account the pressure drag on trees. The displacement height d was estimated to be $d = 3.25$ m. A blending height h_b for the Roughness Sublayer (RSL) of $h_b = 11.24$ m was determined for the modelling subset, taking into account the drag force exerted by trees.

Contents

List of Figures

Glossary

The following abbreviations are often used in this work. They are introduced in the text at their first occurrence and further on used only in their abbreviated form.

ABL - Atmospheric Boundary Layer

CALP - Centre for Advanced Landscape Planning, Forestry Dep. at UBC

CDF - Cumulative Distribution Function, Integral of the PDF

CFD - Computational Fluid Dynamics

CFCAS - Canadian Foundation for Climate and Atmospheric Sciences

DEM - Digital Elevation Model

EPFL - École Polytechnique Fédérale de Lausanne

EPiCC - Environmental Prediction in Canadian Cities

ETHZ - Eidgenössische Technische Hochschule Zürich

FFT - Fast Fourier Transformation

IBM - Immersed Boundary Method

ISL - Inertial Sublayer

LAI - Leaf Area Index

LES - Large Eddy Simulation

LIDAR - Light Detection and Ranging

MKE - Mean Kinetic Energy

MOST - Monin Obukhov Similarity Theory

PDF - Probability Distribution Function

UBC - University of British Columbia

RANS - Reynolds Averaged Navier-Stokes Equations

RSL - Roughness Sublayer

SGS - subgrid-scale

TIN - Triangulated Irregular Network

TKE - Turbulent Kinetic Energy

Symbol definitions and units

The following list comprises full names and symbols of important variables and constants used within this work, along with their physical dimensions and constant values.

Table 1: Symbol definitions and units

z_i	Boundary Layer height	[m]
z_*	Roughness Sublayer height	[m]
u_*	Friction velocity	$[ms^{-1}]$
h_b	Blending height	[m]
z_{sensor}	Tower measurement elevation above ground	24.8 m
h	Space-averaged height of the roughness elements	[m]
d	Displacement height	[m]
z_0	Aerodynamic roughness length for momentum	[m]
g	gravity	9.81 m s^{-2}
κ	von Kármán constant	0.41 [-]
f	frequency (e.g. of tower measurements)	[Hz]
u	Longitudinal wind component	$[ms^{-1}]$
v	Lateral wind component	$[ms^{-1}]$
w	Vertical wind component	$[ms^{-1}]$
C_d	Wind drag coefficient	[-]
a'	Deviations from mean, valid for any variable: a'= a - $\overline{a}$	[unit of a]
$\overline{u'w'}$	Covariance of long. and vert. wind components	[m^2s^-2]
$\overline{u'v'}$	Covariance of long. and lat. wind components	[m^2s^-2]
$\overline{u'T'}$	Covariance of long. wind component and air Temperature	[K ms^{-1}]
$\overline{u'^2}$	Variance of long. wind component	[m^2s-^2]
$\overline{u'^3}$	Skewness of long. wind component	[m^3s-^3]
$\partial T/\partial z$	Mean temperature lapse rate	[°K m^-1]
τ_{ij} = -$\overline{\rho}\overline{u_i'u_j'}$	Reynolds stress, consisting of six stress components with i,j taking the values 1,2 and 3.	[kg $m^{-1}s^{-2}$]
L	Obukhov length	[m]
ν_{air}	Viscosity of air	1.5 10^{-5} m^2s^{-1}
Re	Reynolds number, Re = LU/ν	[-]
ρ	Density of dry air (23% 0_2, 76% N_2) at 20° at sea level	1.293 kg/m^3 (34)
p	Air pressure	[Pa]
R	Ideal gas constant	8.314 [J $K^{-1}mol^{-1}$]
Ri_1	Richardson number, for a 1 minute period	[-]
Dir_1	Wind direction, from 1 minute averaged wind components	[°N]
Ri_{20}	Richardson number, for a 20 minutes period	[-]
Dir_{20}	Wind direction, from 20 min averaged wind components	[°N]
$Magn_1$	Wind velocity magnitude, from 1 min averaged wind components	$[ms^{-1}]$
$Magn_{20}$	Wind velocity magnitude, from 20 min averaged wind components	$[ms^{-1}]$

ω_a	Cyclic frequency of a given variable a, ω=2πf	$[s^{-1}]$
κ_u	Wave number of u [m/s], κ_u=2πf/$\bar{u}$	$[m^{-1}]$
$\hat{F_a}(\kappa)$	Space spectrum of a given variable a	$[m^3 s^-2]$
$\hat{S_a}(\omega)$	Time spectrum of a given variable a	$[m^3 s^-2]$
θ_*	Scaling temperature	[K]
λ_p	Plan area ratio of buildings	[-]
λ_v	Plan area ratio of vegetation	[-]
A_p	Obstacle area seen from top-down	$[m^2]$
A_T	Total ground area	$[m^2]$
A_F	Frontal area of an obstacle	$[m^2]$
S_x	Average inter-element spacing between element centroids	[m]
L_y	Width of the roughness elements perpendicular to the wind	[m]
L_u	streamwise Eulerian integral length scale	[m]
L_w	vertical Eulerian integral length scale	[m]
r_{uw}	correlation coefficient for u and w	[-]
$\left\langle \overline{u_i" u_j"} \right\rangle$	Dispersive flux (spatial covariance of time-averaged fields)	$[m^2 s^{-2}]$
$K_M = \frac{-\overline{u'w'}}{\partial\bar{u}/\partial z}$	Eddy diffusivity of momentum	$[m^2 s^{-1}]$
$K_H = \frac{-\overline{w'\theta'}}{\partial\bar{\theta}/\partial z}$	Eddy diffusivity of heat	$[m^2 s^{-1}]$

Notations

The notations for averages and fluctuating terms of variables employed in this work are explained below.

- $< a >$ denotes the spatial average of a variable a. For LES model results this means that the average of the concerned variable for all grid points over an xy-plane is computed, yielding an average vertical profile of the variable.
- $\bar{a}$ denotes the time average of a variable a. For both LES model results and for Tower data, this means that the time series of a variable is averaged at a given location. In the results section, time and space averages are often combined: The xy-averaged vertical profiles of different variables, that were averaged over many simulation steps in time, are examined.
- a' denotes the fluctuations of a given variable a about its temporal mean.
- a'' denotes the fluctuations of a given variable a about its spatial mean.

1. Introduction

This Master's thesis approaches the study of turbulence in and above the urban canopy from two different angles: On one side there are the high-frequency measurements which give a precise and per se realistic image of flow characteristics in time while they can make only a limited statement on the spatial properties and variations of the flow. On the other side is a Large Eddy Simulation (LES), run over a highly resolved urban geometry and resolving the flow field at a spatial resolution of 2 $\times$ 2 m. Even though the LES is just an approximation of reality, it can give us more information about the spatial distribution and about the physics of the flow than a large array of measurement devices ever could. The main goal of this work was to reconcile the advantages of both methods - measurements and modelling - in order to better understand how the presence of trees is affecting surface roughness, mean flow and turbulence statistics within a real urban neighbourhood and to compare these findings to existing knowledge from experiments and modelling.

A better knowledge of flow within urban canopies can contribute to a wide field of applications: In the field of Environmental Engineering and Atmospheric Science a very direct application is pollutant modelling. In Urban Meteorology, applications are the estimation of evapotranspiration, production, transport and removal of gases such as CO_2 or water regime of lawns, bushes and trees. Meteorology depends on precise subgrid-scale parameterizations of wind and moisture for local weather prediction. And, last but not least, Climate and Atmospheric Science depends on parameterizations of the exchange of momentum, moisture and pollutants at the earth-atmosphere interface, the Atmospheric Boundary Layer, as boundary conditions for Meso scale and Large scale atmospheric models.

1.1 State of the knowledge

Extensive experimental research has been done on turbulence in urban canopies, such as field surveys conducted with measurement towers in real cities by (32), examination of coherent structures within the urban canopy and an analysis of the budget of Turbulent Kinetic Energy (TKE) within an urban boundary layer by (5). In addition to field and wind tunnel experiments, the first Large Eddy Simulations (LES) were run over idealized settings such as rectangular patches of different surface roughness (2) and regular arrays of cubes (23) to gain insights into physical mechanisms undergoing in urban boundary layers. Simulations over real settings were lacking until some years ago, due to extreme computational requirements. As an example, nowadays a simulation of a small domain with full resolution, run on a powerful cluster, can take up to two weeks. But the increasing availability of Digital Elevation Models (DEMs) and

existence of more and more powerful clusters is now allowing, to some degree of freedom, to simulate a little subset of a real city, as it was performed recently for the Digital Elevation Model of a neighbourhood in Basel, Switzerland [Giometto et al., in preparation, 2014].

The effect of trees on airflow and, inversely, the effect of flow on trees, has been studied earlier with wind tunnel (26) and field measurements (18) as well as with RANS simulations (10).

Previous studies on the impact of trees on airflow and pollutant transport in cities have been focusing on the effect of trees on dispersion of pollutants in street canyons. Most of them were conducted using RANS (Reynolds Averaged Navier-Stokes Equations) models. The study by Vos et al. (39) suggests that trees may have a negative effect on pollutant concentrations in street canyons by trapping pollutants inside canyons. A recent study by Krayenhoff et al. (20), submitted June 2014, parameterizes drag and turbulence in 1-D column models (so called Urban Canopy Models for weather and air pollution forecasting) and informs those parameterizations using 3D RANS simulations that include tree foliage.

As a complete Novum in comparison to previous research, the present study implements trees and bushes as roughness elements within the urban canopy layer. Building shapes and vegetation features and their corresponding density were extracted from a high precision LiDAR (Light Detection and Ranging) dataset provided and pre-processed by Dr. Rory Tooke from the CALP (Collaborative for Advanced Landscape Planning), CIRS (Centre for Interactive Research on Sustainability) at UBC (University of British Columbia) (3) in collaboration with Prof. Nicholas Coops of the Integrated Remote Sensing Studio. The data was complemented by Leaf Area Index (LAI) datasets kindly provided by Prof. Andreas Christen of the Department of Geography at UBC. Drag forces induced by the presence of trees were modelled as a volumetric forcing term in the Navier Stokes equations, where the force is proportional to the computed Leaf Area Density (LAD) encountered at a certain height.

Figure 1.1: Example of a neighbourhood street in Sunset Area, looking north from the modelling domain. Image by the author.

1.2 Objectives of this thesis

1. **Surface properties**: Analyze LES results to determine the aerodynamic roughness length z_0, displacement height d and blending height h_b of the urban boundary layer.
2. **Tree implementation:** Process tree LiDAR data and embed it into the computational domain to study the effect of pressure drag on trees on mean flow and turbulence.
3. **Tower measurements:** Validate LES results with/without vegetation with conditionally sampled tower measurements from UBC Research Tower: Compare spectra in time for model results and tower data.

1.3 Geography and climate of the site

The modelling area was chosen mainly for its long history of tower flux measurements with more than six years of continuous high frequency data acquisition, for the extensive use of the site for research yielding more than 40 papers on the tower in the last 40 years, but also for its relatively uniform topography and the regular, rectangular and North-South aligned pattern of houses and streets, which is typical for North American cities.

1.3.1 Geography

The site is located in the single family house neighbourhood 'Sunset' of South Vancouver at approximately 70 m.a.s.l on a gentle hill, at less than 8 km from the sea bay 'Strait of Georgia'. This residential neighbourhood with relatively flat topography is situated south of the town centre and just 2 km north of the tidal Fraser River that flows into the Strait of Georgia. The first range of mountains on the north shore of Vancouver, arising to an elevation of up to 1500 m.a.s.l and situated only 10 km away from the field site, influences the dominating wind directions at Vancouver Sunset.

1.3.2 Climate

The climate of Vancouver is classified as west coast maritime temperate (33), featuring moderate inter-seasonal mean temperature oscillations and a mean daily air temperature that stays above 0 °C over the entire year; while the monthly mean air temperature remains around 5 °C during the winter months, it amounts to 19 degrees during the summer months, with an annual mean of 10.4 degrees Celsius. A dry period during summer months with absence of precipitations for several weeks, lasting up to two months in certain years, is typical. Mean annual precipitation measured at Vancouver International Airport amounts to 1189 mm, of which nearly all occurs in liquid form and only 3 % is snow. The monthly average wind speed is relatively low. Daily mean wind speed measured at a standard height of 10 m above ground remains constantly between 3 and 4 m/s during the entire year. The wind probability is somewhat higher in spring and in autumn, when storms are more frequent. The dominant wind directions depend strongly on the seasons: Between October and March Eastern winds prevail. This changes abruptly in spring,

when West North West winds dominate during April and May. In summer, wind is somewhat less frequent, with the dominating wind direction changing from ESE in June to WNW in July and back to SE in August (40). On a daily scale, mountain/valley effects and land/sea dynamics act together to produce landwards directed winds ("sea-breeze") during daytime and seawards directed winds ("land-breeze") during night time (33). The moderate temperature variations over the year can partly be attributed to the proximity of the sea, acting as a large reservoir of heat. Soil freezing in winter is relatively rare.

2. Theory

2.1 Governing equations

The following formulae are taken from the book "An Introduction to Boundary Layer Meteorology" by Stull (35), and their description is a summary of the more detailed development made in the book. The motion of a fluid can be described by considering conservation of mass and momentum for fluid particles inside a given control volume. If heat, moisture and different scalars play a role, as it is the case in a complex environment such as the Atmospheric Boundary Layer, four additional equations have to be considered:

- Equation of State (Ideal Gas Law)
- Conservation of Moisture
- Conservation of Heat
- Conservation of a scalar quantity (e.g. a pollutant)

The conservation equations below are often called the 'Navier-Stokes' equations, after the scientists who first stated them. Their analytical solution remains impossible to the present day.

Conservation of Mass (Continuity Equation)

$$\frac{\partial \rho}{\partial t} + \frac{\partial(\rho U_j)}{\partial x_j} = \frac{d\rho}{dt} + \rho \frac{\partial U_j}{\partial x_j} = 0 \tag{2.1}$$

If $\frac{d\rho}{dt}\frac{1}{\rho} \ll \frac{\partial U_j}{\partial x_j}$, then the **Incompressibility approximation** is valid:

$$\frac{\partial U_j}{\partial x_j} = 0 \tag{2.2}$$

or

$$\nabla \mathbf{U} = 0 \tag{2.3}$$

Conservation of Momentum (Newton's second law)

$$\frac{\partial U_i}{\partial t} + U_j \frac{\partial U_i}{\partial x_j} = -\delta_{i3} g - 2\epsilon_{ijk}\Omega_j U_k - \frac{1}{\rho}\frac{\partial p}{\partial x_i} + \frac{1}{\rho}\frac{\partial \tau_{ij}}{\partial x_j} \tag{2.4}$$

I II III IV V VI

I - storage of momentum, or local acceleration
II - advection, or advective acceleration
III - vertical action of gravity
IV - coriolis force; influence of the earth's rotation
V - pressure-gradient forces
VI - viscous stress

Einstein summation notation In the governing equations above and for all other equations in this work, the Einstein summation notation is used: The subscripts i and j each take on the values of 1,2 and 3 corresponding to the three spatial dimensions x,y and z. (a) If a subscript occurs twice in a term, this means that the term is summed over all three spatial dimensions. (b) If an index is not summed in one of the terms of an equation, this means that it must not be summed in any other term of the equation. In this case, the equation stands for three equations, with the index taking on the values 1,2 and 3. Description by Rotach (30).

2.2 Reynolds decomposition and averaging

A frequently used approach to describe turbulence is the Reynolds decomposition: All variables are subdivided into their mean and the deviations from the mean in order to separate the mean flow from the turbulent fluctuations in time, e.g. for the streamwise velocity

$$u' = u - \bar{u} \tag{2.5}$$

with u' the fluctuations from the mean, $\bar{u}$ the mean and u the full variable. The Navier-Stokes equations are rewritten in terms of mean variables and fluctuations about the mean and rearranged in order to separate means from fluctuations.

In a second step, these equations are averaged in time. At this point, specific averaging rules significantly simplify the equations. For example, in order to satisfy mathematics, the mean of all fluctuations in time has to be zero

$$\overline{u'} = 0 \tag{2.6}$$

2.3 Atmospheric Boundary Layer

The Atmospheric Boundary Layer (ABL), also called Planetary Boundary Layer, denotes the lowest part of the Earth's atmosphere, in which surface-atmosphere exchanges take place and in which transport is dominated by turbulence.

It can be subdivided into an outer region where $z \gg z_0$ and an inner region where z $\ll z_i$. Here, z_i denotes the boundary layer height, which is typically about 1000 m, but can vary significantly depending on atmospheric stability and underlying surface. It can take on values between 100 and 3000 m.

In the framework of this thesis the focus is entirely onto the inner region of the ABL, which has a typical depth of 100 m, i.e. 1/10 of the ABL height. The inner region is further subdivided into its lower portion, the Roughness Sublayer (RSL), and its upper portion, the Inertial Sublayer (ISL). These Layers are described below (30).

2.3.1 Inertial sublayer

The Inertial Sublayer (ISL) is the layer situated above the Blending height in the inner region of the ABL. For an urban canopy, the ISL is located between $z = 3 - 5h$ and $z = 0.1z_i$. Flow in the ISL is horizontally homogeneous and it is not directly influenced by the individual roughness elements of the Roughness Sublayer. Usually, the streamwise velocity u increases logarithmically with height within this layer.

2.3.2 Roughness Sublayer

"The term 'Roughness Sublayer' will indicate the entire layer dynamically influenced by length scales associated by roughness elements. This layer encompasses z values from (typically) $2h$ to $5h$ (...). It exists below the inertial or logarithmic layer in which $u(z)$ is proportional to $ln(z)$, and is the rough-wall counterpart of the viscous sublayer over a smooth wall." In Rotach (30), cited from Raupach et al. (1991).

The roughness sublayer height is denoted with the symbol z_*. Regular surfaces such as forests, crop fields or suburbs with one-storey houses have relatively low z_* values, while irregular surfaces such as town centres with high buildings have relatively high z_* values (30).

2.3.3 Blending height

The blending height is the height above surface level where streamwise velocity profiles for different locations on a horizontal plane collapse to a single logarithmic law. Local variations in mean wind velocity due to large roughness elements are 'blended out' above this height. In most cases, the blending height defines the limit between the Roughness Sublayer (RSL) below and the Inertial Sublayer (ISL) above. Instantaneous velocities within the ISL are turbulent and nearly random ('disorganized'), while the space-averaged velocity follows a logarithmic law. In this work, the blending height is denoted with the symbol h_b.

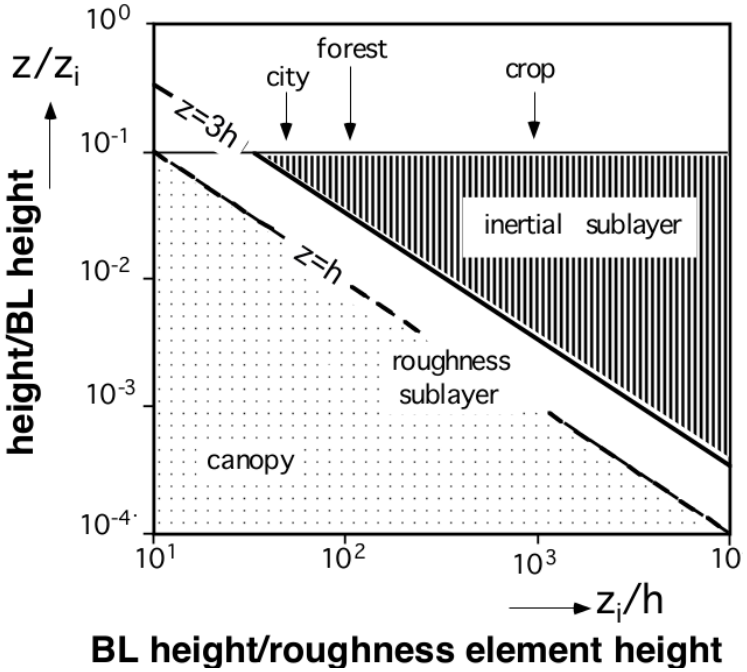

Figure 2.1: Scheme illustrating the dependence of the extent of different layers of the inner ABL on the height of the roughness elements. Source: Rotach (29),

Mason (1988) introduced the blending height as a height "at which turbulent mixing would have blended the internal boundary layers at each transition from one surface type to another into an 'equilibrium or blended layer', wherein the flow is independent of horizontal position (i.e., representing the area-averaged conditions)." From Rotach (30).

"Mason (1988) argued that i) an equilibrium layer [corresponds to ISL] must exist close to the surface where MOST [Monin-Obukhov Similarity Theory] applies and ii) above the blending height a logarithmic wind profile (for neutral conditions) exists."

2.4 Conceptual flow and surface properties

2.4.1 Reynolds number

The dimensionless Reynolds number is determined by the ratio of the external forces acting on a fluid to the internal forces of the fluid.

$$Re = \frac{F_{ext}}{F_{int}} = \frac{u\frac{\partial u}{\partial x}}{\nu\frac{\partial^2 u}{\partial x^2}} = \frac{\frac{U^2}{L}}{\nu\frac{U}{L^2}} = \frac{UL}{\nu} \tag{2.7}$$

The external forces tend to make a flow unstable (i.e. prone to disorder, or turbulence), whereas the internal forces are represented by the viscosity of the fluid, which 'holds the flow together'.

Osborne Reynolds measured this relationship of external to internal forces in a series of experiments in the late 19th century in order to investigate the transition from laminar to turbulent flow. He found that flow becomes turbulent for Reynolds numbers greater than Re = 2000 (30).

For a given fluid (with constant viscosity), turbulence is only a property of the flow, and depends on its velocity and the domain size.

2.4.2 Friction velocity u_*

The friction velocity is a measure for the total vertical flux of horizontal momentum near the surface. It is derived from the magnitude of the Reynolds stress:

$$u_*^2 = [\overline{u'w'_s}^2 + \overline{v'w'_s}^2]^{1/2}, \tag{2.8}$$

where $\overline{u'w'_s}$ and $\overline{v'w'_s}$ denote the covariances between horizontal velocities and vertical velocity at the surface (indice 's'). Written in the form of a Reynolds stress, e.g.

$$\tau_{xz} = -\bar{\rho}\overline{u'w'_s}, \tag{2.9}$$

these terms represent the deformation of a fluid element by the turbulent mixing of air of different speed to one of its faces (35).

2.4.3 Surface Layer Scaling - MOST

The following development is adapted from (30) and from Stull (35). Similarity theory attempts to describe the characteristics of the result of solving the conservation equations for a fluid by describing the 'new' variables arising from the Reynolds decomposition and averaging, i.e. the covariances $\overline{u'w'}$ and $\overline{u'\theta'}$, independently from the conservation equations. This approach is often successful because these covariances, or turbulent fluxes, represent important physical processes such as turbulent transport of momentum and they have been observed to dominate the other terms in the equations in many cases in reality.

For the Surface Layer, i.e. the layer immediately above a rough surface, it has been found from experimental research and dimensional analysis that the dominating variables are $\overline{u'w'_s}$ (surface flux of momentum), $\overline{u'\theta'_s}$ (surface flux of sensible heat), $\frac{g}{\bar{\theta}}$ (buoyancy) and the vertical coordinate z. A dimensionless combination of these variables can be formed that expresses the characteristics of the Surface Layer.

The Monin-Obukhov similarity theory (MOST) uses the same approach for the surface layer, but defines slightly different variables to arrive at the final dimensionless group:
The characteristic temperature

$$\theta_* := -\overline{w'\theta'_s}/u_* \tag{2.10}$$

and the length scale

$$L := \frac{1}{k}\frac{u_*^2}{\theta_*}(\frac{g}{\overline{\theta}})^{-1} = -\frac{1}{k}\frac{u_*^3}{\overline{w'\theta'_s}}(\frac{g}{\overline{\theta}})^{-1} \tag{2.11}$$

which is called the Obukhov length. The resulting dimensionless group is z/L, which differs from the initial surface scaling only by the inclusion of the von Kármán constant k. Any dimensionless variable is now a function of z/L alone.

Thus for the Surface Layer, any mean variable $\bar{a}$ made dimensionless by scaling it with a characteristic term a_* can be expressed as a function of the non-dimensional π-group z/L:

$$\frac{\bar{a}}{a_*} = f_a(\pi_1) = f_a(z/L) \tag{2.12}$$

Based on this general similarity for the Surface Layer, the non-dimensional profile for mean wind speed in the SL is expressed as

$$\frac{\partial \bar{u}}{\partial z}\frac{kz}{u_*} = \phi_m(z/L) \tag{2.13}$$

For ideally neutral conditions we have that $z/L = 0$ and $\phi = 1$. We define a height at which $\bar{u} = 0$, the roughness length z_0 (see below): $\bar{u}(z = z_0) = 0$. Now, integrate the above equation for neutral conditions between z_0 and a height z in the SL by separating variables:

$$\int_{\bar{u}(z_0)}^{\bar{u}(z)} d\bar{u} = \frac{u_*}{k}\int_{z_0}^{z}\frac{dz}{z} \tag{2.14}$$

which yields

$$\frac{\bar{u}(z)}{u_*} = \frac{1}{k}\cdot ln(\frac{z}{z_0}) \tag{2.15}$$

The resulting equation for velocity in dependence of height corresponds to the typical logarithmic velocity profile observed in neutral Surface Layers.

2.4.4 Aerodynamic Roughness length z_0

This length characterizes the elevation above ground at which, for a logarithmic velocity profile, the mean streamwise velocity is zero: $u(z_0) = 0$. This definition is only valid if there is no zero-plane displacement d.

In order to fit a logarithmic velocity profile to wind measurements made above a rough surface, the fit has to be shifted upward by $dz = z_0$, according to equation 2.15 seen above.

Following its name, z_0 is a measure for the roughness of a surface. It typically increases proportionally to the height of the roughness elements of a surface, to their exposed surface and to their density, until a point is reached where the elements are placed densely enough so that shading by neighbouring elements again reduces the drag on a given element. In urban canopies, z_0 is often of the order of magnitude of 0.1h, with h being the average building height.

Roughness parameterizations from literature

Parameterizations of aerodynamic roughness of urban areas can be obtained by two fundamentally different approaches: The first approach considers surface roughness directly by looking at the urban geometry, including the density, fractional surface area and height of houses. Such methods are termed 'morphometric' (13). The second approach, which is called 'anemometric' or 'micrometeorological', focuses on observed flow properties such as standard deviations of wind speed for one-point measurements. As described in (12), this can be done using fast-response or slow-response measurement methods. Examples for such parameterizations will be described more in detail in section 3.7.1 and section 3.7.2.

2.4.5 Displacement height d

Also called the 'zero plane displacement', the displacement height d is the elevation above the base level at which the wind speed starts to increase significantly. The barycenter of wind pressure on the obstacles is located at this height. It is a property of the Inertial Sublayer (ISL) describing the Inertial Sublayer wind speed profile. This quantity is purely theoretical and it appears when a logarithmic velocity profile has to be fitted to wind speed measurements above a very rough surface such as an urban canopy. Only by subtracting d from the height z, a satisfying fit of the logarithmic wind speed profile can be achieved. Above forest and urban canopies, d is often estimated to be $\mathrm{d} = 0.7 \cdot h$. The height d depends on quantities such as the average size of the roughness elements, the inter-element spacing and the shape of the elements (30).

2.4.6 Flow regimes

Flow over rough surfaces depends on three geometric characteristics of a site (14):

1. The mean height of the roughness elements: h
2. The plan area index: $\lambda_P = A_P/A_T$, where A_P is the obstacle area seen from top-down and A_T is the total ground area.
3. The frontal area index: $\lambda_F = \overline{L_y h}/\overline{S_x^2}$, "where $\overline{L_y}$ is the mean width of the roughness elements perpendicular to the wind direction and $\overline{S_x}$ is the average inter-element spacing between element centroids, in the along-wind direction", Grimmond et al. (13).

Three different flow regimes with increasing obstacle density can be distinguished, as determined in (15): If obstacle elements are far apart and the turbulence generated by one element does not interfere with the turbulence generated by the subsequent element, this is called **isolated flow**. **Wake interference flow** occurs if the wake from one element interferes with the subsequent element. If the elements are placed closely enough in order to prevent the wake from reaching the ground in-between the elements, **skimming flow** has developed. The maximum roughness is reached for wake interference flow, while it decreases again for skimming flow because there is less interaction with the canyons in-between obstacles. The roughness type responsible for skimming flow is also called **k-roughness**, while the roughness type that is at the origin of isolated and wake interference flow is called **d-roughness**.

2.5 Turbulent Kinetic Energy (TKE)

While the Mean Kinetic Energy (MKE) informs about the energy contained in the mean flow, the Turbulent Kinetic Energy is a measure of the energy contained in the deviations from the mean flow, the turbulent components of a flow field. The kinetic energy per unit mass, $\frac{1}{2}\overline{u_i u_i} = \frac{1}{2}(\overline{u^2} + \overline{v^2} + \overline{w^2})$, may be expressed as the sum of the mean component (the MKE) and the turbulent component (the TKE): $\frac{1}{2}\overline{u_i u_i} = \frac{1}{2}\bar{u_i}\bar{u_i} + \frac{1}{2}\overline{u_i' u_i'} = MKE/m + e$, where e denotes TKE per unit mass. As can be seen in this equation, e is simply half the sum of the variances of the velocity components (35).

The TKE equation is a second-moment equation, as opposed to the conservation equations presented in section 2.1, from which it can be derived. Second moments of flow variables are indispensable for a better understanding of the nature of the turbulence (28).

The time-averaged TKE budget at a single point is

$$\frac{\partial \bar{e}}{\partial t} + \bar{U}_j \frac{\partial \bar{e}}{x_j} = +\delta_{i3}\frac{g}{\bar{\theta}_v}(\overline{u_i'\theta_v'}) - \overline{u_i' u_j'}\frac{\partial \bar{u}_i}{\partial x_j} - \frac{\partial \overline{u_j' e}}{\partial x_j} - \frac{1}{\bar{\rho}}\frac{\partial \overline{u_i' p'}}{\partial x_i} - \epsilon \tag{2.16}$$

A detailed explanation of the individual terms of TKE can be found in Stull (35).

2.6 Atmospheric stability: Richardson number

In an unstable atmosphere, the gradient of potential temperature is negative, while it is positive in a stable atmosphere. Typically, the atmosphere in the lower ABL becomes stable during night due to surface cooling through back radiation. Especially in the case of intense solar radiation during the day, the atmosphere becomes quickly unstable and convection (upward movement of warm air) develops. An air parcel which is moved from its initial position to an infinitesimally higher elevation in the atmosphere, will continue to rise if the atmosphere is unstable. The same parcel will sink back to its initial position if the atmosphere is stable, and it remains in place in the case of an ideally neutral atmosphere.

Thus, atmospheric stability is determined by the relationship between upward moving forces creating turbulence, such as mechanical shear production, and the restoring force of gravity that tends to suppress turbulence. In order to determine atmospheric stability in a simplified way, especially if limited measurements are available, the so-called Flux Richardson number was defined to be the ratio of the buoyant production term and the mechanical production term of the TKE budget:

$$Ri = \frac{\frac{g}{\bar{\theta}}\overline{w'\theta'}}{\overline{u_i' u_j'}\frac{\partial \bar{u}_i}{\partial x_j}} \tag{2.17}$$

The Richardson number is dimensionless, and its denominator consists of nine terms, as defined by the Einstein summation notation. A more detailed documentation on different types of Richardson numbers can be found in Stull (35).

2.7 Filtering

In different steps of this work, some sort of numerical filtering operation is used. This is the case e.g. for the refinement and smoothing of model input data (1D filter in the vertical, 2D filter in the horizontal) as well as for a neater visualization of spectra by averaging out small spikes. In this work, filtering of the signal in space or time was always done with a running average (top-hat type filter). The corresponding Matlab function *conv* is used together with an appropriate filtering support. In order to ensure energy conservation for the signal, the sum of the elements of such a filter support always has to be equal to one. In case of a 1D filter, the support is an $n \times 1$ vector. In case of a 2D filter, the support is an $n \times n$ matrix, with n the length of the support in each filtering direction.

$$(f * g)(t) = \int_{-\infty}^{\infty} f(\tau)g(t-\tau)d\tau \tag{2.18}$$

where f and g are two functions, shifted in the space or time domain by the amount τ and evaluated at the location or moment t. The symbol "$*$" is the convolution operator, providing a simplified notation of the convolution integral. The weighting function g represents the filter support vector (in 1D) or matrix (in 2D) if the convolution is used for filtering (8).

The discrete form of this equation in one dimension, employed for the numerical computations of the convolution e.g. by the Matlab function, is:

$$(f * g_N)[n] = \sum_{m=0}^{N-1} f[m]g_N[n-m] \tag{2.19}$$

where the durations of f and g are limited to the interval [0,N-1] and either f or g can take the role of the impulse response, while the other function is the input signal (25).

2.8 Spectral Analysis

The main purpose of spectral analysis in the study of turbulence is to determine which size of eddies contributes to what property of the flow field. After passing from the time and space domain to the frequency domain, a power spectrum of the signal is obtained, visualizing the importance of each frequency. A transition to the frequency (or spectral) domain is done using transforms such as the Wavelet transform or the Fourier transform. In the following, the procedure is illustrated using the Fourier transform:

$$\hat{F}_a(\kappa_1) =: \mathcal{F}\{C_a(r_1)\} = \frac{1}{2\pi}\int_{-\infty}^{\infty} C_a(r_1)e^{-i\kappa_1 r_1}dr_1 \tag{2.20}$$

$$\hat{S}_a(\omega) =: \mathcal{F}\{C_a(\tau)\} = \frac{1}{2\pi}\int_{-\infty}^{\infty} C_a(\tau)e^{-i\omega\tau}d\tau \tag{2.21}$$

with κ_1 being the longitudinal component of the wave number, κ_1=2πf/$\bar{u_1}$, f [s^{-1}] the natural frequency and ω=2πf the cyclic frequency. This overview has been adapted from Rotach (30).

3. Methodology

3.1 LES model

3.1.1 Concepts

The EPFL-LES model, which was first developed by (1), solves the filtered Navier-Stokes equations on a regular domain using a Pseudo-Spectral method in the horizontal directions and a second-order accurate centered difference scheme in the vertical direction. Surface roughness derived from a Triangulated Irregular Network (TIN) is directly resolved by embedding the surface in the computational domain and relying on an immersed boundary method to enforce boundary conditions at the interface location. Time advancement is done using the explicit second-order Adams-Bashforth scheme (37).

Of the force terms on the right hand side of the Navier-Stokes momentum equation, only the pressure gradient forces and the viscous stresses are relevant in the present application of the LES. Gravity can be neglected due to the incompressibility assumption and the Coriolis forces are very small because of the relatively small dimensions of the modelling domain in comparison to planetary scales. The equations are implicitly filtered in space, resolving fluid motions explicitly only down to grid resolution. Effects at smaller scales are represented by the Subgrid Scale Model (see below). The filtering operator is denoted with "˜ ", thus the momentum equation to be solved becomes:

$$\frac{\partial \tilde{U}_i}{\partial t} + \tilde{U}_j \frac{\partial \tilde{U}_i}{\partial x_j} = -\frac{1}{\rho}\frac{\partial \tilde{p}}{\partial x_i} + \frac{1}{\rho}\frac{\partial \tilde{\tau}_{ij}}{\partial x_j} \tag{3.1}$$

The **pressure gradient term** can be seen as a volumetric forcing term, which is constant throughout the computational domain and is the main forcing mechanism for the system. It consists of (a) the pressure gradient prescribed between the boundaries (i.e. the imposed gradient), and (b) the pressure drag exerted by the houses and trees in the domain. Viscous or skin friction drag might only be important in regions with attached flow, i.e. some rooftops and some street canyons.

$$-\frac{1}{\rho}\frac{\partial p}{\partial x_i} = -\frac{1}{\rho}\frac{\partial p_{imposed}}{\partial x_2} + \frac{1}{\rho}\frac{\partial p_{buildings}}{\partial x_i} + \frac{1}{\rho}\frac{\partial p_{trees}}{\partial x_i} \tag{3.2}$$

The **viscous effects** at the model resolution are negligible, due to the fact that the roughness Reynolds number is Re >> 1000, and therefore the stresses arise entirely from the subgrid LES model.

Subgrid scale model The subgrid scale (SGS) model used is a basic Smagorinsky model, which is based on the mixing length. This model "expresses the SGS flux as a function of the resolved strain rate tensor $\bar{S}_{ij} = (\partial_j \bar{u}_i + \partial_i \bar{u}_j)/2$ using

$$\tau_{ij} = -2\nu_{sgs}\bar{S}_{ij} = -2(c_{s,\delta}\delta)^2|\bar{S}|\bar{S}_{ij} \tag{3.3}$$

where δ is the filter width (i.e. the grid size) and ν_{sgs} is the SGS viscosity." Tseng et al. (37). The model is based on the mixing-length theory and the viscous analogy. Variations of the Smagorinsky model differ in the way the unknown Smagorinsky coefficient $c_{s,\delta}$ is estimated. Traditionally, this coefficient was set equal to a constant, typically 0.16. This constant was estimated from the theory of isotropic homogeneous turbulence, stating that turbulence statistics are assumed to be independent of direction and location in space (37).

Immersed Boundary Method (IBM) IBM is a method used to prescribe boundary conditions in LES simulations: Instead of modelling surface roughness, it is directly resolved in the IBM. The method uses Monin Obukhov Similarity Theory (MOST) to derive wall stress from the wind velocity at the first grid point above the model surface, assuming a logarithmic velocity profile (9).

Lateral boundary conditions Air flow in the model is generated by a horizontal pressure gradient applied between the inflow boundary south of the domain at $y = 0$ m and the outflow boundary north of the domain at $y = 512$ m. We have embedded periodic boundary conditions due to discrete Fourier spatial expansions that are used to represent the solution in the numerics.

3.1.2 Simulation parameters and conditions

The spatial dimensions of the modelling domain were $128 \times 512 \times 512$ m. Before running the simulation over many steps, short trial simulation runs were made in order to verify that the construction of the ϕ functions (representing the building topography) was completed correctly and that the extent, resolution and orientation of the building geometry and of the Leaf Area Density files were as expected. In a next step, a simulation over the building geometry with more simulation time steps was executed in order to check and verify velocity profiles and their appearance. After these preliminary checks, the long simulations were started.

Both for the model with trees and for the model without trees, the following modelling procedure was taken: In a first execution (a), the LES model was run over 150'000 time steps of $dt = 0.01$ s with a total modelling time of 25 minutes. Then, starting from the final step of the first execution (a) as initial condition for the flow, a second run (b) over 120'000 time steps with a total modelling time of 20 minutes was made in order to obtain a more stationary flow.

Because of restrictions to disk space and because of time required for saving large-size variables such as 3D- resp. 4D-matrices of velocity in space resp. in space and time, the results were saved in three different formats:

- Time-averaged field: Time-averaged variables for each 30'000 simulation time steps were saved at full modelling resolution.

- Time-series field 1: A time series of the last 50'000 steps of the simulation was saved at a temporal resolution of 0.1 Hz and at low spatial resolution: Each variable was sub-sampled at an interval of 32 × 32 × 124 m in space.
- Time-series field 2: A time series of only 300 steps at full resolution both in time and space was saved for each variable.

The model validation, i.e. the computation of time spectra, was done using the Time-series field 1 and the analysis of canopy properties and plotting of the relevant variables in space was done using the Time-averaged field of the last 30'000 simulation time steps. That way, the entirely stationary flow was averaged over a sufficiently long time interval.

Table 3.1: The main LES model parameters.

Parameter	Value
Reynolds number Re	10^5
Pressure gradient $\partial p/\partial x$	0.01 m/s^2
Time step dt	0.01 s
Total number of time steps nsteps	$(1.5 + 1.2) \cdot 10^5 = 2.7 \cdot 10^5$
Length in x-direction Lx	512 m (- 2 m)
Length in y-direction Ly	512 m (-2 m)
Length in z-direction Lz	128 m (-4 m)

3.2 Modelling domain

Figure 3.1: Panorama picture of the neighbourhood 'Sunset', taken from the top of the Urban Climate Research Tower. Image kindly provided by Prof. Andreas Christen. Photographer: Rick Ketler, Geography Dept. at UBC.

The LES is applied to a 512 × 512 m domain placed south-west of the UBC Urban Climate Research Tower in the Vancouver Sunset Area neighbourhood. The tower is located at 123.0784°W/ 49.2261°N in the coordinate system WGS84. The North-eastern corner of the domain overlaps with the tower location by 60 m in both x (South-North) and y (West-East) direction and extends south-westwards. The site in Vancouver Sunset had been chosen for the installation of the Research Tower in 1978 because of its spatially homogeneous pattern of streets and houses, which is representative for the majority of neighbourhoods in Vancouver and

in North American cities in general, because of its relatively smooth topography and because of the possibility to set up a 30 m high tower inside the lot of the Mainwaring substation of BC Hydro.

Within the neighbourhood, the precise location of this 512 × 512 m modelling domain was chosen for various reasons:

- Only wind directions between West and South East are considered for the analysis of tower data because the homogeneous urban surfaces of interest are located in this sector.
- The sector South West - South East of the Mainwaring Substation contains the most regular building and street patterns and no large open areas.
- Topography in this sector is much more homogeneous and flat, as opposed to the areas North and North east of the Mainwaring substation. This is an important criterion because the neighbourhood is modelled as a flat surface in the LES, i.e. topography is removed.
- The high fence and row of trees surrounding the BC Hydro Mainwaring substation creates a wake in the air flow. In order to avoid direct influence by this wake on the measurements at the tower location, the wind should approach the fence from sector south.

3.3 Topography and trees

Vegetation and constructed objects in the area around the Measurement Tower are very well documented thanks to the EPiCC (Environmental Prediction in Canadian Cities) technical reports developed as part of the CFCAS (Canadian Foundation for Climate and Atmospheric Sciences) funded project. EPiCC tech report No. 3 (22) is about Vegetation Characteristics at the Vancouver experimental sites. For a radius of 500 m around the Sunset Measurement tower, the plan area fraction of vegetation is of $\lambda_v = 33.4$ %, with $\lambda_{v,G} = 21.6$ % of ground vegetation (< 2 m) and $\lambda_{v,T}(EPiCC) = 11.9$ % of above-ground vegetation. This value is very close to the value computed for the 512 × 512 m modelling subset: $\lambda_{v,T}(\text{Model}) = 11.44$ %. The proportions of deciduous and coniferous (evergreen) trees within a similar radius of 400 m around the tower are 14.76 and 4.44 stems/ha respectively. Due to the low proportion of coniferous trees, the overall Leaf Area Index (LAI) varies strongly with seasons (75 % of trees are leafless in winter). The overall mean LAI (including surfaces without trees) of the area around the tower is 0.39 and was estimated within the EPiCC project as follows: LiDAR measurements were used for the determination of the maximum tree height. 120 trees were picked manually and the LAI was estimated for these trees based on urban-specific (empirical) relationships for urban trees in the United States of America, distinguishing between coniferous and deciduous trees. The LAI estimate is based on tree height and crown diameter (22).

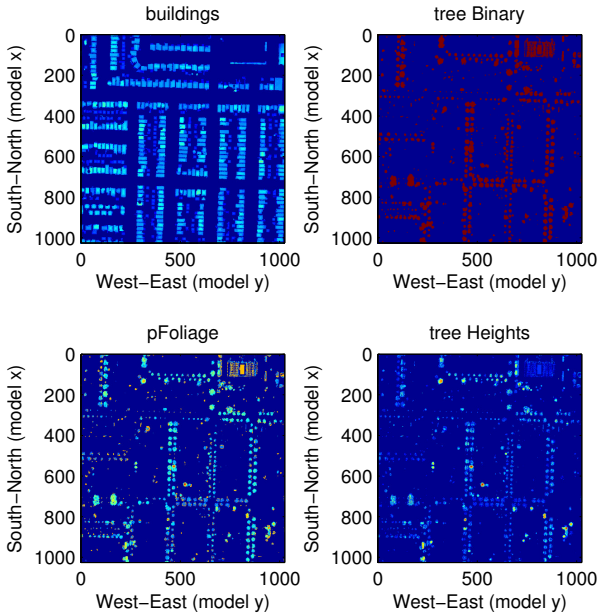

Figure 3.2: Overview of the four main datasets extracted from the LiDAR point cloud: For the distinction between buildings and vegetation, an algorithm based on the number of reflections of a LiDAR beam was used. The 'tree Binary' is 1 for cells classified as trees and 0 for others. pFoliage is a dataset containing the parameters K and λ of the Weibull probability distribution function representing Leaf Area Density.

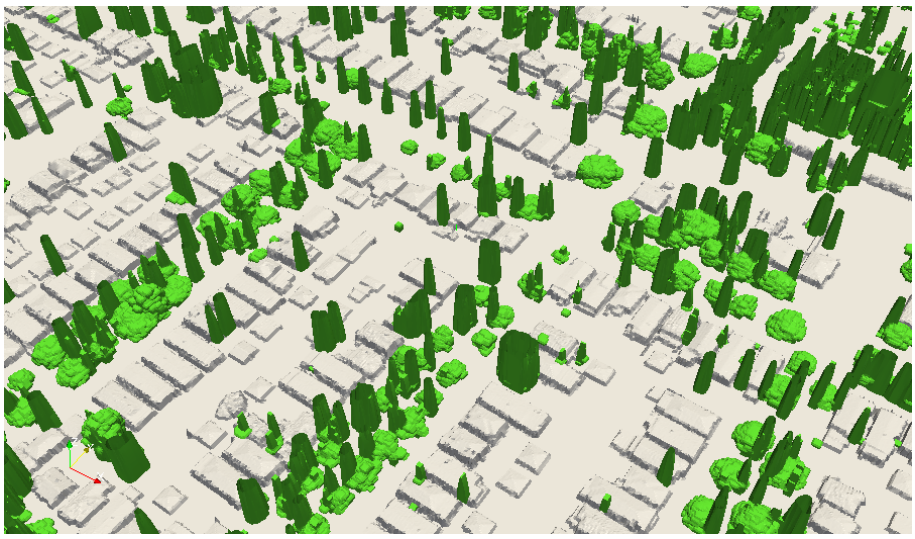

Figure 3.3: Extract of the model domain; visualized here is the triangulation of the buildings (grey) and the isosurface of leaf area density LAD = 0.002 m^2/m^3. This low LAD value approximates the outermost layer of the foliage cover in most cases.

As it has been stated earlier in this report, the average building height in Vancouver Sunset is low. In this type of residential area, only one to two storey houses are encountered. An

exception is a higher commercial building to the east of the tower. This building was excluded from the modelling subset in order to avoid the formation of a large detaching wake. Following the EPiCC report, the mean building roof height for a 500 m radius around the tower is 5.13 +/- 1.85 m. For the model subset situated South West of the tower, the mean building height was computed from the 'building height' grid by averaging the elevation of all points for which $z > 0$. This yielded $h = 4.97$ m, which is close to the value from the EPiCC report that covers an area three times larger. **The mean built obstacle height (= 'canopy height') for scaling purposes in the model results and in the tower data is taken to be $h =$ 5.0 m.** Obviously, this 'mean obstacle height' does not include trees, making it useful for a dimensionless comparison of vertical profiles between modelling results with vs. without trees.

The building plan area fraction λ_b and the plan area fractions of impervious ground surfaces λ_I are 29 % and 37 % respectively. The building plan area fraction computed for the modelling subset is $\lambda_b(Model) = 30.0$ % (38) .

Table 3.2: Modelling area statistics

Domain Property	Value	Source
Mean building height h	4.97 m	Computed from LiDAR data
Plan area fraction of buildings, λ_b	30.0 %	Computed from LiDAR data
Plan area fraction of vegetation, λ_v	11.44 %	Computed from LiDAR data
Nb. of deciduous trees	14.76 stems/ha	EPiCC tech report, (22)
Nb. of coniferous trees	4.44 stems/ha	EPiCC tech report, (22)
Average LAI, over all cells (summer)	0.39	EPiCC tech report, (22)
Average LAI, over all cells (winter)	0.044	Computed from LiDAR data

3.3.1 Building geometry

The Digital Elevation Model (DEM) of the buildings and trees used as a model input is the result of the Light Detection and Ranging (LiDAR) point cloud dataset originating from a measurement campaign in February 2014 with a total flying time of 7 hours, including large parts of the city of Vancouver. The dataset was processed by Dr. Rory Tooke from the Department of Forestry at University of British Columbia (3). The point cloud has a density of at least 20 pts/m^2, reaching up to 100 pts/m^2 in places. For this LES simulation, only the pure building DEM after removal of the underlying topography and after removal of vegetation was used. The DEM of the buildings was triangulated using a Delaunay triangulation with Matlab (extract of the code: see Annex section 9.1.3). No filtering of the building geometry was required.

3.3.2 Vegetation

Informations about tree resp. bush location and density were extracted from the high precision LiDAR dataset by Dr. Rory Tooke from UBC (3). Within a Cartesian grid, presence or absence of trees was determined for each cell using an extraction algorithm based on the number of returns from the LiDAR beam. Locations with two or more reflections, resulting in two or more

returns, were considered as vegetation. Line features such as powerlines or reflections from house walls causing more than one return were treated as an exception in order not to count them as vegetation.

Leaf Area Density

The main goal in implementing vegetation was to determine a height dependent form drag force for each vegetation cell of the domain. Therefore, a measure for height dependent vegetation density had to be considered: A LiDAR beam interception probability representing probability of foliage at a given height was computed from the LiDAR returns for each cell. The Weibull probability distribution with its two parameters k ('shape') and λ ('scale') was fitted to the vertical profile of interception probability.

$$pFoliage(x; \lambda, k) = k/\lambda(x/\lambda)^{k-1} e^{-(x/\lambda)^k} for\ x \geq 0 \tag{3.4}$$

Leaf area density a(z) at a given height, in $[m^2/m^3]$:

$$a(z) = -\ln(1 - pFoliage(z)) \tag{3.5}$$

The function executing the computation and quality adjustments of the 3D-tensor containing the LAD for each grid cell at different heights is shown in Annex section 9.1.4.

The LAD is measured 'top town' and thus represents the leaf area projected onto a horizontal surface. We assumed a random orientation of leaves in space. Therefore, the vertically measured LAD is considered to be as well representative for the leaf density in the horizontal direction and for the horizontal drag force induced by vegetation elements.

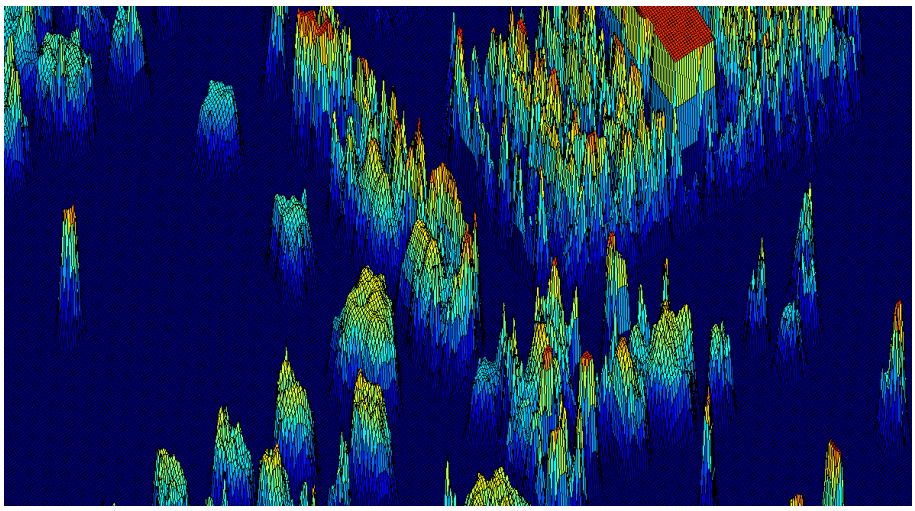

Figure 3.4: Extract of a surface plot of the scale parameter λ west of the research tower

Leaf area density was computed for each cell at discrete heights z ranging from 0 to 30 m, at 1.0 m intervals, by evaluating the Weibull probability distribution function for each 0.5 $\times$ 0.5 m cell of the modelling domain. Thereafter, a two-dimensional convolution filter had to be applied in the horizontal for each height.

Behaviour of the Weibull PDF The frequency of occurrence of Leaf Area Density values at different heights was examined in order to determine if the data were consistent and to detect heights with a frequent occurrence of extreme values (i.e. outliers). A 3D plot of the PDF of the LAD in dependence of height is displayed in figure 3.5.

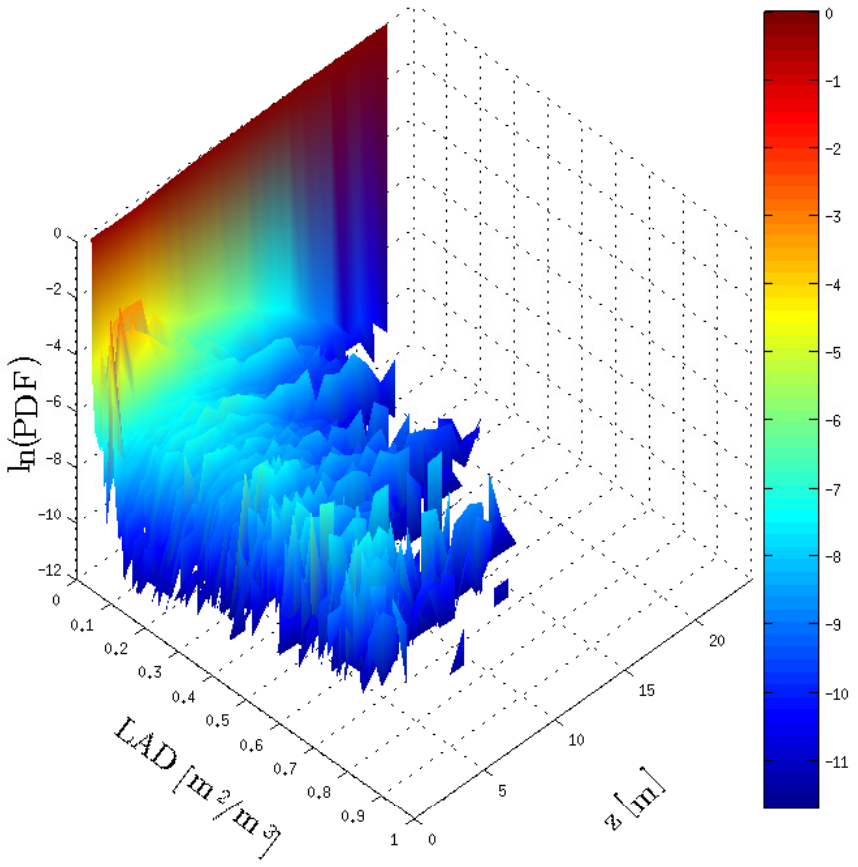

Figure 3.5: Surface plot of the height dependence of the LAD coefficient.

Vertical filtering of LAD Sharp spikes were observed frequently in the distributions computed from the data. In part, they may be due to localized misclassifications of house roofs as trees near a height of 5 m, resulting in an overestimation of LAD between 4.5 and 6 m height. The low variance of some of the generated Weibull distributions, would lead to aliasing effects if raw sampled at the LES resolution, given that the Nyquist frequency of the LES is much lower than that necessary to fully describe the desired Weibull distribution. To avoid such aliasing effects we performed a 1-dimensional (z) low pass filtering of the generated Weibull distributions. The following procedure was adopted:

1. A Weibull PDF was computed from the given parameter set at a high resolution of $dz = 0.1$ m

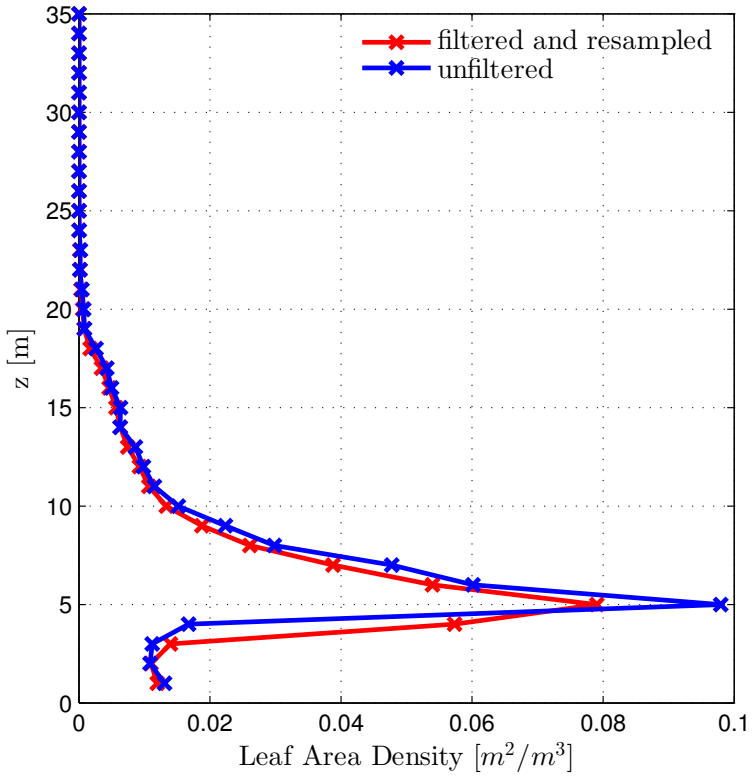

Figure 3.6: 'Typical tree': vertical profile of LAD, averaged over all tree cells. Displayed is the unfiltered versus the filtered profile.

2. This Weibull PDF was filtered with a top-hat running average filter (1D convolution) with a 2 m support.
3. The resulting PDF was again subsampled at a lower resolution of $dz = 1$ m (corresponding to 1/2 of the support length, thus fulfilling the Nyquist-Shannon condition for obtaining a unique signal)

The matlab function that does this filtering and resampling is shown in Annex section 9.1.5.

The 'typical tree' After applying the above described filtering and re-sampling, the vertical profile of Leaf Area Density, averaged for all cells of the modelling domain that contain trees, is designated as the 'typical tree' of our modelling domain. The profile before and after filtering is visualized in figure 3.6. Unfortunately, this step of vertical filtering was added at a later stage of this work and results from running the LES model using the vertically filtered LAD are not presented in this work. Nevertheless, horizontal (2D) filtering was included and is described in the paragraph below.

Horizontal filtering of LAD Once the spikes occurring in the vertical LAD profiles were smoothed, the resulting 3D tensor (of dimensions 512 × 512 × 35 m) was filtered in the horizontal in order to avoid abrupt changes in LAD. Such sudden variations would possibly result in

local oscillations of the wind speed. A 2D convolution was used for this. The Matlab function *conv2D* was used for the numerical computation of the convolution. The input matrix was convoluted with a quadratic matrix for which the number of elements in each dimension were defined by the length of the support (supp) and with all cell values equal to $1/\text{supp}^2$ in order to conserve the total power of the signal. This resulted in a matrix of dimensions $2 \cdot nx \times 2 \cdot ny$, where nx and ny are the dimensions of the input matrix before convolution. The filtering result is the central nx × ny of this resulting matrix.

Drag Force

The pressure drag force exerted on trees by the wind is proportional to the squared wind velocity at a given height z and a form drag parameter C_d, which depends on leaf density. The subsequent derivation follows Thom (36).

The variable a(z) is the sum of projected areas of leaf elements per unit area at height z, on a plane normal to the flow. The leaf area index is obtained by integrating a(z) over height:

$$S_d = \int_0^z a(z)dz, \tag{3.6}$$

The drag force per element (1 m^2) induced by vegetation at a given elevation z is

$$F(z) = \rho C_d(z) u(z)^2 \tag{3.7}$$

The height-dependent drag coefficient $C_d(z)$ can be expressed as a function of the mean drag coefficient $(C_d)_m$ and the leaf area density, which yields

$$F(z) = \rho (C_d)_m a(z) u(z)^2 \tag{3.8}$$

The mean drag coefficient can be obtained from

$$(C_d)_m = \tau_0 / (\rho u_m^2 S_d) \tag{3.9}$$

where the shear stress is

$$\tau_0 = \rho u_*^2 \tag{3.10}$$

and the squared mean velocity is

$$u_m^2 = \int_0^h u(z)^2 a(z) dz \tag{3.11}$$

As the bottom shear stress τ_0 varies significantly in space and the drag coefficient could only be determined iteratively starting from this variable, a spatially constant drag coefficient of $C_d = 0.2$ was applied. This value was used by Krayenhoff et al. (20) for the implementation of drag in their RANS model. While C_d ranges between 0.15 and 0.3 for forest foliage, the value of 0.2

has been found by Katul (17) to be optimal for model implementation. Other values found in literature range from 0.165 ((21), for momentum transport in a forest canopy) to 0.3 (24), which is a relatively high value because no account was taken for sheltering effects. Endalew et al. (10) confirm a leaves-on value of $C_d = 0.2$ with a highly resolved modelling and experimental study of drag on tree branches and leaves, but they obtain $C_d = 0.15$ for leafless trees.

C_d depends on velocity because deformation of the tree crown, bending and shaking of branches and leaves result in a lower overall roughness. Koizumi et al. (18) and Mayhead (26) found in field tests resp. in wind tunnel experiments that C_d decreases with increasing wind speed. But Koizumi et al. show in their field tests that C_d remains nearly constant for wind speeds above 10 m/s. This and the narrow range of wind speeds between 5 and 12 m/s occurring within our LES model at the level of the tree crowns justify the use of a constant drag coefficient.

Due to the small-scale wake and shear production, causing more TKE to be produced and thus more MKE to be consumed, the drag force occurring on a tree may be bigger than for a solid sphere.

3.4 Tower measurements

Data from the Urban Climate Research Tower of UBC was kindly provided by Prof. Andreas Christen of the Micrometeorology research group at the Department of Geography at UBC. The raw data used for this study involves wind speed (u,v,w) and temperature measurements between 1.1.2008 and 22.3.2014, sampled at a frequency of 20 Hz. This data was averaged over 1 minute intervals in order to obtain first to third order moments of the data and in order to compute wind directions over meaningful time intervals for conditional sampling, as will be explained below.

The Research tower is a 30 m high triangular lattice tower situated 5 m from the south-eastern corner of the Mainwaring power substation of B.C. Hydro. The domain of the substation is of rectancular shape, surrounded by dense hedges and trees and extends over 100 m in the west-east direction and over 130 m in the south-north direction. The measurements were made at a height of 28.8 m above local ground. Because the local ground at the substation is shifted vertically downward by 4 m as compared to the surrounding ground, the effective measurement height of the sensor is $z_{sensor} = 24.8m$ (6).

3.4.1 Instruments

The wind and temperature measurements were made with *CSAT 3*, a 3-axis anemometer-thermometer with an internal sampling rate of 60 Hz produced by Campbell Scientific, Logan, UT, USA. Its internal coordinate system is right-handed, where the u+ axis was pointing towards geographic North, the v+ axis towards geographic West and the w+ axis pointing vertically upward (4). An image of the measurement device can be found in the Annex, section 9.3.2.

Figure 3.7: The 30 m high (effective height 26 m) Urban Climate Measurement Tower at the South East corner of the B.C. Hydro Mainwaring Substation at the Vancouver Sunset site. The tower belongs to the Micrometeorology group at UBC. Image by the author.

3.4.2 Data reading

We analyzed a large amount of tower data; the 6.25 years of continuous measurements at a frequency of 20 Hz result in 160 GB of data. According to the norm for the processing of this type of high-frequency measurements, the data was read file-by-file and 1-minute averages were computed within each 30-minutes file, before the high frequency data was again deleted from the temporary memory in order to free space. For each 1-minute mean, the index of the corresponding file name and the number of the minute for which it was computed were saved. As the data is saved in the "binary TOB1 file format" by Campbell Scientific, the number of bytes and the type of binary format had to be determined for each record field (i.e. each data column) and the code had to be provided with this information. With the Matlab function *fread*, each file was read line by line.

3.4.3 Quality control and outlier removal

The data recorded at 20 Hz was controlled for outliers and spikes following the criteria used in the EPiCC Technical Report 1 on Processing and Quality control of turbulent flux measurements during the Vancouver EPiCC experiment (7). First to fourth order Statistics were computed for the raw data of each 30-minutes data file and compared to the quality criteria. For each data file a 'quality flag' was added, taking a value of 1 if the quality criteria were met and a value of 0 if not. The criteria imply the thresholds for absolute values, spikes and statistics, presented in table 3.3.

3.5 Data processing

In order to be able to validate the modelling results with in situ point measurements at the tower, data had to be sampled to retain only the periods during which recorded wind direction

Table 3.3: Quality control thresholds used for high frequency tower data, adapted from (7)

	u [m/s]	v [m/s]	w [m/s]	T [° C]
Absolute thresholds (min/max, physically based)	+/-30	+/-30	+/-30	-20/+40
Spike threshold	6	6	6	6
Standard deviation (min/max)	0.05 / 4.0	0.05 / 4.0	0.02 / 1.5	0.01 / 2.0
Skewness (min/max)	-3.0 / 3.0	-3.0 / 3.0	-2.0 / 2.0	-2.5 / 2.5
Kurtosis (min/max)	-2.0 / 5.0	-2.0 / 5.0	-2.0 / 15.0	-2.0 / 15.0

at the tower matches the imposed wind direction in the LES model and during which the atmosphere is neutrally stratified.

3.5.1 Dimensional analysis and averaging

A dimensional analysis of the modelling area was conducted in order to determine the appropriate durations of filtering time intervals for different spatial scales. In the following, the procedure is described and values for two different spatial scales are presented.

Starting from a spatial scale of interest (e.g. tower height) and looking at the maximum observed wind velocity, a characteristic turbulence time scale can be determined:

$$T = \frac{L}{v_{max}} \tag{3.12}$$

The expectation of the mean velocity is approximated in the following way:

$$E(\overline{u}) \propto 50T \tag{3.13}$$

where the factor 50 is a standard value. This means that the minimum length of the time interval for the scale of interest is $50T$, in order to obtain a good estimate for the expected value.

Values for two spatial scales

Tower scale ('small scale') This scale considers the length scale of the measurement tower in sunset area, with a sensor elevation above ground of 24.8 m. Thus L $\simeq$ 24 m. The maximum observed wind speeds had a magnitude of 24 m/s, resulting in $T = 1$ s and $50 \cdot T = 50$ s. Consequently, **1 minute** was chosen to be an appropriate averaging time interval for this spatial scale. However, this reasoning assumes that there is only mechanical turbulence. Turbulence generated by thermals may cause significantly longer time scales. Because the data will be conditionally sampled for neutral conditions later on in this work, the value of 1 minute can be accepted as a first estimation.

Table 3.4: Symbols adopted for the variables wind direction, wind speed and Richardson number in the conditional sampling process

Variable	**1 min**-mean	**20 min**-mean	$\lvert\sigma\rvert$ among 1 min-means within 20 min
Wind direction	Dir_1	Dir_{20}	$\sigma(Dir_1)_{20}$
Wind speed (magn.)	$Magn_1$	$Magn_{20}$	$\sigma(Magn_1)_{20}$
Richardson number	Ri_1	Ri_{20}	$\sigma(Ri_1)_{20}$

Modelling scale ('large scale') The length scale was chosen to be of the order of the model dimensions: $L = 500$ m. Considering again a maximum observed wind speed of 24 m/s, this results in $T \simeq 20$ s and $50T \simeq 17.5$ minutes. An averaging interval of **20 minutes** was chosen to be appropriate for this scale.

3.5.2 Conditional sampling

Tower data for wind speed and temperature, measured at 20 Hz over a period of 6.25 years, was read piecewise into Matlab and, corresponding to a 'small' and to a 'large' spatial scale, 1-minute averages and 20-minutes averages were computed for each variable u, v, w and T. For these averages, the horizontal wind direction was computed by taking the tangent of the wind components u and v. Subsequently, data was sampled to retain only the periods during which the wind direction was within +/- 10 degrees of the model wind direction. Data was considered for the 'leaves on' period, corresponding to the summer months June through September as well as for the 'leaves off' period corresponding to the winter months December through March. The following sampling procedure is similar to the one employed in (5). Additional knowledge on sampling in the case of the Vancouver tower was provided by Prof. Andreas Christen.

In this section and further on, the symbols defined in table 3.5.2 are used.

Sampling method (a) Sampling method (a) differs from sampling method (b) in the way data is selected for wind direction: Instead of sampling Dir_{20} for the desired wind direction interval (i.e. 180 +/- 10 °) and then choosing intervals with low standard deviation, method (a) samples Dir_1 for a given wind direction interval and then looks for sequences of Dir_1, where Dir_1 remains within the wind direction interval for 20 minutes. Once these 20 minutes intervals are selected, this sampling method proceeds identically to sampling method (b), as described below.

Sampling method (b) The result of the sampling is the extraction of several 20 minutes intervals fulfilling the following requirements:

- recorded wind within +/- 10° of model wind direction South (180°)
- 20 min - average neutral atmosphere: -0.05 $< Ri_{20} <$ 0.05
- low standard deviations of wind direction and Richardson number among 1 minute periods within the selected 20 minutes intervals

- wind speeds between 2 and 12 m/s

In order to obtain the final 20 minutes intervals, the following steps were applied to the data :

1. **Compute 1 min averages** Averages were computed for u,v,w,T as well as for the fluxes $\overline{u'w'}$, $\overline{v'w'}$ and $\overline{w'T'}$.
2. **Sample wind directions** Wind directions were sampled as 20° intervals centered at the model wind direction
3. **Standard deviation of wind direction** For all 20 minutes intervals with sampled wind directions the standard deviations of wind direction among 1 minute intervals was computed. Only intervals with standard deviations $|\sigma| < 15°$ were selected.
4. **Atmospheric stability** The flux Richardson number was computed for each of the above selected 20 minutes intervals. As a simplification, only the subscripts 1 and 3 (corresponding to the velocity components u and w) were considered in the definition of Ri, leading to the following expression for Ri:

$$Ri \simeq \frac{\frac{g}{\overline{\theta}}\overline{w'\theta'}}{\overline{u'w'}\frac{\partial \overline{u}}{\partial z}} \tag{3.14}$$

   Only intervals with 0.05 > Ri_{20} > -0.05 were retained. For these remaining intervals, Ri was computed for each minute (i.e. Ri_1) in order to compare $\sigma(Ri_1)$ between 20 minutes intervals.
5. **Visual comparison** Now, $\sigma(Ri_1)$, $\sigma(Dir_1)$ as well as 1 minute values of Ri (denoted as Ri_1) were examined visually and only the 20 minutes intervals with acceptable appearance were retained.
6. **Wind speeds** The neutral periods with desired wind direction and low standard deviations were conditionally sampled to retain only the 20 minutes intervals with average wind speed (i.e. magnitude) between 2 and 12 m/s.

The conditional sampling, combining methods (a) and (b), resulted in 102 selected intervals of 20 minutes for the summer months June through September of the years 2010 through 2013 which were used for the validation of the LES model results.

3.6 Validation of modelling results: spectra

Validating modelling results covering a domain of 512 × 512 × 128 m at two meters resolution with single-point data is difficult. It has to be accomplished in a way that the validation is meaningful in spite of having only a single measurement point. An advantage in the present case is the fact that the tower measurements are available for a relatively long continuous time period of 6.25 years, allowing to find atmospheric conditions very similar to those simulated by the LES. To compare data series at a single point in space, the most powerful tool are time spectra. The following properties of the spectra have to be verified and compared:

- Slopes of the inertial subrange and of the production range
- Frequency observed at the slope change
- Occurrence of peaks, indicating coherent structures in the flow field

3.7 Canopy properties

Over urban canopies, the friction velocity is difficult to determine because one cannot simply consider the velocities resp. covariances over a homogeneous rough surface. Instead, the urban geometry is composed of rough surfaces such as surfaces of houses, bushes and streets at small scales. The geometry of street canyons and individual objects can be viewed as a large 'rough surface' at domain size scale, with the entire street canyon depth being analogous to the grain size of a gravel bed in a river channel or the grass length on a pasture. Therefore it becomes difficult to determine the height at which to sample the 'surface velocity' u_s. These considerations lead to the concept of a 'displacement height' d , the height of an imaginary 'surface' near the top of the canopy height. In order to compute the friction velocity from the modeling results, the space-averaged value of $\overline{u'w'}$ and $\overline{v'w'}$ at z = d can be used:

$$u_* = [\overline{u'w'_{xy}(z=d)}^2 + \overline{v'w'_{xy}(z=d)}^2]^{1/4} \tag{3.15}$$

Another option is to use the maximum value of the xy-average of these covariances encountered over the entire modelling depth:

$$u_* = max([\overline{u'w'_{xy}(z)}^2 + \overline{v'w'_{xy}(z)}^2]^{1/4}) \tag{3.16}$$

To be physically consistent, this value has to be equal to the resulting friction velocity due to the imposed pressure gradient in the LES model. In a hypothetical case of 'zero friction' inside the model, the pressure gradient would be equal to the friction velocity.

3.7.1 Displacement height d

The displacement height d can be determined in various ways. One possibiliy is to examine a scaled velocity profile in a semilogarithmic plot: ln(z-d) is plotted repeatedly versus u(z-d) for different values of d until the linear part of this vertical profile starts at z - d = h, thus at the mean building height. This calibration may be applied to different locations in the xy-plane as well as to the space averaged profile.

Other methods are (1) the 'rule of thumb' that estimates $d = 0.7h$ (assuming a triangular distribution of pressure force on buildings),(2) the comparison of the imposed friction velocity to the friction velocity computed from the flow field, (3) the computation of the barycenter of pressure force on a building and (4) morphometric parameterizations (see below). Methods (1) through (3) are described directly in the Results, section 4.5.2.

Morphometric parameterization

A morphometric displacement height for our modelling subset in Vancouver Sunset area can be computed with the method of Bottema (1995), documented in (12):

$$\frac{d}{\overline{h}} = (\frac{\sum A_{rb} + \sum (1-p)A_{rt}}{A_T})^{0.6} \tag{3.17}$$

,

where A_{rb} is the area of buildings, A_{rt} is the area of trees, A_T is the total area of the subset, and p is the porosity of trees. For p a value of 0.2 is usually adopted for summer months. The mean obstacle height h can be taken as the mean building height or as the weighted average of building and tree heights.

3.7.2 Aerodynamic roughness length z_0

Once d has been found, z_0 can be determined by considering the 'log-layer', the portion of the vertical velocity profile where the velocity increases logarithmically with height. A linear fit is applied to the log-layer found in the semilogarithmic plot. The intersection of this linear fit with the z-axis, i.e. with $u(z-d)/u_* = 0$, yields z_0. The corresponding law reads

$$\frac{u(z)}{u_*} = \frac{1}{\kappa} \ln(\frac{z-d}{z_0}) \tag{3.18}$$

The code that performs the fit and displays the fitting result is shown in section 9.1.6 in the annex.

A recursive check to ensure the proper functioning of the fitting algorithm was performed. A logarithmic velocity profile was computed for typical values of z, z_0, h and d and a linear fit applied. The value of z_0 resulting from this fit had to match exactly the input value of z_0 used for the computation of the logarithmic velocity profile. Such a test is presented in figure 3.9.

Anemometric parameterization

An example for an anemometric parameterization from high frequency measurements is the eddy correlation stress method (Es method) assessed in (12):

$$z_0 = (z_{sensor} - d) \cdot \exp(-\frac{\bar{u}_z \cdot \kappa}{u_*}) \tag{3.19}$$

where z_{sensor} and κ are known, d is estimated and $\bar{u}_z$ as well as u_* are computed from high frequency tower measurements resp. from LES model results.

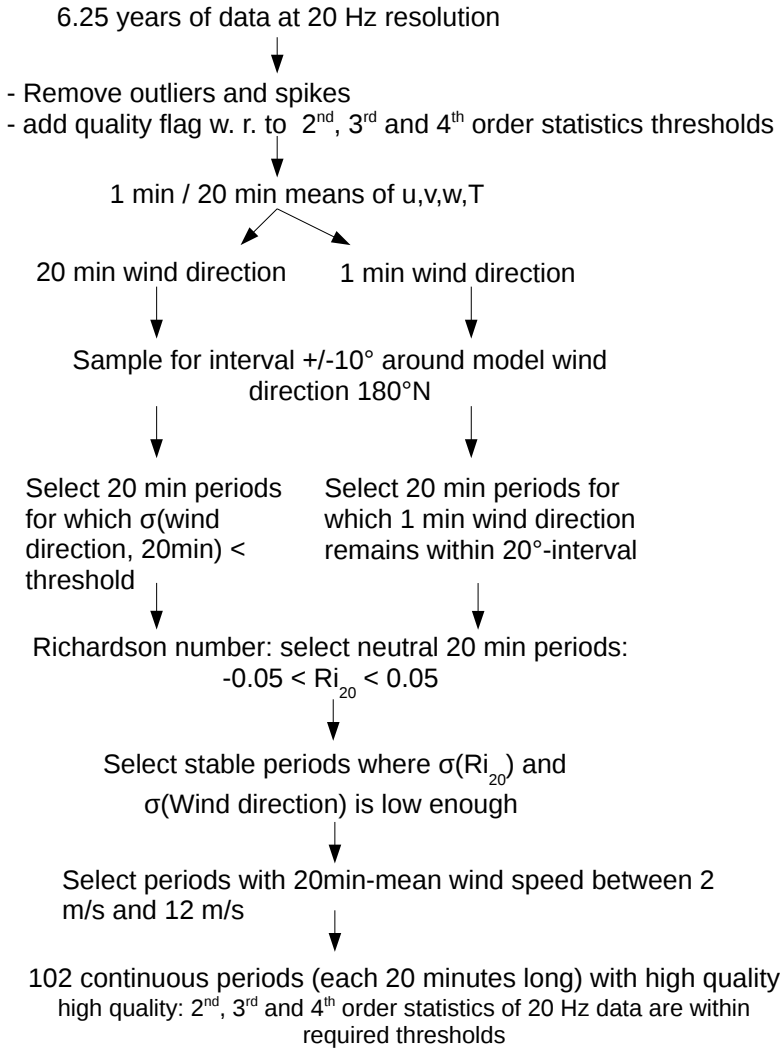

Figure 3.8: Scheme of the sampling procedure applied to tower data

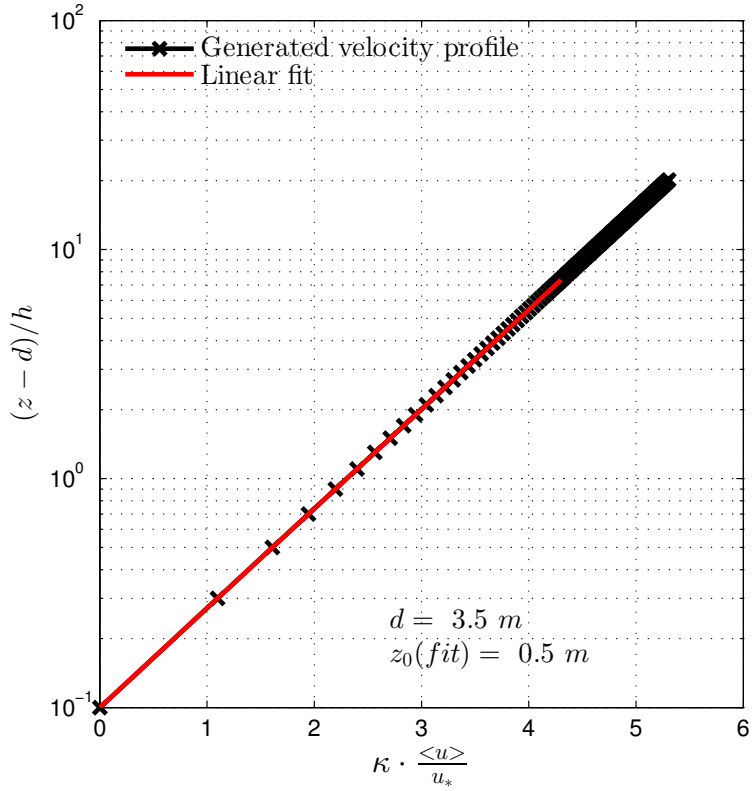

Figure 3.9: Result of a test of the fitting algorithm to a logarithmic velocity profile. $u(z)/u_* = 1/\kappa \cdot ln(z/z_0)$ was computed starting from $z = z_0 : 1.0 : 100\ m$, $z_0 = 0.5m$, $u_* = 0.9m/s$, $\kappa = 0.41$, and $h = 5m$.

4. Results and Discussion

4.1 Tower data sampling

In the following, statistics and results from the conditional sampling of the UBC climate research tower data are presented.

4.1.1 Mean wind and temperature characteristics

Wind

The wind roses in Figure 4.1 show 1 minute averaged wind direction for the four years' measurement period 2010 - 2013 at the Sunset tower. Out of the total 6.25 years of measurements, only this four years' period was considered because (a) there are more period with missing data in the years 2008-2009 and it was problematic to read all this data, (b) the amount of data is largely enough for statistical relevance and for validating modelling results and (c) because this way it can be compared more directly to (6). The wind roses in figure 4.1 look identical to the wind roses published in (6) who worked with measurements of the very same tower and thus serve as a check for the correct computation of the wind directions and the right usage of the data.

The most frequent wind directions in the Vancouver Sunset area are North East over East to South East as well as, although with rarer occurrence, South West. The latter wind sector is prevailing during summer months, while winter months are dominated by North Eastern to Eastern winds coming down from the valleys of the coast mountains. Also, Eastern winds are dominant during the night (= land breeze) and South Western winds during the day (= sea breeze). Data for all seasons was processed and analyzed, whereas only the data for the summer months June through September, during which all deciduous trees carry leaves, was used for the validation of the modelling results since the simulations were done for 'leaves on' conditions.

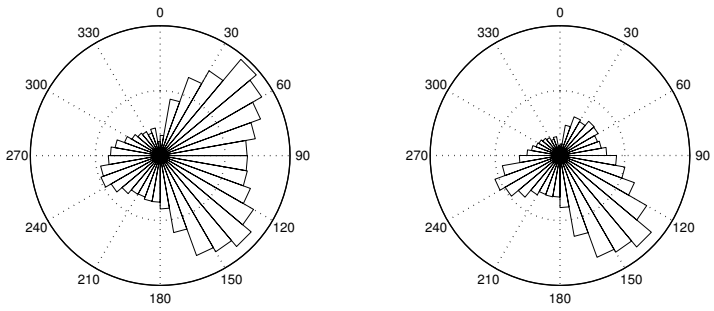

Figure 4.1: Wind roses of Vancouver Sunset tower data for the years 2010 through 2013 are displayed. Wind directions are in degrees North and indicate where the wind is blowing **from**. **(a) is for all months** and **(b) for 'leaves on' months only**, i.e. June through September. For the comparison to the model results, only the 'leaves on' period (summer) was used because the simulation was done for 'leaves on' conditions.

Mean daily evolution in summer

Figure 4.2 and figure 4.3 show the mean daily evolution of key variables averaged over 1 minute intervals at the Sunset Tower during the summer ('leaves on') months June through September. Wind speeds rise in the course of the morning and are followed by a temperature increase. The wind direction changes from South West to South-east simultaneously to an increase in wind speed. As expected, all variables show a sinusoidal day-night cycle.

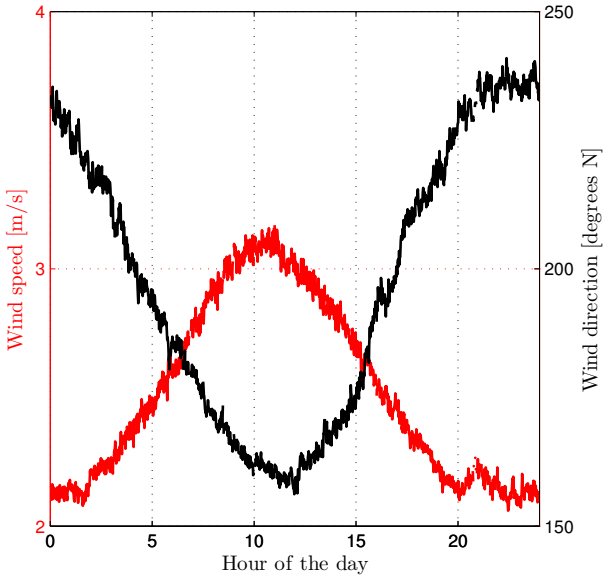

Figure 4.2: Mean evolution of wind speed (i.e. magnitude) and wind direction over the course of an ensemble day for the 'leaves on' months June through September during the years 2010 to 2013.

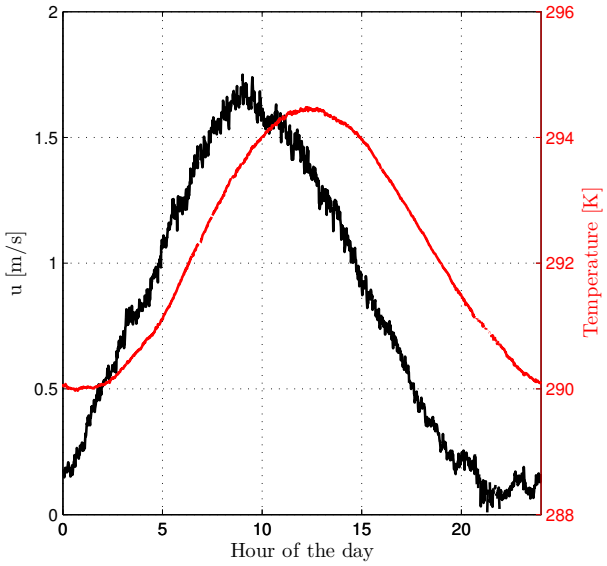

Figure 4.3: Mean evolution of longitudinal wind velocity u and temperature over the course of an ensemble day for the 'leaves on' months June through September during the years 2010 to 2013.

4.1.2 Sampling results

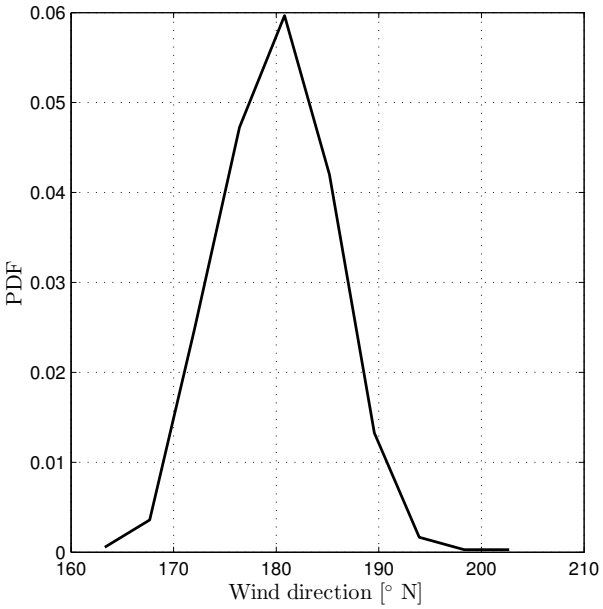

Figure 4.4: PDF of wind direction of 1 minute averages, sampled for periods where 1 minutes-average wind direction remains within an interval of +/-10° of wind direction 180° for 20 minutes, i.e. sampling **method (a)**.

The result of sampling method (a) is depicted in Figure 4.4. After sampling 1 minute averaged wind data for the given wind directions, the sampled data was examined to find 20 minutes periods for which the 1 minute averaged wind direction continuously remains within a 20° interval centred at the sampling wind direction.

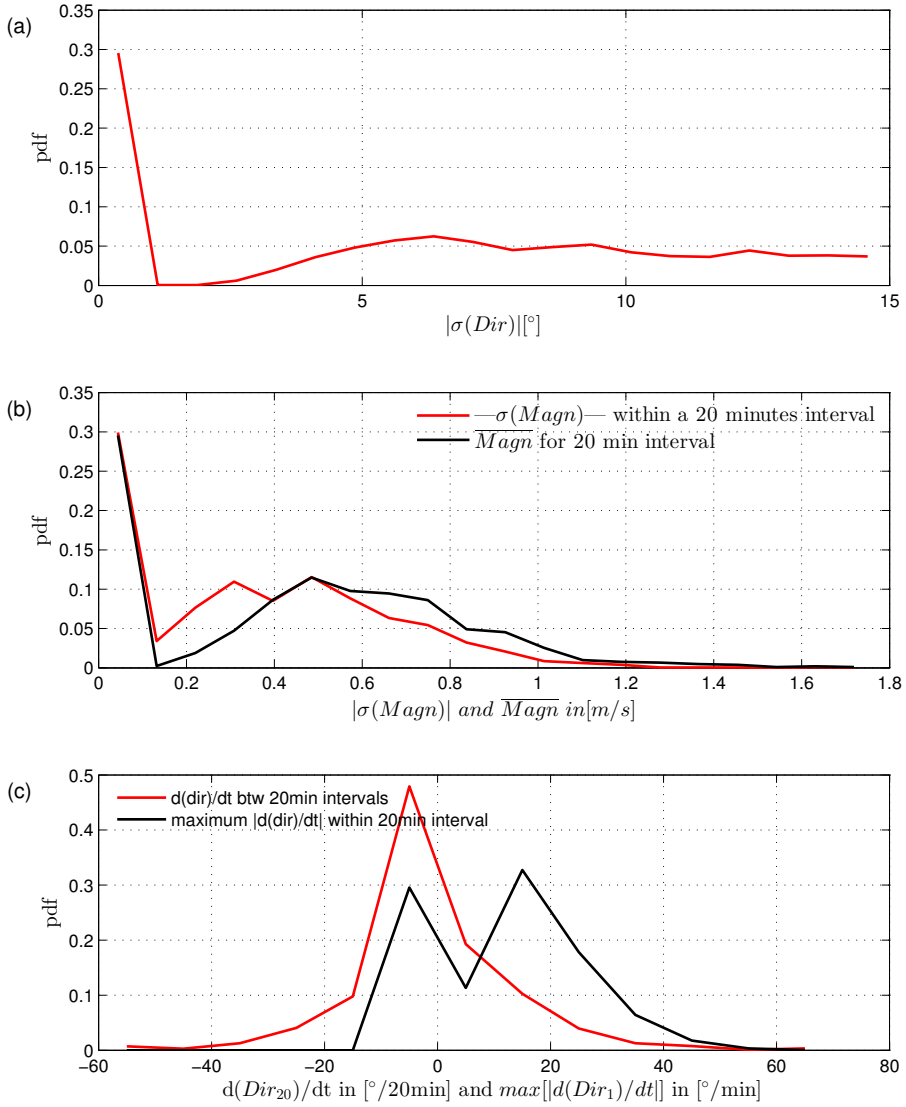

Figure 4.5: PDFs of (a) standard deviations of wind direction and (b) velocity magnitude within 20 minutes periods and of mean velocity magnitude for 20 minutes periods. (c) PDF of change in wind direction between 20 minutes periods and maximum change in 1 minute averaged wind direction within 20 minutes periods. Displayed are PDFs of values sampled for wind direction and low standard deviation of wind direction for 180 +/- 10° during the 'leaves on' period.

A large number of 20 minutes intervals resulting from sampling method (b) can be found: The number of sampled intervals for wind direction South is n = 625. These intervals correspond to periods where the 20 minutes-averaged wind direction is within the sampling interval and

has a low enough standard deviation of wind direction among 1 minute averages within the interval (i.e. $|\sigma(Dir_1)_{20}| < 15°$). Wind velocity magnitudes and their corresponding standard deviations remain relatively low for the sampled periods. Figure 4.5 displays the PDFs of these sampling results.

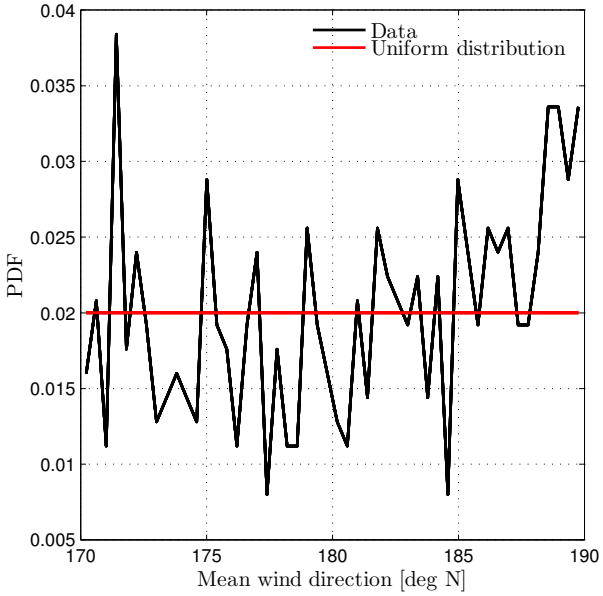

Figure 4.6: PDF of the 20 minutes mean wind direction, sampled with method (b): Periods with model wind direction 180+/-10° and low standard deviation, compared to a uniform distribution law.

Plotting the PDFs of standard deviations of Dir_{20} and of Ri_{20} in Figure 4.8 shows that an important variability of Dir_1 implies as well a high variability of Ri_1. Physically, this makes sense, because a change in wind direction often goes along with a change in wind speed and it implies as well that a different source area (with possibly different temperatures) influences the air masses that reach the sensor. Such a short-term change may occur during the passage of a microfront. It could also be associated with the turning of the diurnal wind system, e.g. when winds turn from sea breeze to land breeze.

The standard deviation of the 1 minute Richardson number within neutral 20 minutes intervals, $|\sigma(Ri_1)_{20}|$, can vary significantly and reach values as high as 10^4 for certain intervals. Such values correspond to outliers in the 1 minute Richardson numbers, Ri_1. All intervals with $|\sigma(Ri_1)_{20}| > 20$ were not used for comparison to modelling results. A certain variability among the 1 minute Richardson numbers can not be avoided if a statistically relevant number of 20 minute intervals has to be selected. This variability, with Ri_1 reaching absolute values of more than unity, can be explained by short term dynamics in the Boundary Layer, termed as microfronts, or by large termals (Prof. Andreas Christen, personal communication). Thermal turbulence has a much larger wavelength than the mechanical turbulence. Physically it does not make sense to compute Richardson numbers over short time intervals such as one minute. Nevertheless, these values can be used as an indicator for variability.

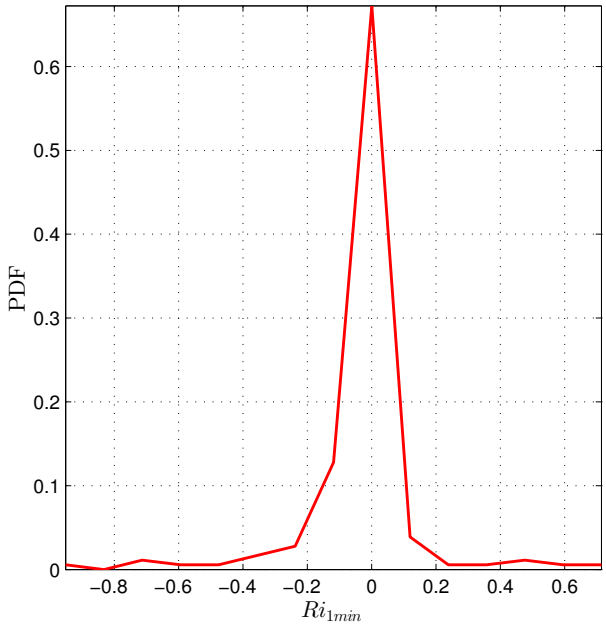

Figure 4.7: PDF of 1-minute Richardson numbers, taken from neutral 20 minutes periods obtained with **method (a)**. The corresponding plot for sampling method (b) is shown in Annex section 9.2.2.

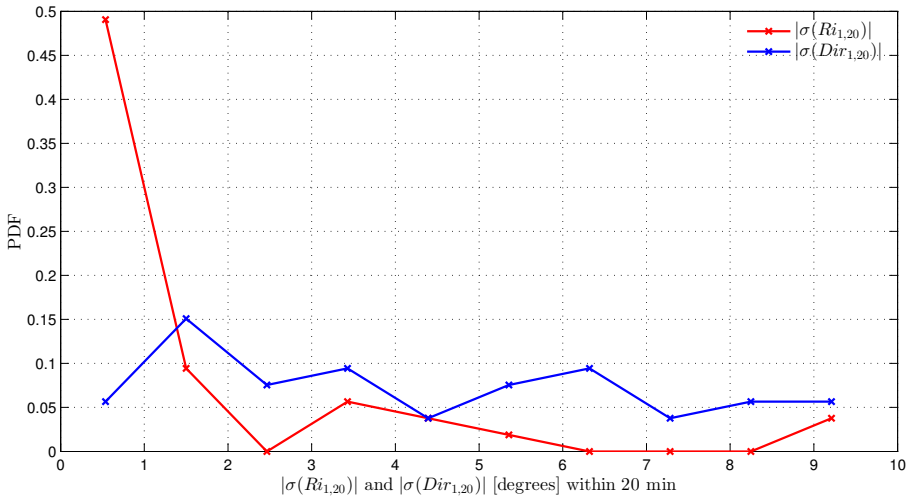

Figure 4.8: Pdf of standard deviations of Richardson numbers and wind directions of periods that are neutral for 20 minutes, from method (b). The standard deviations were computed for variation of 1 minute averages within 20 minutes periods, i.e $|\sigma(Ri_1)_{20}|$ and $|\sigma(Dir_1)_{20}|$. Large outliers of standard deviations have been removed.

Table 4.1: Tower data statistics: 'Overall' denotes the entire data, without sampling. 'Selected' denotes the data that was sampled for wind direction and for a neutral atmosphere.

Period	$\sigma(Dir_1)_{20}$	$\overline{Dir_{20}}$	$\sigma(Magn_1)_{20}$	$\overline{Magn_{20}}$	median of Ri_1
4 years Overall 1'	+/- 91.3 °	214.9 °	+/- 1.71 m/s	2.77 m/s	-
4 Summers Overall 1'	+/-83.9 °	197.4 °	+/-1.24 m/s	2.53 m/s	-
4 Summers **selected** 1'	+/-6.88 °	184.3 °	+/-0.52 m/s	4.37 m/s	-0.0224

4.2 Model validation

4.2.1 Time Spectra

In the following, time spectra at the tower location are compared in terms of their slopes in the inertial subrange and in the production range as well as in terms of the location of slope change. The tower spectra reach a maximum frequency of 10 Hz, while the model spectra end at a frequency of 5 Hz. The first time series field ('ts_1 field') of the model results is sampled at a frequency of 10 Hz, therefore a relevant frequency of $10/2 = 5$ Hz is considered. The tower data was sampled at 60 Hz and averaged to output at 20 Hz by the anemometer, so that a frequency of $20/2 = 10$ Hz can be considered. Only half the maximum sampling frequency is displayed because of the Nyquist-Shannon theorem that states that a signal has to be sampled with more than double the frequency of the signal.

Figure 4.9 shows that both tower data and model results at tower location contain a clearly distinguished inertial subrange with its typical slope of -5/3, according to the equation

$$F(\kappa_1) = \alpha_1 \kappa_1^{-5/3} \epsilon^{2/3} \tag{4.1}$$

where α_1 is the proportionality factor (Kolmogorov constant), κ_1 the wave number and ϵ the dissipation rate. This relationship was first found by Kolmogorov (19) and is well documented in Stull (35), and in Rotach (30).

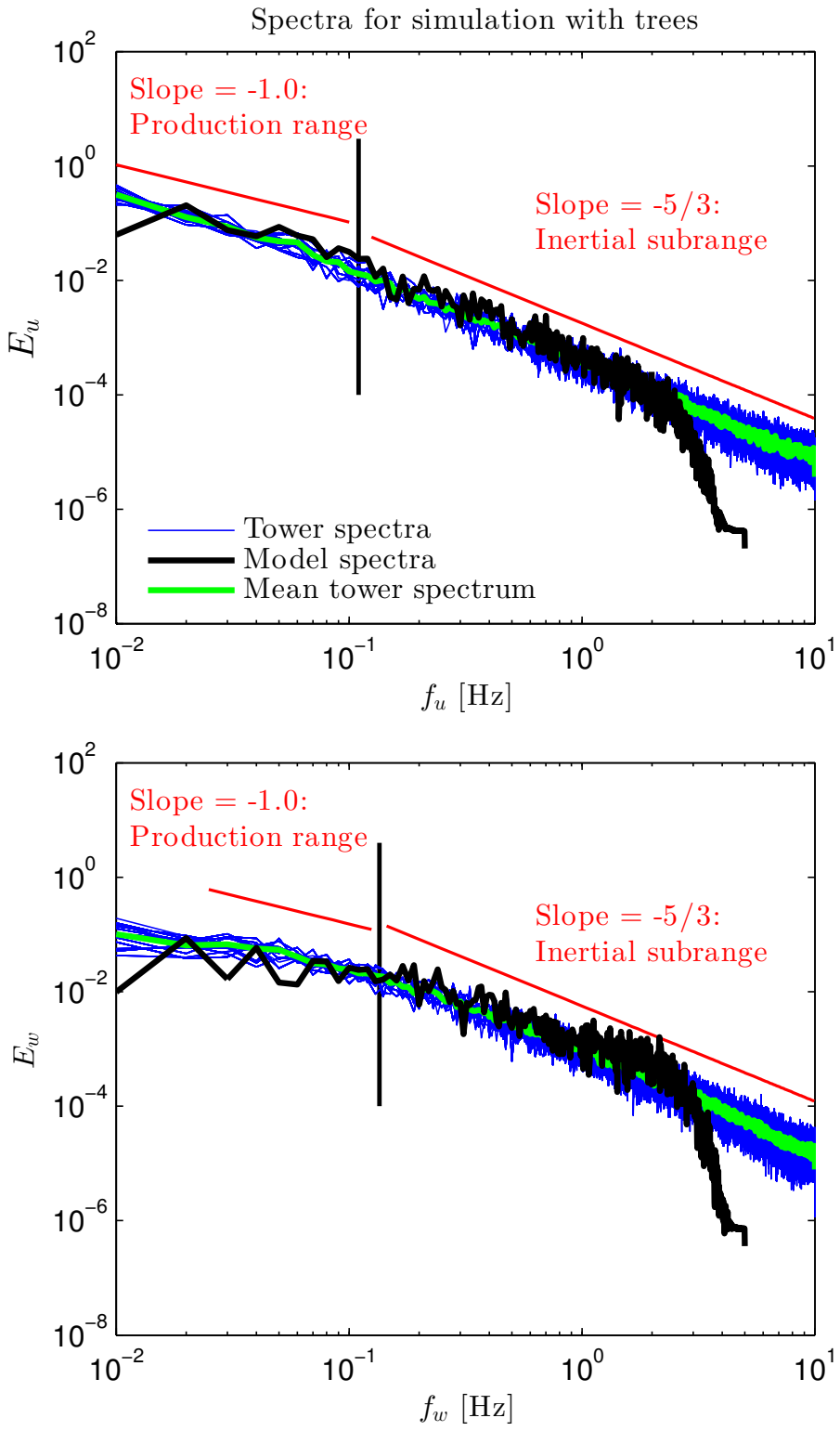

Figure 4.9: Spectra of tower data and model results **including** trees. Model results at tower location (5000 steps at 10 Hz: T = 8.3 min) are compared to spectra from 102 conditionally sampled 20 minutes periods of tower data (each 24000 steps at 20 Hz).

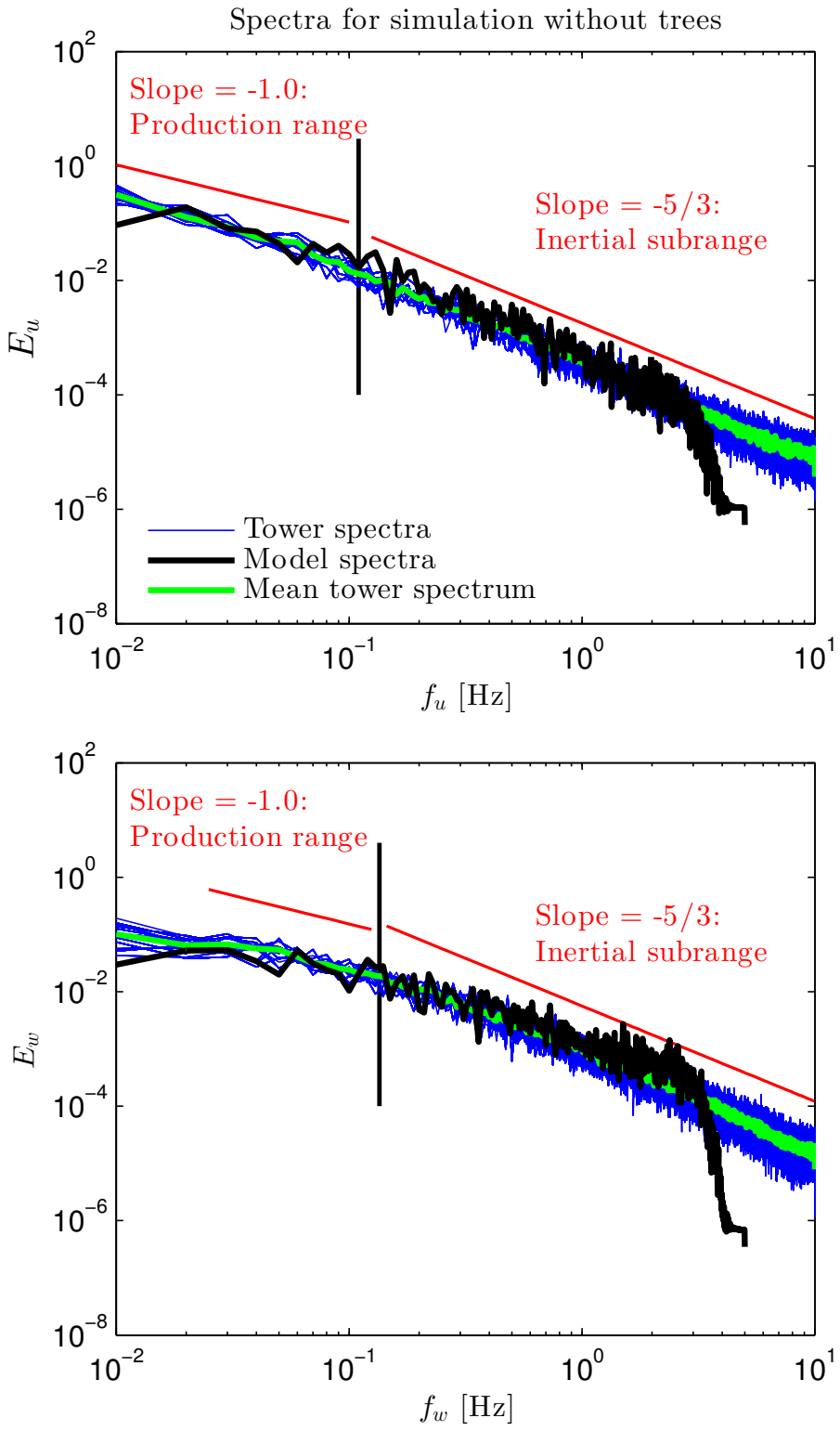

Figure 4.10: Spectra of tower data and model results **without** trees. Model results at tower location (5000 steps at 10 Hz: T = 8.3 min) are compared to spectra from 102 conditionally sampled 20 minutes periods of tower data (each 24000 steps at 20 Hz).

The change between the production range (slope of -1.0) and the inertial subrange (slope of -5/3) is clearly apparent in the tower spectra and also visible in the model spectra. The change in slope occurs at a frequency of approximately 0.11 Hz (for u) resp. 0.135 Hz (for w) for both the tower and the model spectrum, which indicates that the turbulent flow simulated by the LES model matches the flow observed at the tower location well. The spatial scale of this slope change is in the range of 75 - 90 m, for a mean wind velocity of approximately 10 m/s.

The spectra of the model results show a sudden drop in energy at a frequency of 2-4 Hz. This is due to an oversampling occurring at high frequency: The temporal resolution of the model output is limited by the grid spacing and the wind speed. For our LES model runs, grid spacing is δx = 2 m and the maximum wind speed computed by the model at the sensor is $v = 15\,m/s$. The minimum wave length in space resolved by the model is $\lambda_s = 4$ m (two grid cells) and the minimum wave length resolved by the model in time is $\lambda_t = \lambda_s/v = 0.27$ seconds. Thus the maximum frequency in time that is resolved by the model is $f_t = 1/\lambda_t = 3.75\,Hz$. The drop in spectral energy in figure 4.9 starts at 2 Hz and goes on until 4 Hz, which matches very well the computed maximum resolved frequency of 3.75 Hz. (The small part of the model spectrum situated at frequencies higher than 3.75 Hz can be ignored. It consists mainly of 'noise', i.e. random fluctuations of the 'signal' in time.)

4.2.2 Characteristic scales

Dimensional analysis and spectra

Prominent peaks or valleys in the spectra can indicate wake shedding of the flow by obstacles such as houses and trees. The range of velocity frequencies at which large scale coherent structures are to be observed can be narrowed down by considering the model scales: The tower height of the order of 20 m and a mean wind speed of approximately 10 m/s yield λ_s = 2 - 40 m and λ_t = 0.2 - 4 s, but values for λ_t of more than 20 s are possible for lower wind speeds. Therefore, the time frequency range in the velocity spectra within which peaks or valleys that indicate coherent structures can be observed is f_t = 0.25 - 5 Hz, with possible values as low as 1/(20 s) = 0.05 Hz. Significant peaks (and valleys) occur in the model spectrum for u at frequencies of 0.06 to 0.7 Hz and at frequencies of 0.06 to 2 Hz in the model spectrum for w, as seen in figures 4.10 and 4.9. These values are within the range predicted by the dimensional analysis above. However they do not occur in the measured spectrum. The reason is that the measured spectra were sampled at different wind speeds, then normalized by the absolute value of standard deviation of wind speed (but not by the wind speed itself) and averaged. This averaging of peaks at different locations, corresponding to spectra for periods with different wind speeds, leads to a smoothing out of the peaks.

Correlations in time

Plotting the time correlations of the fluctuations about the mean $u' = u - \bar{u}$ for the simulation **without trees** at tower location shows that the maximum time lag for which $\rho > 0$ is between 20 and 30 seconds for heights between 4.5 and 24.5 m, as displayed in figure 4.11. This is a much longer time scale than assumed above and it is probably due to both lower flow velocities and larger spatial dimensions of big eddies. Nevertheless, correlations are only significant (i.e.

bigger than 0.5) for time lags smaller than 3 s, supporting very well the values suggested by the dimensional analysis made above, which found a maximum $\lambda_t = 4$ s. Secondary peaks appearing for lags of 13 s and 28 s at 9.5 m height resp. for a lag of 40 s at 24.5 m height indicate that oscillating wakes at 'large' scale are present, possibly emerging from obstacles such as houses upstream in the flow.

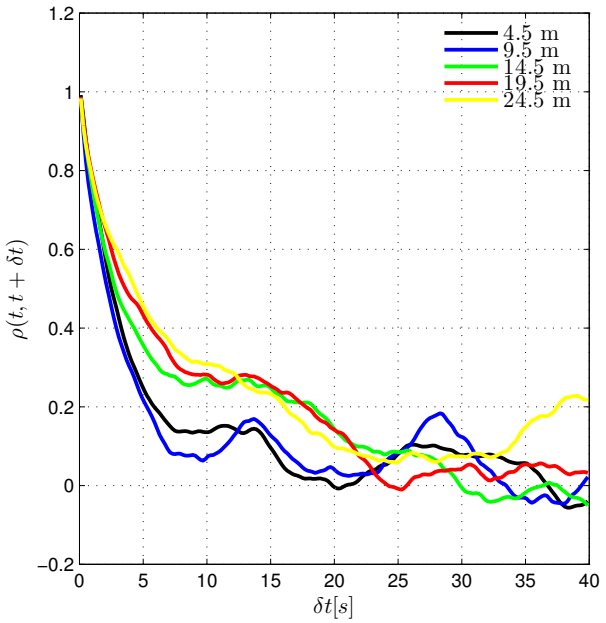

Figure 4.11: Correlations of fluctuations of streamwise velocity in time $\rho_{u'}(z; t, t + \delta t)$ at tower location, for different lags and different heights for the simulation **without trees**.

Considering the same plot of correlations for changing lag at tower location, but now for a simulation with trees, reveals that generally correlations remain higher for a given lag if trees are added. This effect is especially true for the heights 14.5, 19.5 and 24.5 m, as displayed in figure 4.12. While the correlations fall below 0.5 for time lags greater than 4 seconds in the case without trees, they remain higher than 0.5 up to time lags of 10 - 15 s for the heights greater than 10 m. It seems that the characteristic length and time scales above tree height are bigger when trees are present. This may be due to wake shedding from trees, which have bigger dimensions than houses in Vancouver Sunset area.

However, if the same comparison of time correlations is conducted at a different location in the modelling domain, nearly the opposite findings can be observed: For a given lag, the simulation with trees leads to lower correlations than the simulation without trees. Therefore, the influence of trees on the size of the wakes seems to vary in space.

Spatially averaged correlations in time were computed for the entire modelling domain, for one cell per patch of 32 × 32 m: The results displayed in figure 4.13 and in figure 4.14 show that there is a small but clear difference between the spatially averaged correlations in time computed for the simulation without trees and those computed for the simulation with trees. By observing the passage of the correlation curves at time lags of 5 and 10 seconds, it becomes clear from

the two figures that, for a given lag, correlations in time remain higher for the simulation with trees.

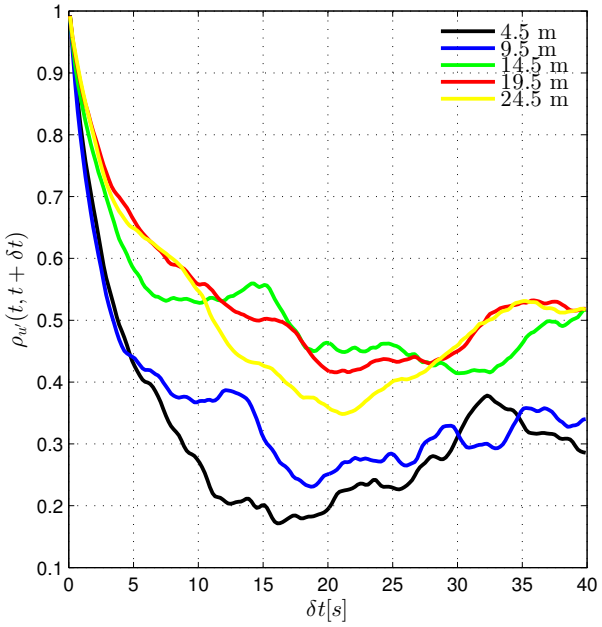

Figure 4.12: Correlations of fluctuations of streamwise velocity in time $\rho_{u'}(z; t, t+\delta t)$ at tower location, for different lags and different heights for the simulation **with trees**.

If correlations in time are plotted at tower location for the entire model depth (see figure 9.5 in the Annex), it becomes apparent that they decrease more quickly at heights 80.5 to 120.5 meters than closer to the surface. Important negative correlations exist at 40.5 and 120.5 m. The same as for lower heights is true for small scale motions: significant positive correlations exist only for time lags smaller than 3-4 seconds. The negative correlations observed at larger heights may be due to locked structures extending over the entire model domain length, but further investigation is needed on this topic.

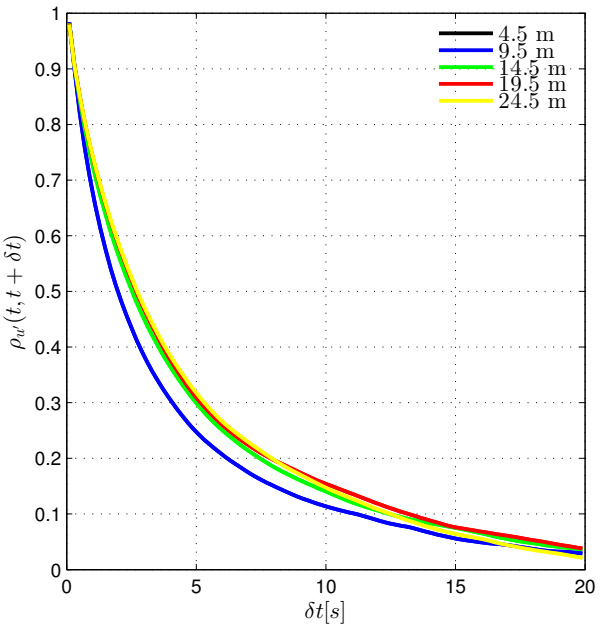

Figure 4.13: Horizontally averaged correlations of fluctuations of streamwise velocity in time $\rho_{u'}(z; t, t+\delta t)$, for different lags and different heights for the simulation **without trees**.

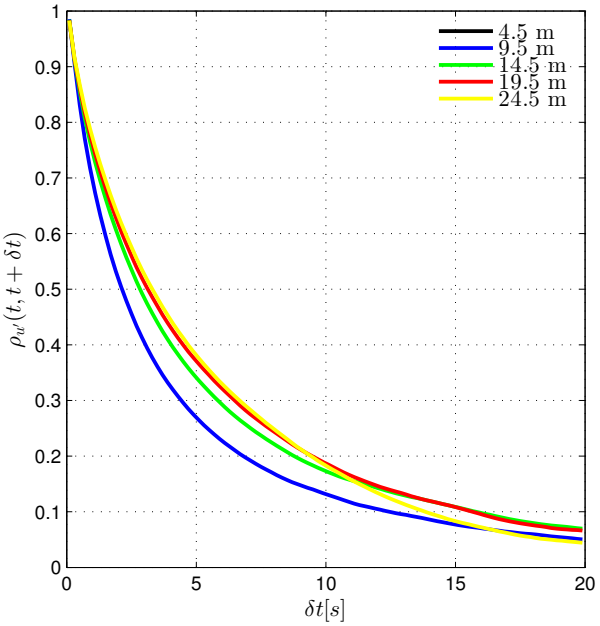

Figure 4.14: Horizontally averaged correlations of fluctuations of streamwise velocity in time $\rho_{u'}(z; t, t+\delta t)$, for different lags and different heights for the simulation **with trees**.

4.3 Visual analysis of the instantaneous flow field

For both simulations it is clearly visible how the flow slows down from top of the domain to the bottom. The slowest wind speeds are encountered behind buildings. Above a certain height, velocities are no more dependent on the immediate topography of the houses and the velocity field becomes disorganized: This is the Inertial Sublayer.

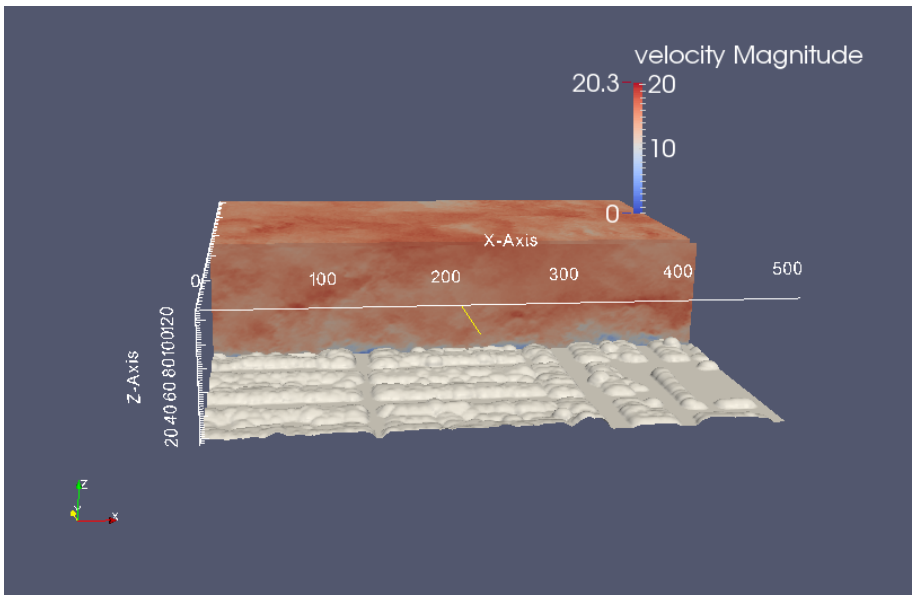

Figure 4.15: Sectional cut across the flow field along an x-z plane, displaying wind velocity in the centre of the modelling subset, embedded into the urban geometry. The flow field displayed is part of the results of the simulation **without trees**. All spatial dimensions are in [m] and velocity magnitude is in [m/s].

The overall difference in wind speed between the two simulations is visible at first glance due to the velocity-dependent colouring of the flow field, having the same scale for both pictures figure 4.15 (without trees) and figure 4.16 (with trees): The flow field without trees contains much more red and dark red colour than the flow field with trees. Especially the flow velocities close to the ground, up to z = 2 h seem to be significantly lower.

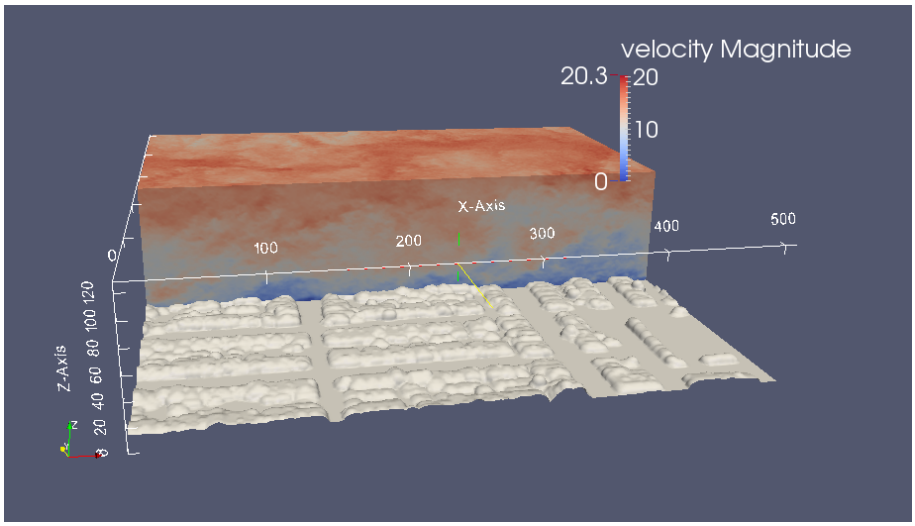

Figure 4.16: Sectional cut across the flow field along an x-z plane, displaying wind velocity in the centre of the modelling subset, embedded into the urban geometry. The flow field displayed is part of the results of the simulation **including trees**. All spatial dimensions are in [m] and velocity magnitude is in [m/s].

In figure 4.17 the wakes produced by buildings are very well visible, as well as the back circulation behind buildings, leading to negative velocities. Also, the difference in velocity between the two simulations is clearly detectable. For the simulation with trees, the wakes produced by the buildings seem to be somewhat less strong. This phenomenon, a consequence of the additional pressure drag exerted onto the flow by the trees, will be examined in section 4.4.3 with relation to the dispersive fluxes.

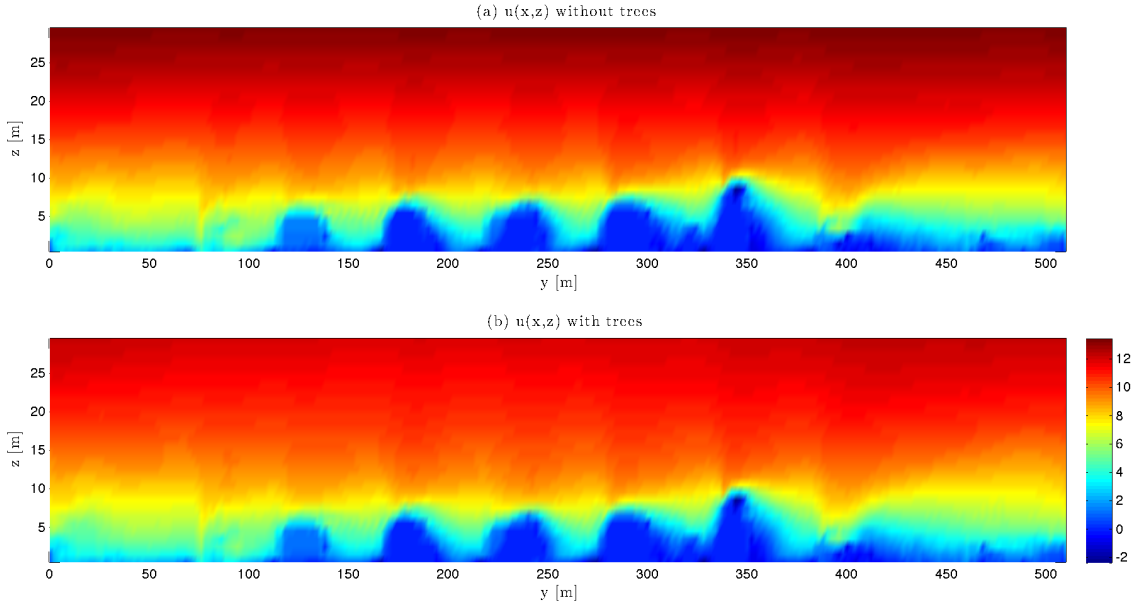

Figure 4.17: Sectional cut across the flow field along an x-z plane, comparing u-velocity for both simulations in the centre of the modelling subset along y = 400 m and up to a height of 30 m.

4.4 Vertical profiles

In the following, vertical profiles of essential variables are drawn for the buildings only ('no trees') and the buildings with trees ('with trees') case. The profiles are assessed regarding their representativeness of typical urban canopy layer properties, their information content on the flow field, turbulence production and consumption as well as their information content on the roughness of the underlying surface. The effect of the drag force induced by trees on different variables such as the longitudinal space-averaged velocity, the momentum fluxes and the velocity variances is discussed.

4.4.1 Longitudinal velocity

For a given height, wind speeds for the simulation without trees are clearly higher than for the simulation with trees. This is a direct result of the modified roughness properties due to the presence of trees. The total force remains the same, since it is balancing the pressure gradient. The roughness felt by the flow in the domain increases slightly.

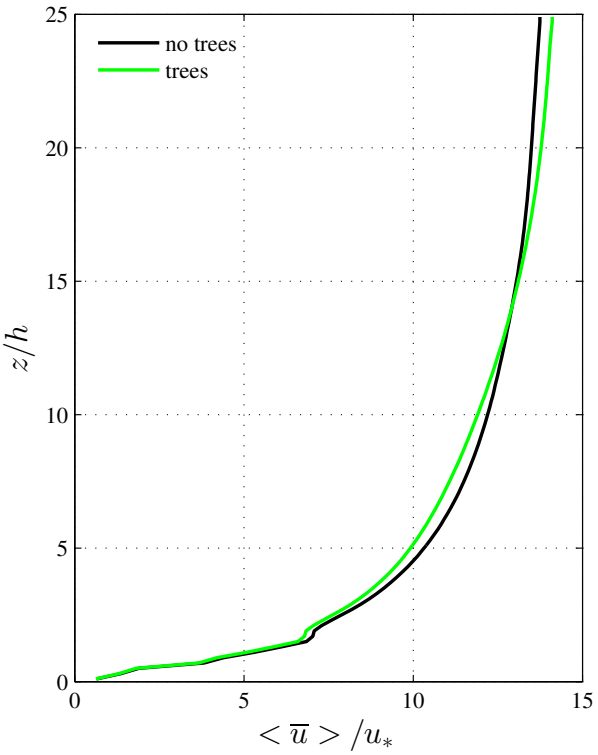

Figure 4.18: Vertical profile of the horizontally averaged longitudinal velocity

4.4.2 Variances

Figure 4.19 shows immediately that, in the lower part of the ABL (for $z < 5h$), longitudinal velocity varies more with trees than without, whereas the opposite is true for the upper part of the model depth. This suggests that the drag force on trees leads to more variation of the flow in time. The height of the cross over, $z = 5h = 25$ m, is situated approximately 2-3 h above the tree crowns. At that height, the flow is more uniform again. The lower variance obtained for the case with trees as opposed to the case with buildings only can be explained by the trees 'filling the holes' in-between the buildings, leading to a transition from z-roughness to d-roughness. The same can be observed for the vertical velocity, but in a less pronounced way.

In figure 4.19, a behaviour comparable to a typical plant canopy can be observed especially for the 'buildings only' case; the profiles between z = 0 and z = 2h are similar to profiles obtained from wind tunnel measurements and field experiments, as documented in (11): σ_u/u_* begins at a value of 1.5 (too high for plant canopies) near the ground and reaches a value of 2 (same value as for plant canopies) at z=h.

A comparison of the spatially averaged variances of the streamwise velocity and the vertical velocity for the trees versus no trees case is made in figure 4.19. For both simulations the variance of w just above the buildings at 7.5 m (i.e. at $z = 1.5h$) is by half an order of magnitude smaller than the variance of u. This can be explained by the fact that vertical movements are restrained by the pressure force acting upward from the underlying surface,

while horizontal movements are only restrained in-between buildings. Below a height of 10 m (i.e. $2h$), the variance of u for the simulation with trees is lower than for the simulation without trees. The top of the tree crown is located in many cases near a height of 10 m, indicating that trees seem to reduce turbulent fluctuations at larger wavelengths (while they may enhance it at small wavelengths, see TKE profiles below). A cross over of this behaviour occurs between $2h$ and $7h$, which may be explained with the wake shedding by the trees, inducing more variability in the log-layer. Above $7h$, the variability with trees is again lower than without trees. For the variance of w, the same effects can be observed, but at a larger scale: The inversion is located between $5h$ and $15h$.

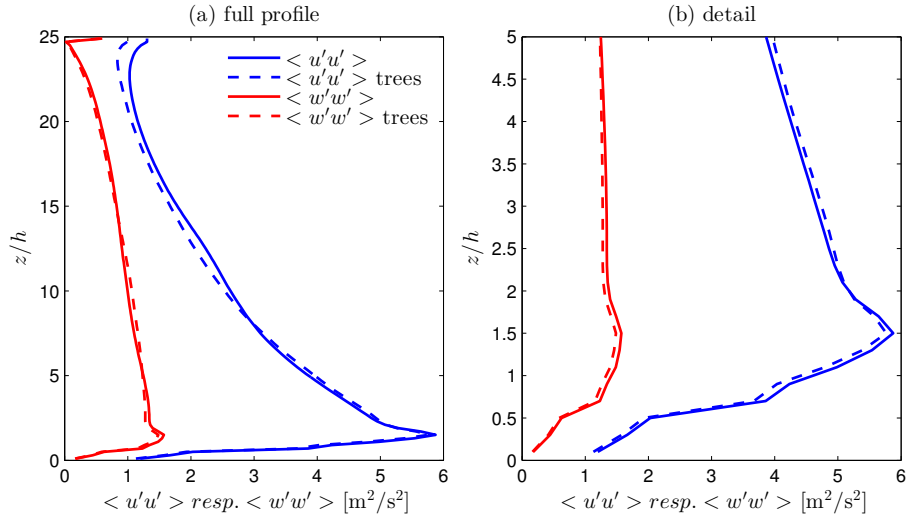

Figure 4.19: Vertical profiles of the horizontally averaged variance of longitudinal and vertical wind velocity for the simulation with trees and without trees. Plot (a) shows the profiles of the variances over the full domain depth and plot (b) shows the same profiles in detail, up to $z = 5h$.

4.4.3 Fluxes

The Reynolds flux, i.e. the vertical transport of horizontal momentum $\overline{u'w'}$, below $z = 5h$ is slightly smaller with trees than without, but becomes larger above. Trees seem to inhibit transport of momentum into the canopy. The dispersive flux $< \overline{u"} >< \overline{w"} >$ with trees remains lower than without trees over the entire domain depth, suggesting that trees inhibit the exchange of momentum in the spatial dimension at all scales. It shows a local maximum at roof height, where important velocity differences in space occur due to the obstacles. Higher up in the inertial sublayer, this term is smaller with trees than without. An explanation for this behaviour is that, even if the trees enhance turbulence locally, they reduce wake production on buildings on a larger scale: a tree located in-between two buildings slows down and deviates the wind before it hits the next building. Instead of hitting a building at full speed and being deviated upward, the wind is dampened by the trees and small scale TKE is produced. It is also deviated upwards, but with less energy. The subgrid stress τ_{xz} is naturally relatively small for both the simulations with and without trees. But it experiences an important peak at $z \cong h$,

where the house roofs are located. This realistic behaviour is produced by the immersed SGS model that reproduces shear on walls. In the upper 2/3 of the modelling domain, dispersive fluxes seem to dominate the budget of fluxes. This behaviour is not entirely realistic and is a result of the architecture of the LES model that has been observed previously. In order to get rid of this effect, the results would have to be averaged over several model runs.

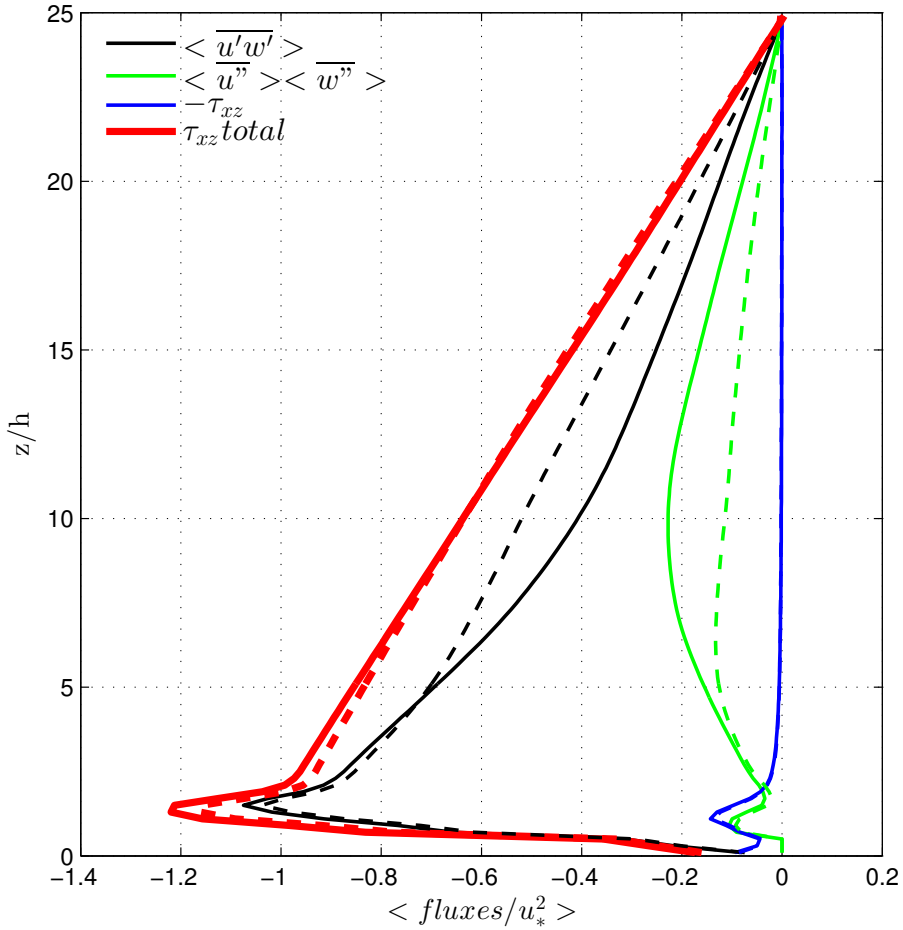

Figure 4.20: Vertical profiles of the horizontally averaged eddy covariance fluxes (i.e. Reynolds fluxes), dispersive fluxes and total fluxes. Shown are results from the simulation **without trees (solid lines)** vs results from the simulation **with trees (discontinuous lines)**. All spatial averages were computed as xy-averages over the entire domain for each height z.

4.4.4 Blending height and spatially distributed velocity

An important spread of velocity magnitudes in space can be observed below z = h in figure 4.21, while a very neat collapse of the velocity profiles occurs above the blending height. This collapse is due to the fact that velocities are displayed along the x-axis, thus along the axis of the streamwise velocity, for three characteristic locations on the y-axis: (a) In the interspace between buildings, i.e. in the backyards, (b) at the location of a row of buildings running in x-direction

and (c) at the location of a street running in x-direction. It can be seen that for all plots, the streamwise velocity varies significantly below the blending height, with the highest variance in the building interspace. The height of the collapse of the profiles varies slightly in-between the locations, but it is in the same range. Above the blending height, elongated streaks are responsible for a very uniform velocity distribution along the x-direction.

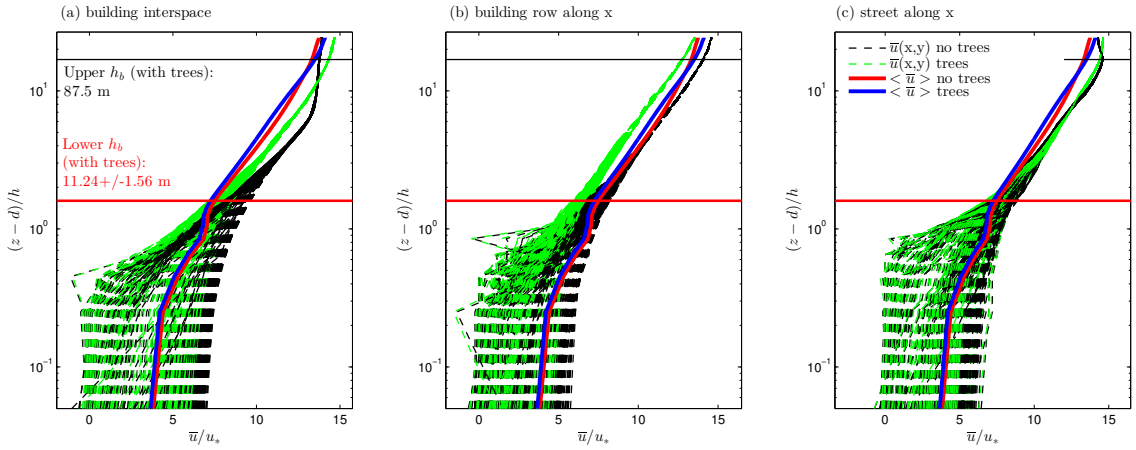

Figure 4.21: (a) Vertical profiles of streamwise velocity at all grid points along the x-direction for the location y = 256 m. (b) Vertical profiles of streamwise velocity at all grid points along the y-direction for the location x = 256 m. The xy-averaged velocity profiles are represented by the blue and red lines. The blending height of 11.24 m that is indicated (red line) is the 'lower' blending height for the simulation without trees. The 'upper' blending height $h_b = 87.5$ m is hyptothetical and valid for the simulation with trees only. It is indicated with a thin black line

The blending height of the Roughness Sublayer (further on called the 'lower' blending height) may be estimated visually from figure 4.21 as the height at which the velocity profiles collapse. As a stringent criterion, the height where $|\sigma(u(x))|/u_{xy} \simeq 0.05$ is taken to be the blending height. Above this height, the deviations from the mean velocity are statistically speaking small enough to be negligible. This criterion is evaluated for all grid points along the y-direction, with standard deviations among all velocities along the x-axis, which yields 256 values for the lower blending height (one at each grid point along the y-direction). These values are averaged to yield one final value for the lower blending height. The application of the criterion is visualized in figure 4.22. Determined this way, the lower blending height with trees becomes $h_b = 11.36$ m, and the lower blending height without trees $h_b = 11.5$ m. This result is somewhat surprising as a bigger variability among velocity profiles would be expected for the simulation with trees at first hand. But as figures 4.23 and 4.24 show, trees may even reduce the overall variability of streamwise velocity in the horizontal. As mentioned earlier, smaller trees tend to 'fill up' interspaces in-between houses. They can also make a house-to-street transition appear less sharp by reducing the mean height difference between the street level and the houses.

Along the y-axis, velocities vary much more than along the x-axis above $z = h$, as shown in figures figures 4.23 and 4.24. Surprisingly, there is very little correlation between velocities along the dimension orthogonal to the flow direction. This might be due to previously observed elongated structures, scaling with height z from the surface and spanning several building

heights in length. Nevertheless, even the velocity profiles along the y-direction show some sort of collapse above the lower blending height $h_b = 11.24$ m. But this collapse is much less pronounced than for the velocity profiles along the x-direction.

The absence of a collapse of velocities along the y-axis suggests that there must be some sort of 'upper' blending height, which takes into account the standard deviation among the velocities of all grid points of the domain, without following the flow direction. The same strict criterion that was used for the determination of the lower blending height was also applied to this overall standard deviation: $|\sigma(u(x,y))|/u_{xy} \simeq 0.05$. Only for the simulation with trees, a height inside the modelling domain where this criterion holds could be found: Upper $h_b = 87.5$ m. For the simulation without trees, on the other hand, the blending height would be situated outside the modelling domain. These results suggest that, in order to confidently determine such an upper blending height where all velocity profiles collapse, a larger modelling domain would be needed, with a domain height H of up to 500 m. Due to high computational costs, such a setting is currently not feasible for a model resolution of 2 × 2 m.

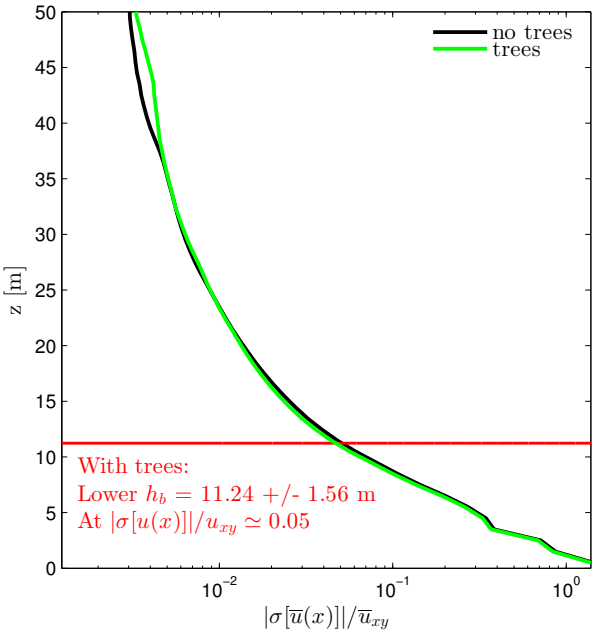

Figure 4.22: Determination of the lower blending height from the fraction of velocity standard deviation along the x-axis over spatially averaged velocity. A blending height was computed from this fraction for each location along the y-direction. The average of all blending heights along the y-direction was taken to yield the final blending heights $h_b = 11.24$ m (σ = +/- 1.56 m)for the simulations with trees and $h_b = 11.5$ m (σ = +/- 1.88 m) for the simulation without trees. The profile displayed is a mean profile for all locations along the y-direction.

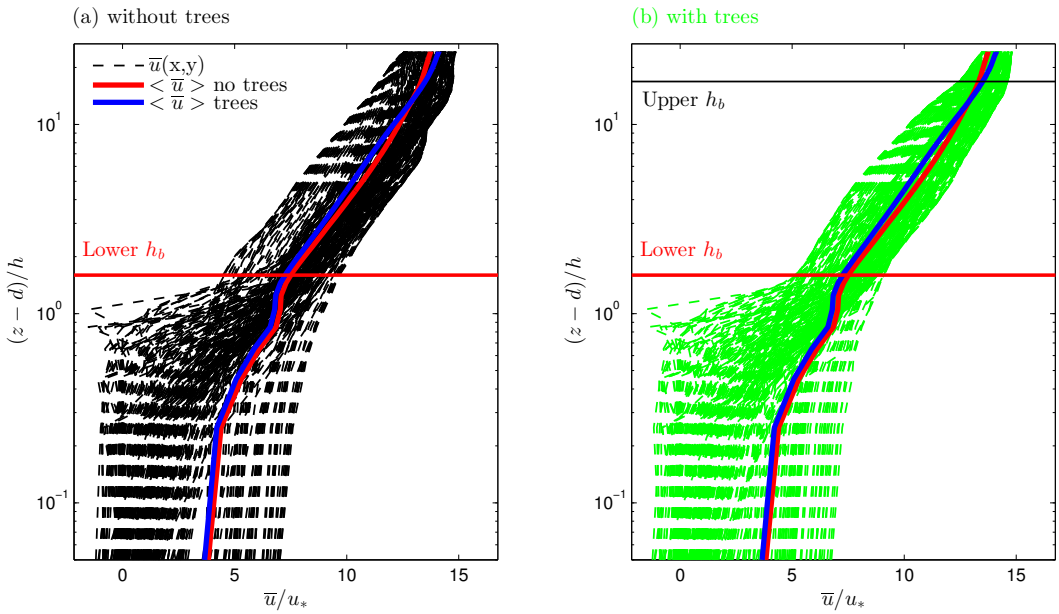

Figure 4.23: Vertical profiles of streamwise velocity **along y-direction** for a given location x = 348 m, where a row of **buildings** stretches over the entire extent of the domain in y-direction. The left plot shows results from the simulation without trees (a) and the right plot shows results from the simulation with trees (b). Lower h_b = 11.24 m, upper h_b = 87.5 m.

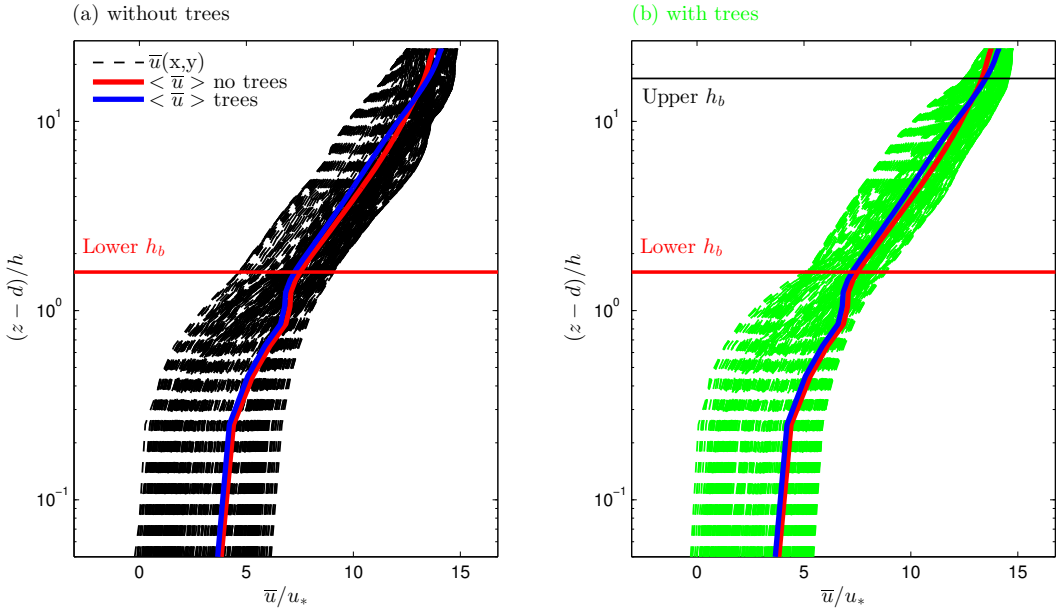

Figure 4.24: Vertical profiles of streamwise velocity **along y-direction** for a given location x = 156 m, where a **street** stretches over the entire extent of the domain in y-direction. The left plot shows results from the simulation without trees (a) and the right plot shows results from the simulation with trees (b). Lower h_b = 11.24 m, upper h_b = 87.5 m.

The influence of the elongated streaks that lead to a high correlation of the flow in streamwise direction can be observed well in figure 4.25. This phenomenon is also responsible for the existence of a 'lower' blending height, characterizing the blending of velocities along x-direction and delimiting the Roughness Sublayer.

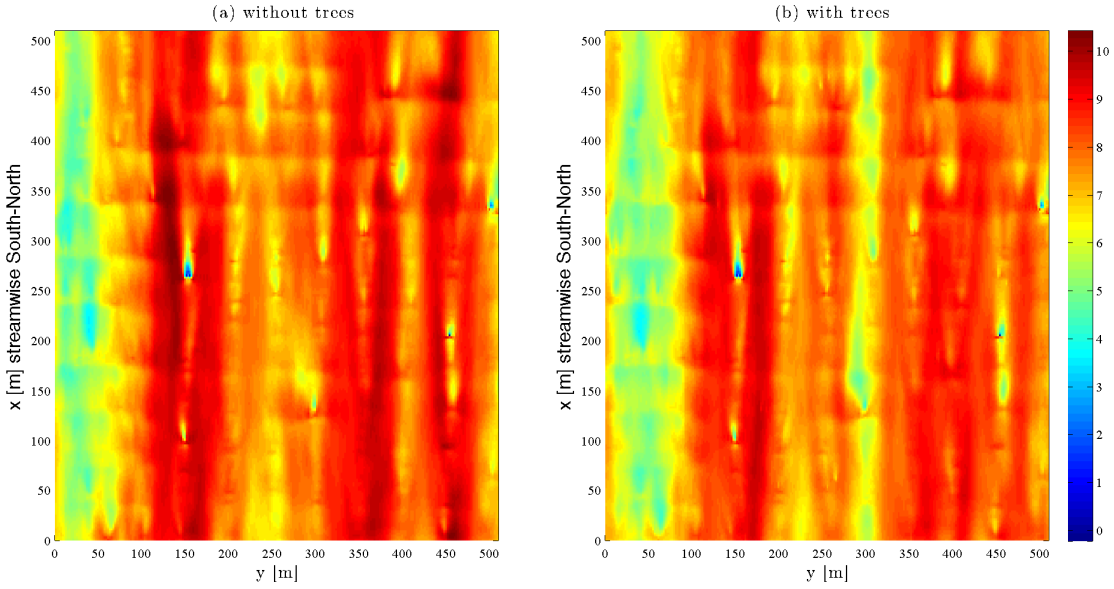

Figure 4.25: Surface plots of streamwise velocity u [m/s] at a height z = 10.5 m for **(a)** the simulation **without trees** and **(b)** the simulation **with trees**. The scaling bar on the right is valid equally for both plots.

4.4.5 Turbulent Kinetic Energy

The shape of the profile of absolute TKE of both simulations in figure 4.26 shows how it increases quickly between $z = 0$ and $z = 1.5h$, reaching its maximum close to $2h$, thus in the Roughness Sublayer, where wakes of buildings and trees occur. Above $z = 5h$ TKE decreases strongly, indicating that a bigger part of the energy is present in the mean flow in the form of Mean Kinetic Energy and less small scale velocity variations occur. Due to the subgrid model, TKE at the ground is not zero.

The profile of absolute turbulent kinetic energy suggests that less TKE is present if the drag force induced by the trees acts on the flow. The additional roughness seems to dampen turbulence, instead of enhancing it. This behaviour can be observed up to a height of approximately $5h$, above which the TKE for the simulation with trees becomes slightly larger than for the simulation without trees before a second inversion takes place at approximately $10h$. This first impression suggesting that TKE is smaller with trees than without may not be the right conclusion: The trees take away energy from the mean flow, slowing it down. If the results with and without trees are compared, the total kinetic energy of the flow in the simulation with trees is lower due to the pressure drag on trees, which converts a part of the kinetic energy into TKE that further dissipates to heat. That is why the **absolute** TKE recorded with trees must not necessarily be higher than for the case without trees. In order to compare the two simulations

properly, the kinetic energy needs to be scaled to account for the overall loss in kinetic energy due to the pressure drag on trees. This was done by dividing the horizontally averaged TKE by the MKE. The result is displayed in figure 4.27. As can be seen in the plot on the right for the Roughness Sublayer, the normalized term TKE/MKE is slightly higher for the simulation with trees than for the simulation without trees. This confirms the hypothesis made above: As for the roughness sublayer, in relative terms, there is more TKE present in the flow for the simulation with trees than for the simulation without trees.

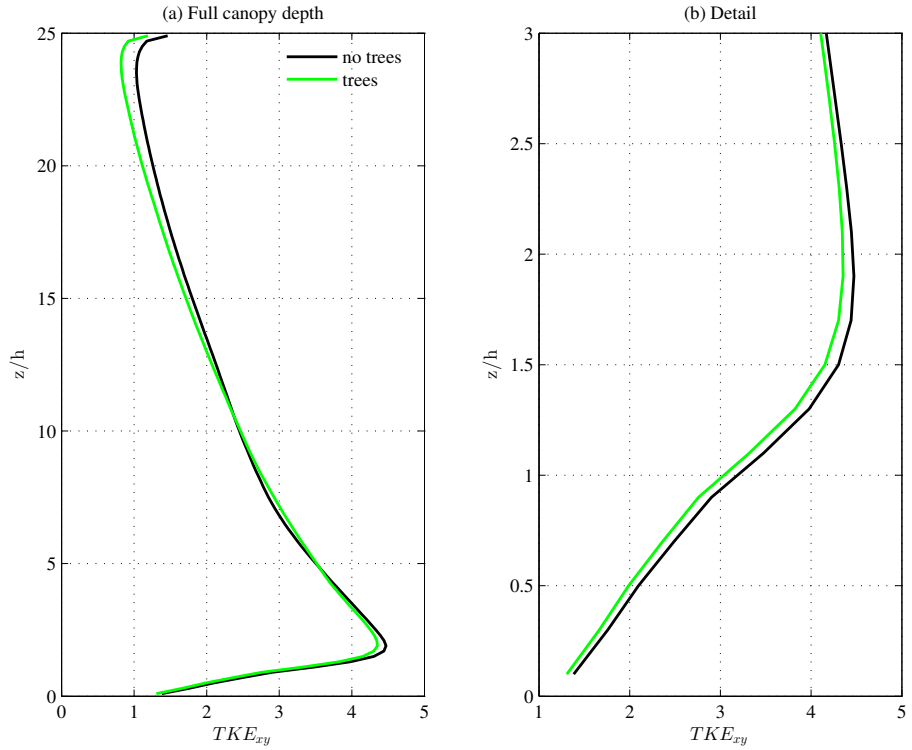

Figure 4.26: Horizontally averaged vertical profiles of the turbulent kinetic energy (TKE) for the simulation with trees and without trees.

4.5 Canopy properties

Variables of the flow in the urban canopy are visualized in order to show the differences between the pure building canopy and the canopy including pressure drag on trees. Two important parameters that characterize the roughness of a surface are derived: The displacement height d and the aerodynamic roughness length z_0. Further, it is assessed if typical urban canopy properties can be observed in the profiles.

4.5.1 Friction velocity

The spatially averaged maximum friction velocity for the simulation without trees is $u_* = 1.13$ m/s, while it is of 1.11 m/s for the simulation including the pressure drag on trees. Surprisingly,

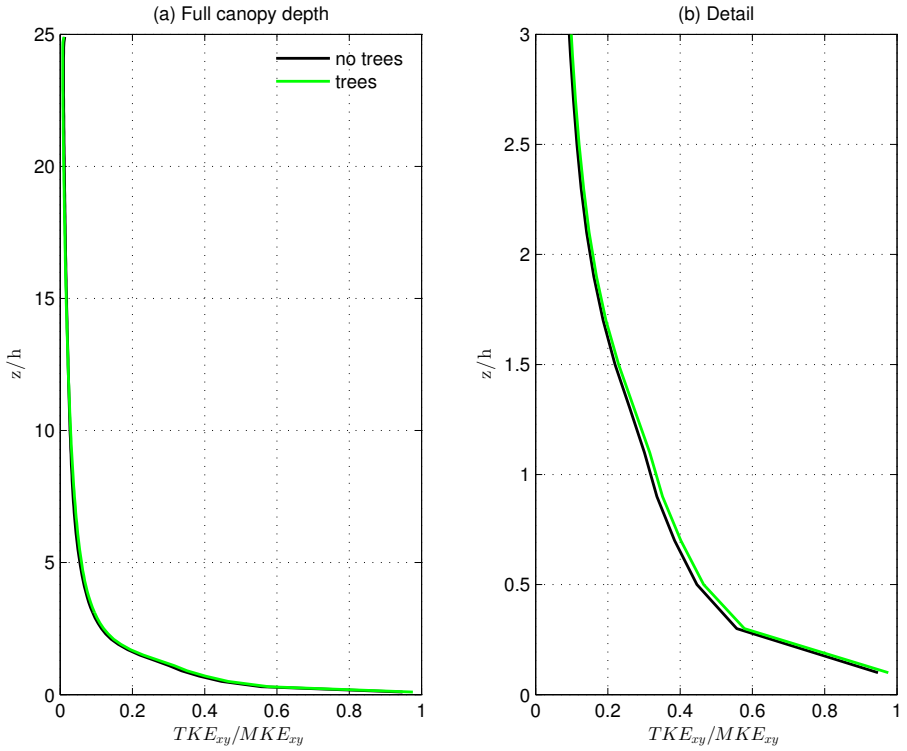

Figure 4.27: Horizontally averaged vertical profiles of the turbulent kinetic energy (TKE), **normalized with mean kinetic energy (MKE)** for the simulation with trees and without trees.

the maximum value with trees is smaller than without trees. On the other hand, if the spatially averaged friction velocity is computed for all heights z and averaged, this yields a different image: $\overline{u_{*,xy}(z)} = 0.615$ m/s without trees and $\overline{u_{*,xy}(z)} = 0.664$ m/s with trees. This value can be regarded as an integral value representing the effect of the surface roughness on the flow over its entire depth. These values of the friction velocities give a first idea of the increased overall roughness of the modelling subset when a pressure drag is added. The maximum friction velocities for the case with and without trees are both reached at a height of $1.5h$, i.e. 7.5 m. This height is well in accordance with measurements made in urban canopy layers, such as Oikawa and Meng (1995) (27) in the urban canopy of Sapporo, Japan, and Rotach (1993) (31) in the urban canopy of Zurich, Switzerland, where $u_{*,max}$ was located at $1.5h$ and $1.7h$ respectively. Similar values were found in wind-tunnel measurements made for the model of the real urban canopy of the city of Nantes by Kastner-Klein et al. (2001) (16).

The friction velocity can be computed in a third way: it is the friction velocity defined by the drag that the surface imposes on the model under the application of the constant pressure gradient of $\partial p_{kin}/\partial x = 0.01\ m/s^2$, imposed between the lateral model boundaries in order to drive the flow in the LES model:

$$u_{*,imp} = \sqrt{\frac{\partial p_{kin}}{\partial x} \cdot (H - d)} \tag{4.2}$$

Where $H = 125$ m is the domain height and d is the displacement height. Pressure is used in the form of kinematic pressure: $p_{kin} = p/\rho$, in units of m^2/s^2. For a displacement height d = 3.5 m, the imposed friction velocity becomes $u_{*,imp} = 1.1023$ m/s, which is slightly lower than the maximum friction velocity determined from the flow ($u_{*,max}$) but significantly higher than the mean friction velocity of the entire flow field. If larger values are chosen for d, $u_{*,imp}$ becomes smaller, which is not realistic, considering the value of $u_{*,max}$. If we choose d = 0 m, $u_{*,imp}$ is still slightly smaller than $u_{*,max}$. $u_{*,imp}$, the imposed friction velocity, is employed to scale all variables when comparing the simulations including trees to simulations without trees.

For comparison, the mean friction velocity computed from the conditionally sampled tower data (102 files of 30 minutes each) is $u_* = 0.543$ m/s and the maximum is $u_{*,max} = 1.016$ m/s. The friction velocity at tower height obtained from the LES model is 0.925 m/s. The difference to the maximum values obtained for the tower data is quite important. Therefore, scaling the spectra with the variance of the streamwise velocity can be justified because the Reynolds number is very high, and the viscous term is considered negligible.

Mapping the friction velocity u_* computed from the flow field with and without trees shows very clearly the difference in surface roughness occurring due to trees. Especially the 'high' trees (i.e. trees higher than approximately 10 m) have a strong effect, as can be seen in figure 4.28. Important effects of tree roughness can be detected inside street canyons aligned with the main flow direction (from South to North), where regular patterns of tree rows along the sides of the streets are encountered, which is very typical for this kind of suburban residential neighbourhood.

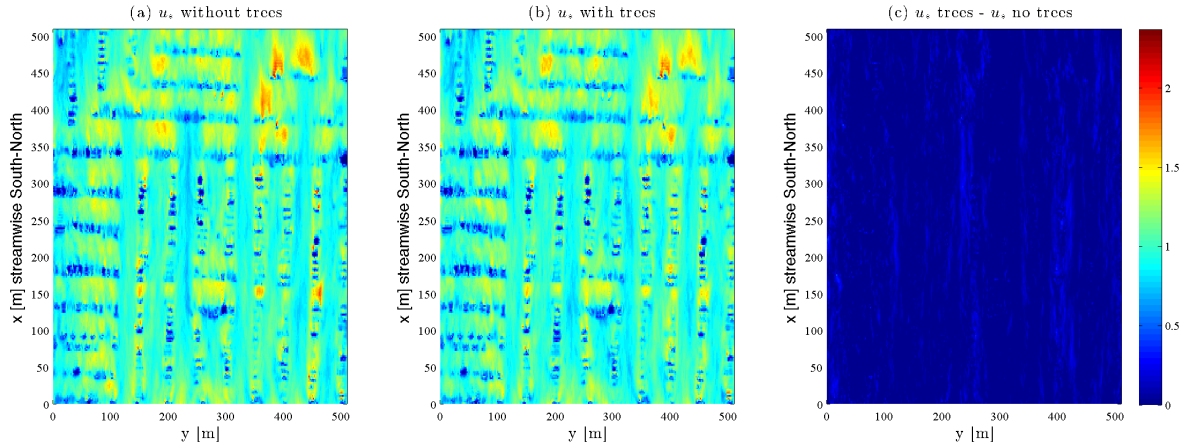

Figure 4.28: 2D plot of friction velocity u_*, with colour representing u_* in [m/s]. The friction velocity is displayed for the case **(a) without trees**, **(b) with trees** and **(c) for u_*(trees) - u_*(no trees)**. The scale bar on the right is valid equally for all plots.

4.5.2 Displacement height d

Rule of thumb

The displacement height is often estimated to be $d \simeq 0.7h$ (30), yielding d = 3.5 m for the present case with h = 5 m. This value serves as a good reference in a first place, but d needs

Table 4.2: Friction velocity for different model results and for tower data

u_* [m/s]	Explanation	with trees	without trees	100x(trees/none-1) [%]
$u_{*,imp}$ (d = 3 m)	Imposed by $\frac{\partial p_{kin}}{\partial x}$	1.105	1.105	0
$u_{*,imp}$ (d = 0 m)	Imposed by $\frac{\partial p_{kin}}{\partial x}$	1.118	1.118	0
$max[< u_*(z) >]$	Max. of xy-mean	**1.114**	**1.133**	-1.73
$< u_* >$	Overall mean	0.664	0.616	+7.9
$< u_*(z_{tw}) >$	xy-mean at z=z_{tw}	0.921	0.916	+0.53
$u_*(x_{tw}, y_{tw}, z_{tw})$	At tower coord.	1.017	0.88	+15.6
$max[u_{*,tw}(t)]$	Max measured	1.016	-	-
$\overline{u_{*,tw}(t)}$	Mean measured	0.543	-	-

to be determined more precisely in dependence of the properties of the flow.

From velocity profiles

Semi-logarithmic profiles of the stream wise velocity u were compared for different values of d and assessed for their 'straightness' and form of the bend in the velocity profile occurring in the lower part of the logarithmic layer. Displacement heights between d = 3.0 m and d = 4.5 m all yield a quite satisfying appearance of the velocity profile. Without any further quantitative information it is difficult to determine d with this method.

Imposed friction velocity

A third way to determine and confirm d is the comparison of the imposed friction velocity $u_{*,imp}$, computed for a given displacement height d, to the horizontally averaged friction velocity computed from the flow field: If d is chosen correctly, one should obtain $u_{*,imp} \simeq u_{*,max}$. As it has been shown above, the imposed friction velocity here never reaches the value of $u_{*,max}$, not even for d = 0 m. Nevertheless, this suggests that a relatively low value for d should be considered.

Barycenter of pressure force

A reliable method to obtain the displacement height d is the examination of pressure forces in the LES model results. For both simulation with and without trees, the average barycenter of pressure was approximated with the help of the horizontally averaged pressure: Between the lowest grid point at z = 0.5 m and the obstacle height h = 5.0 m, the barycentric height z_b was determined according to the well-known equation 4.3.

$$z_b = \frac{\sum_{z=0.5m}^{z=h} p(z) \cdot z}{\sum_{z=0.5m}^{z=h} p(z)} \tag{4.3}$$

The results for z_b are summarized in table 4.3. In spite of the approximative nature of the approach used, the heights obtained are all in the same range, between 2.75 and 3.85 m.

Table 4.3: Barycentric heights h_b determined from the xy-averaged pressure force for the simulation with trees and for the simulation without trees

$z_b[m]\ for\ z_{max} = h$	xy-averaged	at building
without trees	3.23	3.12
with trees	3.24	3.14

After visual inspection of the pressure field in an xz-plane (see figure 9.6 in Annex), locations of interest with direct pressure drag on exposed buildings were determined. Henceforth, pressure at both the luv ($p_{luv}(z)$) and lee ($p_{lee}(z)$) sides of a building was averaged over several selected points in the horizontal (located immediately in front resp. in the back of the building) and the resulting pressure force $p_{res}(z)$ acting on the building at each height was computed: $p_{res}(z) = p_{luv}(z) - p_{lee}(z)$. The pressure force profile $p_{res}(z)$ was then used in equation 4.3 to compute the barycentric height z_b for this building: $z_b = 3.12$ m (without trees) resp. 3.14 m (with trees). A vertical profile of the pressure $p_{res}(z)$ acting on this house is displayed in figure 4.29. A pressure peak at $0.7h$ is clearly visible. The pressure barycenter obtained from the simulation results with trees differs very little from the one obtained from the simulation without trees. Although here the derivation of the pressure baricenter was restricted to one location and an approximative domain-averaged value, these values are quite close to each other and in the same range as the values for the displacement height d found above. Considering the values in table 4.3 and the values obtained for one building, this method suggests that d is situated near 3.2 m.

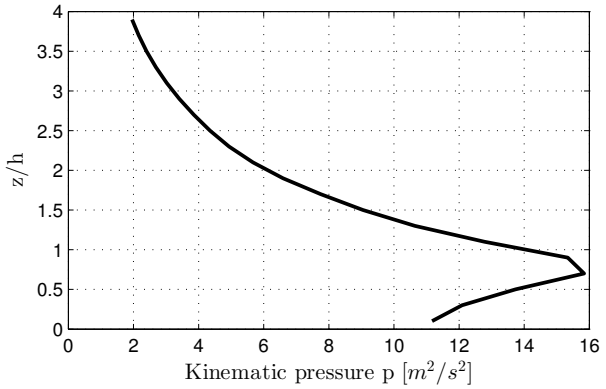

Figure 4.29: Vertical profile of horizontally averaged resulting kinematic pressure $p_{res}(z)$ in front of a building.

Morphometric parameterization

We determined the displacement height d according to the method of Bottema (1995) introduced in section 3.7.1. This yielded $d = 2.83$ m for $h = 5.0$ m. If h is estimated from the weighted average among tree and building heights, h becomes 4.8 m and d becomes 2.75 m. If only trees with a height greater than 5 m are considered, the weighted average obstacle height h changes to $h = 5.85$ m and the displacement height becomes $d = 3.33$ m. These results support a choice

of $d = 3.0$ m.

After estimating barycentric heights and confirming relatively low values for d by applying the morphometric parameterization, we choose a value of $d = 3.25$ m for the displacement height.

4.5.3 Aerodynamic roughness length z_0

The value obtained for the aerodynamic roughness length z_0 that characterizes the modelling subset depends on the precise determination and choice of the following parameters:

1. displacement height d
2. blending height
3. height range and length of the chosen portion of the linear velocity profile for which the fit is computed

Necessary conditions for a realistic and credible fit can be determined:

1. The displacement height used for the fit should be determined carefully and fits should be tested for a range of possible values of d.
2. The linear fit has to be parallel to the velocity profile (on a semilogarithmic plot) over the entire distance of the fit.
3. The height z_1 at which the fit begins clearly has to be above the blending height $h_b = 11.5m$.
4. In the range where the linear fits are applied both velocity profiles with and without trees should be **parallel** to each other. This criterion is the most important one as it demands that both velocity profiles have the same slope and are therefore scaled with the same friction velocity.
5. The slope of the velocity profile (on a semilogarithmic plot) should be different for the portion of the fit than before and after the fit. Ideally, the velocity should accelerate more above the fitting interval than within the fitting interval.
6. The plot should be done only under neutral conditions.

Table 4.4: Results for z_0 for different displacement heights for both simulations. The linear fit to the logarithmic part of the velocity profile was applied for the height interval between 25 and 40 m. This range was chosen such that the fit itself is parallel enough over the fitting portion and such that the fitting lines of the two simulations are parallel. The displacement heights chosen correspond to the range of values found in section 4.5.2, centred around the chosen value of $d = 3.25$ m

d (all in [m])	3.0	3.25	3.5
z_0	0.40	0.38	0.36
z_0(trees)	0.46	0.44	0.42

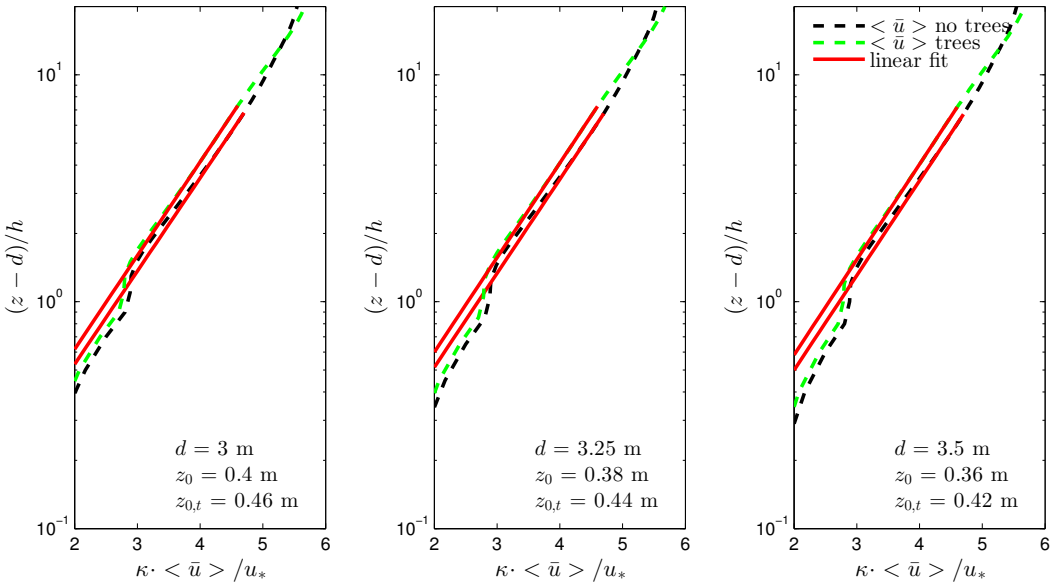

Figure 4.30: Linear fits to the horizontally averaged logarithmic u-velocity profile for the determination of z_0 are presented. Fits and resulting z_0 are computed for three displacement heights: (a) $d = 3.0$ m, (b) $d = 3.25$ m and (c) $d = 3.5$ m, where $d = 3.25$ m has been determined to be the most realistic value for d. The height range of the linear fits is $z = 25$ - 40 m for all plots.

The linear fits displayed in figure 4.30 show that z_0 with trees is higher than z_0 without trees. As discussed above, the outcome of such a linear fit depends on the height interval over which the fit is applied, and on the displacement height d. Therefore, a range of values for z_0 has to be given as a result, rather than one single value. We consider the results for d = 3.0 m and for d = 3.5 m to be equally representative because the linear fits are in a reasonable height range and because the range in-between these displacement heights is the most realistic as it has been shown in section 4.5.2. Linear fits for alternative choices of displacement heights are shown in Annex section 9.2.6. Without trees, $z_0 = 0.36$ - 0.40 m and with trees, $z_0 = 0.42$ - 0.46 m. The ranges of values for z_0 with trees versus without trees are close. This suggests that the effect of the trees on the flow field above an urban canopy is very complex. Because trees fill empty space in-between houses and therefore reduce the force with which wind hits the walls of

houses, the urban canopy becomes more uniform and the average distance between roughness elements decreases. Up to a certain inter-element distance, the overall roughness of the canopy will rise. But if the elements are placed densely enough, shading effects take over and the overall roughness 'felt' by the wind decreases again. In the canopy of the Sunset site, there are many locations where trees clearly increase the roughness, for example along large streets. But there are as well situations where bushes and smaller trees inside courts and in backyards seem to reduce the overall roughness by shading. Nevertheless, there is a large number of trees that are significantly higher than the average building height of 5 m and that certainly increase the overall roughness.

4.6 Effect of the trees on the flow

First conclusions on the effect of trees on the flow were made from the analysis of vertical profiles of different variables.

In order to compare the amount of TKE available and to better quantify the spectral power present in the flow at different spatial scales, spectra of the results with and without trees at the approximate location of the measurement tower are compared in figure 4.31 for a height z = 24.5 m.

The spectrum for the simulation without trees has somewhat more energy in the range of medium frequencies, between 0.1 and 2 Hz. This observation may be a result of the stronger wakes produced by the buildings if no trees are added, leading to important oscillations of the flow. The same comparison of spectra was also conducted at a height of 10.5 m. The spectra look very similar to those in figure 4.31, except that the excess in energy observed for the spectrum without trees seems to be smaller. The corresponding figure can be found in the annex.

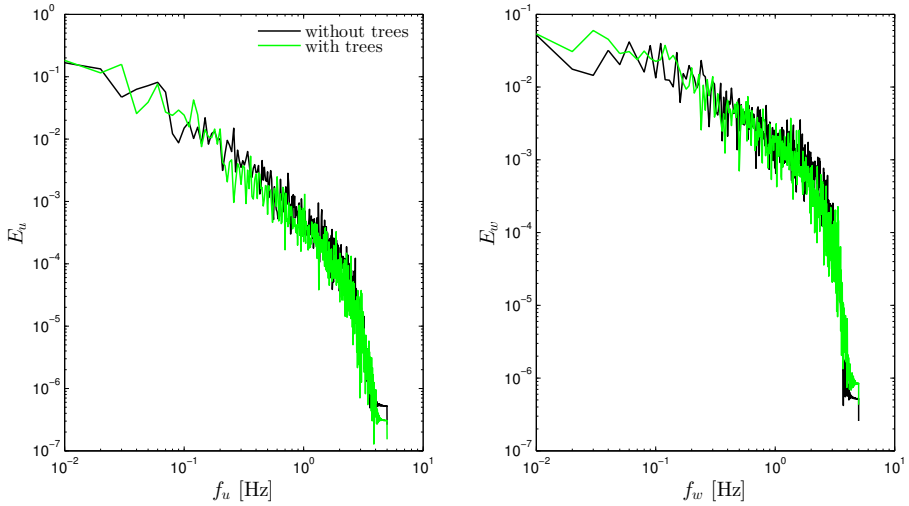

Figure 4.31: Spectra of streamwise and vertical velocities u and w at tower location and z = 24.5 m, plotted on logarithmic axes and compared for the simulations with and without trees. Spectra were computed for five segments of 1000 data points each, divided by the standard deviation of the signal of each chunk and the spectra for the five segments averaged.

4.7 Roughness parameterizations from literature

4.7.1 Displacement height d

Anemometric and morphometric parameterizations of d performed for the neighbourhood of Sunset Area in (12) resulted in a displacement height d = 4.5 m. But in this study, the mean height of the roughness elements was h = 8.7 m, which is significantly larger than the value of h = 5 m computed for the average building height in this work. It is therefore problematic to compare the two values for d. But a comparison of the relative value d/h can still be made: d/h = 0.52 in (12) while d/h = 0.65 in the present study. Thus (12) assumed that the mean wind acts at a lower height, yielding a slightly higher value for z_0. The significant difference between the values found for h has different reasons: (1.) In (12) a larger subset was considered for the computation of the urban geometry statistics. The subset also included higher commercial buildings on the east side that are not included in our subset. (2.) The trees were included in the computation of h. In the present work they were deliberately omitted in order to scale the two different simulations with the same height h referring to the building geometry only. (3.) In (12), h was computed as a mean maximum building height, weighted with the frontal area of the individual roughness elements. In the present work, h was computed as the mean height of all grid cells classified as buildings.

4.7.2 Aerodynamic Roughness length z_0

In the same study as for the displacement height, (12) obtained a value of z_0 = 0.6 m from a selection of **anemometric** parameterizations. The same reservations regarding the comparison of the values of this study to values obtained with our model are true here.

(13) applied various **morphometric** methods to different types of urban surfaces. They indicate a possible value range for z_0 of 0.3 - 0.8 m for suburban one- to two storey house neighbourhoods. The values of z_0 found for Vancouver Sunset in the present study are situated well inside this range.

We applied the Es method described in section 3.7.2 to the LES model results: The input values to the equation are $\bar{u}(z = z_{sensor}) \simeq 10.8$ m/s, $u_{*,max} = 1.114$ m/s, $d = 3.5$ m and $z_{sensor} = 24$ m. This yielded

$$z_0 = (z_{sensor} - d) \cdot \exp(-\frac{\bar{u}_z \cdot \kappa}{u_*}) = 0.40m \tag{4.4}$$

The value is in the lower half of the range of values for z_0 obtained from the linear fits to the streamwise wind velocity, but still supports the fitting results.

If we choose $d = 4.5$ m, the Es method yields $z_0 = 0.38$ m, confirming the expected trend: A higher d leads to a lower z_0.

4.7.3 Comparison to model results

The displacement heights d determined with the morphometric method are in the same range but somewhat lower than the displacement heights obtained in the present work with various methods. The aerodynamic roughness lengths determined with the Es method are almost identical to the values obtained from the linear fits to the LES model data and support these results. On the other hand, typical values for a larger domain of the Vancouver Sunset area presented in (12) and (13) are somewhat different from our results: d/h is slightly lower in these studies than in the present work. However, it is delicate to compare d between the present work and the earlier studies for the various reasons explained above. $z_0 = 0.6$ m obtained in (12) and (13) is somewhat higher than our values for z_0. It goes along well with the relatively low displacement heights found in these studies; usually a smaller d implies also a larger z_0. The difference between the aerodynamic roughness lengths found in the present work and the values found in (12) and (13) may be attributed to an imprecise fitting procedure on our side, to the properties of the anemometric and morphometric methods used in those studies or, in general, to the difference in chosen displacement heights as well as to the different extent of the study areas.

5. Conclusions

Topography and trees Including the building geometry into the simulation was a standard task that did not cause any complications. The implementation of the drag force on trees, on the other hand, was more work intensive. Various corrections, modifications and filtering operations had to be applied to the LiDAR dataset although the dataset had been very well prepared by Dr. Rory Tooke (3) beforehand. And even now, more optimizations could be done to the data; an attempt of representing the vertical distribution of the LAD with a different function than the Weibull distribution could be made. Also, the classification of trees and buildings near roof level may be improved in order to avoid misclassifications, although this is difficult to achieve.

Validation The modelling results have been validated satisfactorily with the conditionally sampled tower measurements, indicating that the model approximates the real flow conditions quite well in stable atmospheric conditions. Thereby, it has to be kept in mind that a validation with single-point measurements is not as relevant as one with several points, e.g. a vertical array of measurements.

Model results: With vs without trees Both the simulation results without trees and with trees show profiles of fluxes, variances and friction velocity that are typical for urban canopies. For the simulation with trees, the flow is clearly slower than for the simulation without trees. Thus the effect of the tree force is as expected and the implementation of trees into this LES model can be termed as successful. Nevertheless, the trees also have the effect of 'filling up' spaces between roughness elements at certain locations in the modelling domain, such as in-between houses. In this case, trees lead to a shift from k- to d-roughness, yielding a lower overall roughness in these locations.

Only after scaling TKE with MKE for each simulation, the creation of additional small scale TKE by the trees in the Roughness Sublayer can be seen. By running the LES model at a higher resolution, e.g. 1 m, this behaviour could probably be investigated with more accuracy.

Time correlations of the longitudinal velocity component u for varying lag and height show that characteristic length and time scales are larger for the simulation with trees than for the simulation without trees, especially up to a height of $z = 5h$. A possible explanation are trees that are larger than the average buildings, producing wakes that reach bigger dimensions than wakes originating from buildings.

Canopy properties A displacement height of $d = 3.25$ m (+/- 0.25 m) and a range of aerodynamic roughness lengths of $z_0 = 0.36$ - 0.40 m (without trees) resp. $z_0 = 0.42$ - 0.46 m (with trees) has been found. The numerous orders of freedom of the linear fit to the logarithmic velocity profile have been reduced by (a) determining d as precisely as possible and (b) performing the fit only over the interval for which the velocity profiles for both simulations are parallel, following a scaling by the same friction velocity. The values found for d and z_0 are realistic and comparable to displacement heights resp. roughness lengths found in earlier studies such as (12) and (13) for the very same neighbourhood.

Blending heights of $h_b = 11.24$ m (with trees) resp. $h_b = 11.5$ m (without trees) have been found. These heights are representative for the upper limit of the Roughness Sublayer, but the collapse of velocities is only significant along the x-direction. In order to precisely determine an 'upper' or overall blending height, a deeper modelling domain would be required. A temptative 'upper' blending height for the simulation with trees was determined to be $h_b = 87.5$ m. The determination of blending heights gave insights into the variability of vertical velocity profiles in the horizontal: The variability of such profiles is lower for the simulation including trees, suggesting that the trees are responsible for a smoothing of the velocity field, while they increase the overall roughness of the urban canopy.

6. Outlook

Results analysis A more detailed analysis of the existing modelling results should be conducted: First, focus could be on the different terms of TKE at different locations and heights in the modelling subset, comparing their magnitudes for the results with and without trees. Second, a thorough quadrant analysis of the Reynolds stresses should be conducted in order to quantify the importance and proportion of sweeps and ejections for modelling results without trees versus modelling results with trees. A quadrant analysis of the model results could also be easily compared against the measurements.

Model input The building geometry used as a model input in this work is of good quality. The LAD profiles representing trees can still be improved significantly. First, the model could be re-run with a better, fully filtered version of the LAD profiles. Second, the input data originating from the pre-processing of the LiDAR data could be improved. Despite a careful pre-processing of the LiDAR data by R. Tooke (3), important spikes remain in the data. These may in part be a consequence of the algorithm that classifies LiDAR beam returns into returns from trees resp. buildings; in certain cases, parts of house roofs were classified as 'trees'. By optimizing this algorithm, some of the spikes in the data could be removed.

Model resolution In order to improve the accuracy of model outputs and to resolve small scale structures such as narrow gaps in-between houses and small trees, the LES model has to be run at a lower resolution of 1 m. This will take time (more than two weeks simulation time), but it is more than worth the patience.

Field measurements In a further study, the tower in Vancouver Sunset area could be equipped with sensors at different heights in order to obtain measurements of velocity and temperature profiles. These can be used for a better validation and possible improvement of the LES model as well as for the analysis of vertical profiles of fluxes, TKE terms and velocity, similarly to what has been done for the simulation of turbulent flow over Basel by Giometto et al. (2014). Locations of interest from the point of view of fluid dynamics could be detected within the neighbourhood with the help of model results. At these locations, additional sensors could be deployed for a limited time period in order to measure wind velocities at characteristic locations in the flow field, such as the back-circulation behind houses or the shading occurring immediately downstream of trees.

Code efficiency Thanks to the ongoing parallelization of the present LES code, a significantly larger subset of 1024 × 1024 m can be modelled at the same resolution of 2 m and, with longer simulation time, even at 1 m. The larger domain size implies a better accounting for larger spatial structures such as the overall geometry of a neighbourhood and allows for including the effect of large obstacles placed further apart. In short, a larger portion of the source area at tower height will be covered. This extension of the code will be achieved in the near future. In the long term, increase in computational power will lead to further improvement in computation speed and thus allow for the modelling of even larger domains at lower resolution.

7. Acknowledgements

Academics First of all, I want to thank Professor Wolfgang Kinzelbach and Professor Marc Parlange for supervising this thesis and for making possible such a unique exchange between the ETH Zurich, the EPFL Lausanne and the UBC in Vancouver. Prof. Kinzelbach kindly supported this special topic for a student in Environmental Engineering and assisted me with various questions regarding the organization of the thesis. Prof. Parlange assisted me in scientific questions, helped me to organize my stay in Vancouver and connected me to many people, and accompanied me on several runs on the UBC campus.

I further want to thank my internal supervisor Marco Giometto for the very proficient supervision of this thesis, the assistance in all aspects of my thesis and the great collaboration and passion in developing this work.

For his engaged supervision I want to thank Professor Andreas Christen from the Micrometeorology Laboratory, Department of Geography at UBC in Vancouver. Together with Marco Giometto, I collaborated closely with him and his group. He provided us with a very extensive high frequency eddy-flux dataset and gave us precious informations about the domain of investigation. He also assisted us in various questions regarding the choice of the modelling domain, dominant wind directions and vegetation cover.

Special thanks go to the scientific collaborators of UBC in Vancouver with whom we interacted during this work: Dr. Rory Tooke from the CALP and his collaborator Dr. Nicholas Coops from the Forestry Department at UBC, invested a large amount of work in preparing the LiDAR datasets for the simulations, and were always available to assist us with questions regarding topography and tree implementation. I further acknowledge Scott Krayenhoff, PhD student of Prof. Andreas Christen, for precious discussions about the implementation of wind drag on trees into our model.

Family My warmest thanks go to my parents Marianne-Vera Staub and Thomas Egli and to my sister Rahel Egli for making my studies possible and for supporting me in reaching my goals.

Friends I want to thank my friends, who inspired me both scientifically and personally, for their support and company during my studies: Katarina Kuba, Giulia Mazzotti, and Stephanie Westerhuis especially for proofreading and peer-reviewing. Fabian Bärenbold, Jonas Haller, Mélina Manzini, Franziska Zahner, Barbara Gehrig, Dersu Alther, Michael Kälin, Timo Walser †, Benjamin Ryser, Jonas Wichert, Pauline Dayer, Stephanie Wietlisbach, Camille Dussouillez, Clément Levasseur and Théo Cormon, for their company and support.

8. References

8.1 Bibliography

[1] John D Albertson and Marc B Parlange. Surface length scales and shear stress: Implications for land-atmosphere interaction over complex terrain. *Water Resources Research*, 35(7):2121–2132, 1999.

[2] Elie Bou-Zeid, Charles Meneveau, and Marc B Parlange. Large-eddy simulation of neutral atmospheric boundary layer flow over heterogeneous surfaces: Blending height and effective surface roughness. *Water resources research*, 40(2), 2004.

[3] CALP office, CIRS (Centre for Interactive Research on Sustainability) , University of British Columbia. *LIDAR DEM, DSM and vegetation datasets*. Tooke, Rory, April 2014.

[4] Andreas Christen. *Atmospheric turbulence and surface energy exchange in urban environments : results from the Basel Urban Boundary Layer Experiment (BUBBLE)*. PhD thesis, University of Basel, 2005.

[5] Andreas Christen, Mathias W Rotach, and Roland Vogt. The budget of turbulent kinetic energy in the urban roughness sublayer. *Boundary-layer meteorology*, 131(2):193–222, 2009.

[6] B Crawford and A Christen. Spatial source attribution of measured urban eddy covariance co2 fluxes. *Theoretical and Applied Climatology*, pages 1–23, 2014.

[7] Ben Crawford, Andreas Christen, and Rick Ketler. Processing and quality control procedures of turbulent flux measurements during the vancouver epicc experiment. 2012.

[8] Bernard Dacorogna and Chiara Tanteri. *Analyse avancée pour ingénieurs*. PPUR presses polytechniques, 2002.

[9] Marc Diebold. *Snow-Atmosphere Interactions over a Mountain Terrain*. PhD thesis, Ecole Polytechnique Federale de Lausanne, 2014.

[10] A Melese Endalew, Maarten Hertog, M Gebreslasie Gebrehiwot, Martine Baelmans, Herman Ramon, BM Nicolaï, and Pieter Verboven. Modelling airflow within model plant canopies using an integrated approach. *Computers and Electronics in Agriculture*, 66(1):9–24, 2009.

[11] John Finnigan. Turbulence in plant canopies. *Annual Review of Fluid Mechanics*, 32(1):519–571, 2000.

[12] C.S.B. Grimmond. Aerodynamic roughness of urban areas derived from wind observations. *Boundary-Layer Meteorology*, 89(1):1–24, 1998.

[13] CSB Grimmond and Timothy R Oke. Aerodynamic properties of urban areas derived from analysis of surface form. *Journal of Applied Meteorology*, 38(9):1262–1292, 1999.

[14] CSB Grimmond and Timothy R Oke. Aerodynamic properties of urban areas derived from analysis of surface form. *Journal of Applied Meteorology*, 38(9):1262–1292, 1999.

[15] M Hussain and BE Lee. A wind tunnel study of the mean pressure forces acting on large groups of low-rise buildings. *Journal of Wind Engineering and Industrial Aerodynamics*, 6(3):207–225, 1980.

[16] P Kastner-Klein and MW Rotach. Parameterization of wind and turbulent shear stress profiles in the urban roughness sublayer. In *This Conference*, 2001.

[17] Gabriel Katul. An investigation of higher-order closure models for a forested canopy. *Boundary-Layer Meteorology*, 89(1):47–74, 1998.

[18] Akio Koizumi, Jun-ichi Motoyama, Kei Sawata, Yoshihisa Sasaki, and Takuro Hirai. Evaluation of drag coefficients of poplar-tree crowns by a field test method. *Journal of wood science*, 56(3):189–193, 2010.

[19] Andrey Nikolaevich Kolmogorov. The local structure of turbulence in incompressible viscous fluid for very large reynolds numbers. In *Dokl. Akad. Nauk SSSR*, volume 30, pages 299–303, 1941.

[20] E Scott Krayenhoff, Jose-Luis Santiago, Alberto Martilli, Andreas Christen, and Timothy R Oke. 10.6 parameterization of drag and turbulence for urban neighbourhoods with trees (submitted june 2014). 2014.

[21] ZJ Li, DR Miller, and JD Lin. A first-order closure scheme to describe counter-gradient momentum transport in plant canopies. *Boundary-Layer Meteorology*, 33(1):77–83, 1985.

[22] Kate Liss, Thoreau Rory Tooke, Eli Heyman, Nicholas C Coops, and Andreas Christen. Vegetation characteristics at the vancouver epicc experimental sites. Technical report, University of British Columbia, 2010.

[23] Alberto Martilli and Jose Luis Santiago. Cfd simulation of airflow over a regular array of cubes. part ii: analysis of spatial average properties. *Boundary-layer meteorology*, 122(3):635–654, 2007.

[24] William Massman. A comparative study of some mathematical models of the mean wind structure and aerodynamic drag of plant canopies. *Boundary-layer meteorology*, 40(1-2):179–197, 1987.

[25] Mathworks. Matlab r 2014a, student version for linux os obtained from eth zurich, 2014.

[26] GJ Mayhead. Some drag coefficients for british forest trees derived from wind tunnel studies. *Agricultural Meteorology*, 12:123–130, 1973.

[27] Susumu Oikawa and Yan Meng. Turbulence characteristics and organized motion in a suburban roughness sublayer. *Boundary-Layer Meteorology*, 74(3):289–312, 1995.

[28] MR Raupach and A St Thom. Turbulence in and above plant canopies. *Annual Review of Fluid Mechanics*, 13(1):97–129, 1981.

[29] Mathias W Rotach. On the influence of the urban roughness sublayer on turbulence and dispersion. *Atmospheric Environment*, 33(24):4001–4008, 1999.

[30] Mathias W Rotach. Course notes of 'boundary layer meteorology', chapters 1-10. *ETH Zurich*, 2013.

[31] MW Rotach. Turbulence close to a rough urban surface part i: Reynolds stress. *Boundary-Layer Meteorology*, 65(1-2):1–28, 1993.

[32] MW Rotach. Profiles of turbulence statistics in and above an urban street canyon. *Atmospheric Environment*, 29(13):1473–1486, 1995.

[33] KE Runnalls and TR Oke. Dynamics and controls of the near-surface heat island of vancouver, british columbia. *Physical Geography*, 21(4):283–304, 2000.

[34] several contributors. *Formulaires et Tables - Mathmatiques, Physique, Chimie*. Commissions romandes de mathmatique, de physique et de chimie, 2000.

[35] Roland B Stull. *An introduction to boundary layer meteorology*, volume 13. Springer, 1988.

[36] AS Thom. Momentum absorption by vegetation. *Quarterly Journal of the Royal Meteorological Society*, 97(414):414–428, 1971.

[37] Yu-Heng Tseng, Charles Meneveau, and Marc B Parlange. Modeling flow around bluff bodies and predicting urban dispersion using large eddy simulation. *Environmental science & technology*, 40(8):2653–2662, 2006.

[38] Tooke R. Christen A. Coops N. Heyman E. Olchovski I. van der Laan, M. 'statistics on the built infrastructure at the vancouver epicc experimental sites'. epicc technical report no. 4. Technical report, Technical Report of the Department of Geography, University of Britisch Columbia. http://circle.ubc.ca/, 30pp, Version 1.2, 2012.

[39] Peter EJ Vos, Bino Maiheu, Jean Vankerkom, and Stijn Janssen. Improving local air quality in cities: To tree or not to tree? *Environmental Pollution*, 183:113–122, 2013.

[40] Weather and Climate service of the Government of Canada. 1981-2010 climate normals and averages, station data of: Vancouver international airport and vancouver oakridge, 06 2014.

8.2 Software

The main software used for this thesis was the following.

- Matlab R2014a by Mathworks, Student version for Linux OS obtained from ETH Zurich
- ParaView Viewer, freeware
- QGIS Desktop, freeware
- TeXStudio, freeware
- JabRef, freeware

9. Annex

9.1 Matlab code extracts

9.1.1 Tower data sampling

Sampling for neutral 20 minutes periods An extract of the function executing the sampling by Richardson numbers is presented below.

```
for i=1:l_IND1
    clear section
    if cont==0 % data from method (b)
        % Consider a 20min-section in the 1min-avg data. Multiply the
        % 20min-index by dT to obtain the index inside the 1min-data:
        section=IND1(i)*dT:(IND1(i)+1)*dT-1;
    elseif cont==1 % data from method (a)
        section=IND1(i):IND1(i)+19; % Choose a 20min-section in the 1min-avg data.
    end

    % Average the 1min-terms:
    wTa20(i)=nanmean(wTa1(section)); % wT-covariance
    wTa20b(i)=nanmean(w(section).*all(section,4)); % Different method for 20min w't'avg
    uwa20(i)=nanmean(uwa1(section)); % uw-covariance
    theta20(i)=nanmean(all(section,4));

    % Fluctuations between 20min-mean and 1min-means:
    udd=u(section)-nanmean(u(section));
    wdd=w(section)-nanmean(w(section));
    Tdd=all(section,4)-theta20(i);

    % COVariances for 1min-data within 20min-intervals:
    wTa22(i)=nanmean(wdd.*Tdd);
    uwa22(i)=nanmean(udd.*wdd);

    % Corrected covariances:
    wTa20(i)=wTa20(i)+wTa22(i);
    uwa20(i)=uwa20(i)+uwa22(i);

    % Richardson number for each 20 min-period:
    %-----------------------------------
    Ri20(i)=g/theta20(i)*(wTa20(i))*(zSensor-d0)*K/(abs(uwa20(i))^1.5);

    % Conditional sampling for neutral atmosphere:
```

```
    %--------------------------------------
    if  abs(Ri20(i))<ri_lim %Ri20(i) > -ri_lim && Ri20(i) < ri_lim

        % index for storing and aggregating the selected 20min periods as 1min-resolved data.
        loc=1+dT*a:dT*(a+1);

        % sample and aggregate the 1min-avg data chunks...
        sampDat(loc,:)=all(section,:);
        sampWT(loc,1)=wTa1(section);
        sampWTb(loc,1)=w(section).*all(section,4);
        sampUW(loc,1)=uwa1(section);
        sampDir(loc,1)=dir(section);

        % sample 20min-average Ri number for this neutral 20min period:
        Ri20n(a+1)=Ri20(i);

        if cont==0
            % sample 20min-average mean wind direction for this neutral
            % 20min period:
            Dir20n(a+1)=Dir(IND1(i));
        elseif cont==1
            % compute 20min-avg-wind direction of the concerned interval:
            Dir20n(a+1)=winddir(1,nanmean(all(IND1(i):(IND1(i)+dT-1),1)),...
                nanmean(all(IND1(i):(IND1(i)+dT-1),2)));
        end

        % The fully resolved data reading/extraction for each selected period is still
        % missing. But probably this step is not needed, after all.

        a=a+1;

    end
end
```

9.1.2 LiDAR datasets

In a first step, LiDAR datasets were read into Matlab and unrealistic values removed.

```
% READ .tif files:
[dsm, R] = geotiffread([path 'ndsm']);
[dem, R1] = geotiffread([path 'dem']);
[treeBinary,R2]=geotiffread([path 'treeBinary']);
[pFoliage,R3]=geotiffread([path 'pFoliage']);
[bld,R4]=geotiffread([path 'bldHeights']);
[treeHeights, R5]=geotiffread([path 'treeHeights']);

% resolution of the data, check files [m]
res = resolution(dsm,dem,treeBinary,pFoliage,bld,treeHeights);
factor=floor(1/res);
tc=floor(tc./res); % adjust tower coord. to resolution

bld(bld<-5)=0; % remove unrealistic values at the borders of building file
pFoliage(pFoliage<0)=0; % remove negative values in Parameter file
```

9.1.3 Triangulation of buildings

The buildings in the modelling domain were triangulated using the built-in Matlab function 'delaunay'. An extract of the building triangulation and the storing of points into 'node' form is presented below.

```
% %-------------------------------------

if building_triang_switch==1

% Create a grid:
x=1:l_dtm; y=1:l_dtm;
[X,Y]=meshgrid(x,y);
clear dem_xyz R

% Triangulate
disp('Triangulating buildings...')
TRI=delaunay(X,Y);
disp('Delaunay Triangulation finished')

disp('Writing building nodes to matrix...')
% Construct xx and yy vectors with unique point locations for (x,y):
for i=1:l_dtm
    int=(i-1)*l_dtm+1:i*l_dtm;
    xx(int,1)=i;
    yy(int,1)=[1:l_dtm]';
end

% Build 'Nodes' matrix:
% Triangulation stored in the form of a 'structure' (same triangulation as above)
TR=delaunayTriangulation(xx,yy);
Nodes=zeros(l_dtm^2,4); n=0;
for i=1:l_dtm
    for j=1:l_dtm
        y_meters=floor(l_dtm/2)-(i-1)/2-0.5;
        x_meters=j/2-0.5;
        n=n+1;
        index = nearestNeighbor(TR,i,j);
        Nodes(n,1)=index;
        Nodes(n,2:4)=[x_meters,y_meters,bld(i,j)];
    end
end
%Edges = edges(TR); % Write edges.
disp('done.')
```

9.1.4 Computation of the Leaf Area Density tensor

The parameters λ and k representing a Weibull pdf fitted to each LAD profile were extracted from the LiDAR datasets provided by Dr. Rory Tooke, (3).

Then, foliage probability is computed at each grid cell and at each height and then converted to Leaf Area Density. The result is a 3D-tensor.

Various conditions are applied, such as the maximum tree height (as an input matrix) and the requirement that $\lambda > 0$.

```
function [z,dLeaf,pFol,Lambda,K] = LAD(pFoliage,treeHeights,treeBinary,dz)

disp('Computing LAD...')

% Read the parameters 'scale' and 'shape' from pFoliage file:
p1=mod(pFoliage,1);                      % take decimals; they represent the SHAPE parameter
Lambda=0.01.*(pFoliage-p1);         % units (integers) stand for SCALE PARAMETER Lambda
K=1000.*p1;                                    % SHAPE PARAMETER K

l_dtm=length(pFoliage);

% % Compute FOLIAGE probability:
zmax=35; % max elevation for which dLeaf is computed
zmin=1.0; % min elevation for which dLeaf is computed
z=zmin:dz:zmax; % vertical coordinate

pFol=zeros(l_dtm,l_dtm,length(z));

for i=1:l_dtm
    for j=1:l_dtm
            if treeBinary(i,j)==1
                % probability of foliage at every level dz, between 0 and 30 m above ground:
                     for k=1:length(z)
                         % crop tree to height, avoid cells where Lambda=0:
                          if z(k) <= treeHeights(i,j) && Lambda(i,j)~=0
                             % WEIBULL DISTRIBUTION:
                             pFol(i,j,k)=(K(i,j)/Lambda(i,j))*(z(k)/...
                                 Lambda(i,j))^(K(i,j)-1.0)*exp(-(z(k)/Lambda(i,j))^K(i,j));
                           else
                             pFol(i,j,k)=0;
                          end
                     end
              else
               pFol(i,j,:)=0;
        end
    end
end

pFol(pFol>0.9999)=0.9999; % if pFoliage > 0.9999, set it to 0.9999
num_pFol_Equal_1=sum(sum(pFol(pFol==0.9999))); % Check where pFol was equal to 1

dLeaf=-log(1.0 - pFol); % LEAF (area) DENSITY in [m2/m3]

dLeaf(dLeaf>5)=4.0; % clip excessively high values
clear pFoliage

disp('done.')

end
```

9.1.5 Filtering of the LAD profiles

Filtering of individual LAD profiles in the vertical direction in order to smooth out spikes was performed. Shown below is the function executing this task for different discretizations in height dz.

```
function [z_resamp,dLeaf_resamp] = filtLAD( dLeaf,dz,dz_fine,dz_coarse )
% Filter LAD in the vertical direction with a top-hat filter.
% Re-sample it at a new resolution.

disp('Filtering and resampling LAD profiles...')

% support: vector of 2 m length
support=ones(1,floor(dz_coarse/dz_fine))/(dz_coarse/dz_fine)
rescaleFactor=floor(dz/dz_fine) % e.g. 1m/0.1m=10
[lx,ly,lz]=size(dLeaf);
dLeaf_filt=zeros(lx,ly,lz);
dLeaf_resamp=zeros(lx,ly,floor(lz*1/rescaleFactor));

for i=1:lx
    for j=1:ly
        dLeaf_filt(i,j,:)=conv(squeeze(dLeaf(i,j,:))',support,'same'); % filter
    end
end
clear dLeaf

% do the re-samp and filter actions in two different loops in order to
% clear dLeaf in-between (otherwise the memory is filled!)

for i=1:lx
    for j=1:ly
        a=0;
        for k=1:rescaleFactor:lz
            a=a+1;
            dLeaf_resamp(i,j,a)=dLeaf_filt(i,j,k);  % re-sample
        end
    end
end
clear dLeaf_filt
z_resamp=1.0:dz:35.0;

disp('done.')
```

9.1.6 Linear fit to determine z_0

```
d=[3.0,3.25,3.5];
xdetail=[2 6]; ydetail=[1e-1 2e1];
h=5.0;

figure(13),

x_width=10;
```

```
y_width=5;
set(gcf, 'PaperUnits', 'inches');
set(gcf,'position',[10 10 x_width*100 y_width*100]...
    ,'color','white','PaperPosition', [0 0 x_width y_width])

for i=1:length(d)

zd=(z-d(i))/h;
zd(zd<0)=0;

% no trees:
%--------------------------------------
% Linear fit between u=start m/s and u=end m/s

z1=25; z2=40; % fitting interval [m]

%startfit=7; endfit=12; xyswitch=1; % start/end fit depending on wind velocity
startfit=(z1-d(i))/h; endfit=(z2-d(i))/h; xyswitch=2; % start/end fit depending on elev.
[u_xy_fit,zd_fit,p] = supps.linfit(kappa*u_xy/ustar_mod,log(zd'),startfit,endfit,xyswitch);

% Prolongate fit to intersect with y-axis, in order to get z0:
xinters=1.0:0.1:max(u_xy_fit);
yinters=exp(p(1)*xinters+p(2));

z0=exp(p(2))*h; % Compute z0 from the fitting parameter
z0=round(z0*100)/100;

% with trees:
%--------------------------------------
% Linear fit between u=start m/s and u=end m/s

z1=25; z2=40; % fitting interval [m]

%startfit2=7; endfit2=12; xyswitch2=1; % start/end fit depending on wind velocity
startfit2=(z1-d(i))/h; endfit2=(z2-d(i))/h; xyswitch2=2;  % start/end fit depending on elev.
[u_xy_fit2,~,p2] = supps.linfit(kappa*u_xy2/ustar_mod,log(zd'),startfit2,endfit2,xyswitch2);

% Prolongate fit to intersect with y-axis, in order to show ln(z0):
xinters2=1.0:0.1:max(u_xy_fit2);
yinters2=exp(p2(1)*xinters2+p2(2));

z0_trees=exp(p2(2))*h; % Compute z0 from the fitting parameter
z0_trees=round(z0_trees*100)/100;

%-----------------
subplot(1,length(d),i)
%-----------------

% plot the xy-averaged u-velocity without trees on a semilog axis:
H13(1)=semilogy(kappa*u_xy/ustar_mod,zd,'k--','linewidth',2); hold on

% plot the (prolongated) linear fit:
plot(xinters,yinters,'r-','linewidth',2)

% plot the xy-averaged u-velocity with trees on a semilog axis:
H13(2)=semilogy(kappa*u_xy2/ustar_mod,zd,'g--','linewidth',2);
```

```
% plot the (prolongated) linear fit:
H13(3)=plot(xinters2,yinters2,'r-','linewidth',2);

% Labels:
xlabel('$\kappa\cdot<\bar{u}>/u_* $','Interpreter','LaTex','fontsize',13),
ylabel('$(z - d)/h $','Interpreter','LaTex','fontsize',13),
xlim(xdetail); ylim(ydetail)

% Textbox:
H={['$d$ = ' num2str(d(i)) ' m'],['$z_0$ = ' num2str(z0) ' m'],...
    ['$z_{0,t}$ = ' num2str(z0_trees) ' m']};
text(0.4,0.1,H,'Units','normalized','Interpreter','LaTex','fontsize',12)

end

h13l=legend(H13,'$<\bar{u}>$ no trees','$<\bar{u}>$ trees','linear fit');
set(h13l,'location','Northwest','Interpreter','LaTex','fontsize',12)

legend boxoff

saveas(13,[ppath,'changeD_linearFit_u','.eps'],'epsc');
```

9.1.7 Computation of spectra

Shown is the function that separates the data into chunks, computes spectra for each chunk, normalizes each spectrum by the variance of the signal of the chunk and finally averages the spectra from all chunks to obtain one representative spectrum.

```
% Compute spectra by chunks, normalize, average and classify (if required):
function [f,z] = spec(x,div,nclass,fmax)

% div: The fraction of the data that is taken for
% fourier transformation and then averaged over all fractions.

% length of one chunk of the dataset:
L_chunk=length(x)/div;
% initialize frequency and power vectors with length according to fft
% output (Nyquist!):
f=zeros(L_chunk/2+1,1); z=zeros(L_chunk/2+1,1);

for i=1:div
    xchunk=x((i-1)*L_chunk+1:i*L_chunk); % (1) Split into chunks
    xchunk=xchunk/std(xchunk);                % (2) Normalize by StdDev of the chunk
    % (3) psd_1d: fast fourier transform and computation of power,
    % Input data vector x, size of fft, length(x):
    [fchunk, zchunk] = psd_1d(xchunk,L_chunk, fmax);
    f=f+fchunk;
    z=z+zchunk;
end
f=f./div; z=z./div; % (4) Average over all data fractions

% Classify into bands, if required:
if nclass>1
    [f,z]=class(f,z,nclass);
end
```

```
end
```

9.2 Additional plots of results

9.2.1 LiDAR data

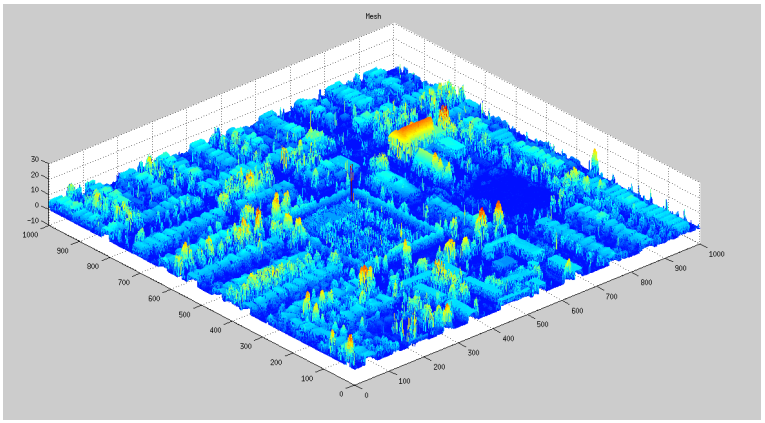

Figure 9.1: Matlab visualization of the LiDAR point cloud of a 500 × 500 m domain at 0.5 × 0.5 × 1 m resolution, centered at the Urban Climate Research Tower in the Sunset neighbourhood. The point cloud has a density of at least 15 pts/m^2, but up to 100 pts/m^2 in certain places. Data was recorded in February 2014.

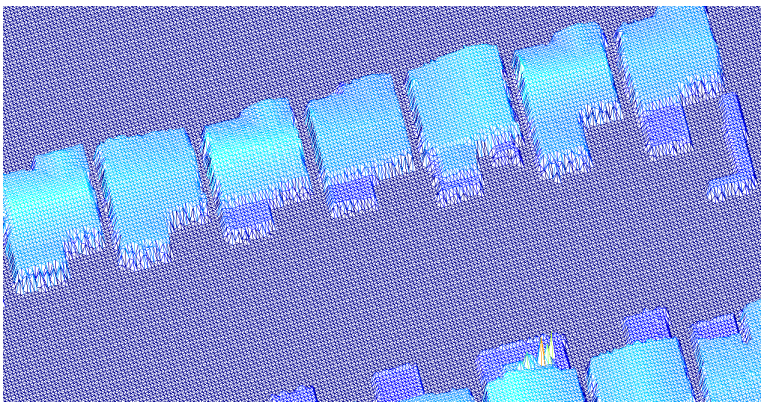

Figure 9.2: Extract of the triangulated building surface of Vancouver Sunset. No filtering was required for the buildings.

9.2.2 Tower data sampling

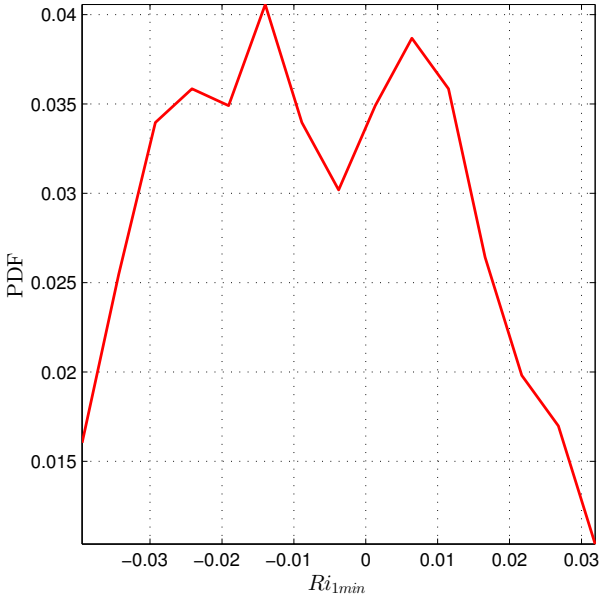

Figure 9.3: PDF of 1-minute Richardson numbers, taken from neutral 20-minute periods obtained with sampling method (b)

9.2.3 Spectra at a lower height

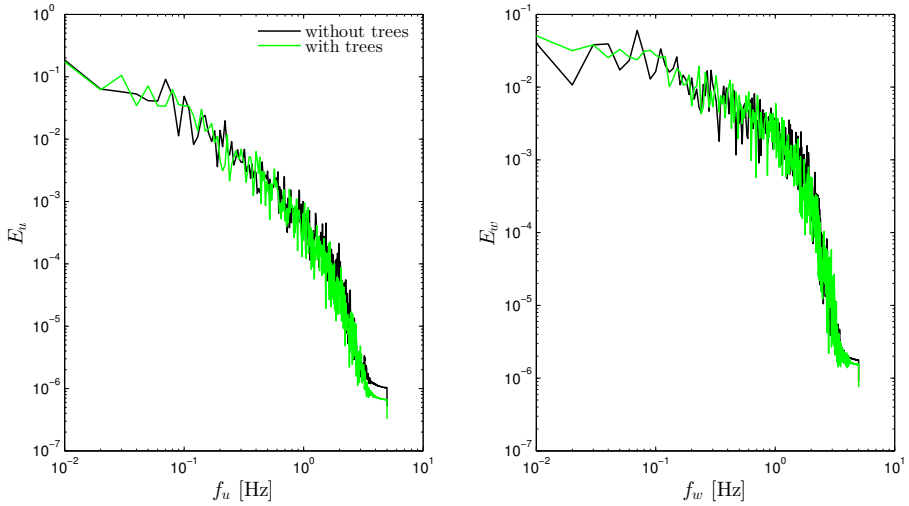

Figure 9.4: Spectra of streamwise and vertical velocities u and w at tower location and **z = 10.5 m**, plotted on logarithmic axes and compared for the simulations with and without trees. Spectra were computed for five chunks of 1000 data points each, divided by the standard deviation of the signal of each chunk and the spectra for the five chunks averaged.

9.2.4 Correlations in time

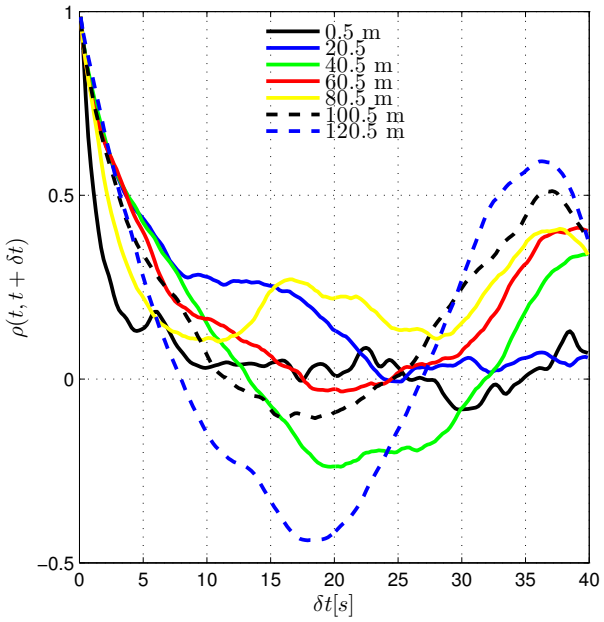

Figure 9.5: Correlations of streamwise velocity in time $\rho_u(z; t, t+\delta t)$ at tower location, plotted for the entire domain depth.

9.2.5 Pressure field

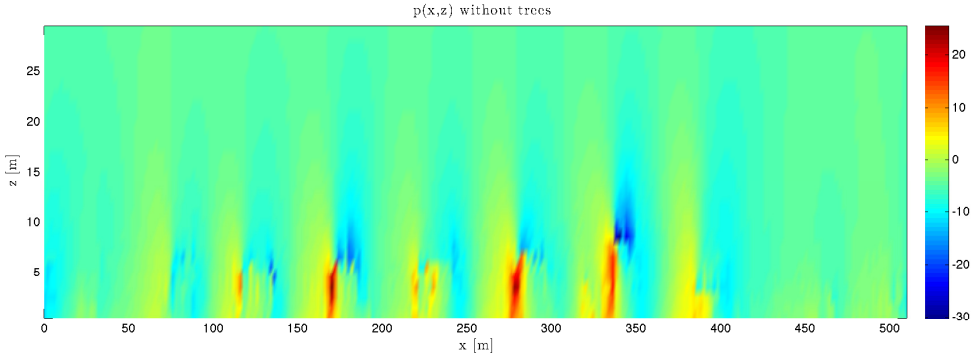

Figure 9.6: Field of kinematic pressure p $[m^2/s^2]$ in the xz-plane for the entire length of the modelling subset. High pressure on buildings and wakes with negative pressure are visible.

9.2.6 z_0: alternative linear fits

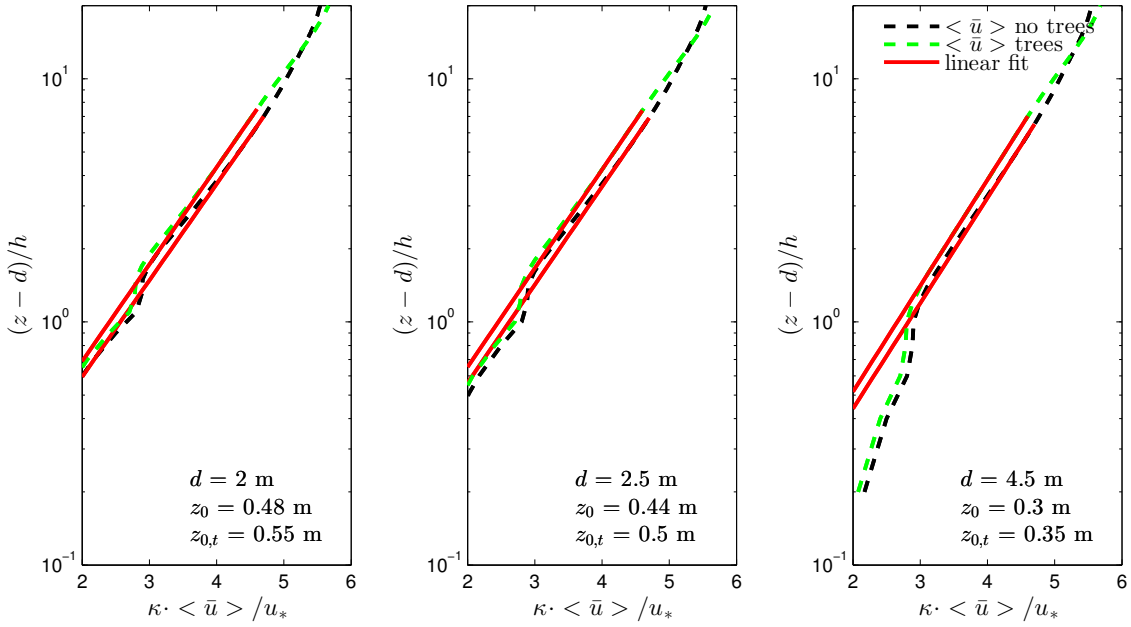

Figure 9.7: Linear fits to xy-averaged u-velocity profiles for alternative values of displacement height d. The fits were all performed over the height range z = 25 to 40 m, which is identical to the height range used for the fits in section 4.5.3.

9.3 Additional relevant images

9.3.1 Images of the modelling area

Images documenting parts of the investigation area Vancouver Sunset, such as the tree dimensions, shape and appearance are presented below.

Figure 9.8: A deciduous tree in Vancouver Sunset Area in the beginning of April. The tree is typical for the area and it is one of the taller individuals.

Figure 9.9: Coniferous trees in Vancouver Sunset Area in the beginning of April.

Figure 9.10: The Mainwaring Substation of B.C. Hydro in Vancouver Sunset. The UBC Research Tower is visible in the background on the right.

9.3.2 Anemometer-thermometer instrument

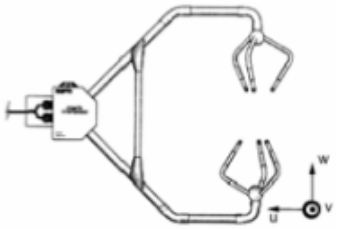

Figure 9.11: Drawing of the 3-axis anemometer-thermometer *CSAT3* of Campbell Scientific, used for the wind and temperature measurements at the UBC research tower. Information and drawing kindly provided by Andreas Christen, Micrometeorology group, Dept. of Geography at UBC.